Synthesis and Characterization of Surface Mounted Chiral Metal-Organic Frameworks

Zur Erlangung des akademischen Grades eines

DOKTORS DER NATURWISSENSCHAFTEN

(Dr. rer. nat.)

Fakultät für Chemie und Biowissenschaften

Karlsruher Institut für Technologie (KIT) - Universitätsbereich

genehmigte

DISSERTATION

von

M. Sc. Zhi-Gang Gu

aus

Jiangxi, P. R. China

Dekan: Prof. Dr. Peter Roesky

Referent: Prof. Dr. Christof Wöll

Korreferent: Prof. Dr. Stefan Bräse

Tag der mündlichen Prüfung: 15.07.2014

I declare hereby, that this dissertation has been elaborated by me and not used other than the sources, references and resources mentioned in the body of this manuscript. I present this work with the best of my knowledge and to fulfill the requisites of the Karlsruhe Institute of Technology to ensure good scientific practices.

Karlsruhe, 03.06. 2014

ABSTRACT

Metal-organic frameworks (MOFs), composed of metal ions and multitopic organic ligands, have been studied recently owing to their fascinating structures and potential applications. In particular, chiral MOFs are very promising materials for an efficient enantiomer separation. However, the impact of the pore size of the MOF on the enantioselectivity has not yet been investigated. By studying the adsorption of chiral molecules in isoreticular chiral surface mounted MOFs (SURMOFs) $[Cu_2(Dcam)_2(L)]$ (Dcam = (1R,3S)-(+)-camphoric acid; L = dabco (diazabicyclo[2.2.2]octane), bipy (4,4′-bipyridyl) and bipyb (1,4-bis(4-pyridyl)benzene)) with identical chiral centers and different pore sizes, it was found that the adsorption capacity and enantioselectivity is significantly influenced by the pore size and structure of chiral MOFs.

Oriented circular dichroism (OCD) was used to investigate chiral SURMOFs $[Cu_2(Dcam)_{2x}(Lcam)_{2-2x}(dabco)]$ ($0 \leq x \leq 1$) in this thesis. The growth orientation could be switched between the [001] and [110] direction by using either hydroxyl or carboxyl functionalized substrates. These SURMOFs were characterized by using OCD, which confirmed the desired ratio as well as the orientation of the enantiomeric molecules. Theoretical computations demonstrate that the OCD band intensities of the enantiopure $[Cu_2(Dcam)_2(dabco)]$ grown in different orientations are a direct result of the anisotropic nature of the chiral SURMOFs. Finally, the enantiopure $[Cu_2(Dcam)_2(dabco)]$ (or $[Cu_2(Lcam)_2(dabco)]$) SURMOFs were loaded with a pair of chiral enantiomers. An enantioselective enrichment was observed by OCD when the chiral host framework was loaded from the racemic mixture.

The quality of SURMOF is very important for many applications and the improvement of SURMOF quality becomes an interesting task currently. In this work, a new setup dipping robot is introduced to improve the quality of SURMOFs. Due to the introduction of ultrasonic bath in the dipping robot, the rising steps are efficiently enhanced for cleaning the sample and improved the quality. The SURMOF HKUST-1 and SURMOF-2 were prepared by the dipping robot with different concentrations of reagent solutions, which show the quality of SURMOFs is good from the optical microscopy, scanning electron microscopy (SEM) and atomic force microscopy (AFM) images, as well as the thicknesses and roughnesses of the SURMOF increase with increasing reagent concentrations.

ZUSAMMENFASSUNG

Metall-organische Gerüstsystemee (MOFs), zusammengesetzt aus Metallionen und organischen Liganden, werden auf Grund ihrer faszinierenden Strukturen und Anwendungsmöglichkeiten vielfach untersucht. Insbesondere sind chirale MOFs sehr vielversprechende Materialien, die eine effiziente Enantiomerentrennung erlauben. Jedoch ist der Einfluss der Porengröße des MOFs auf die Enantioselektivität noch nicht untersucht worden. Durch die Untersuchung der Adsorption chiraler Moleküle in chiralen oberflächenverankerten MOF Filmen (engl.: *surface mounted MOFs*: SURMOFs) vom Typ $[Cu_2(DCam)_2(L)]$ (Dcam = (1R,3S)-(+)-camphersäure, L=dabco (Diazabicyclo[2.2.2]octan), bipy (4,4′-Bipyridyl) und bipyb (1,4-Bis-(4-pyridyl)benzol)) mit identischen chiralen Zentren und verschiedenen Porengrößen wurde herausgefunden, dass die Adsorptionskapazität und die Enantioselektivität beträchtlich durch die Porengröße und Struktur beeinflusst sind.

Orientierter Circulardichroismus (OCD) wurde verwendet, um chirale SURMOFs $[Cu_2(DCam)_{2x}(LCam)_{2-2x}(dabco)]$ ($0 \leq x \leq 1$) zu untersuchen. Auf Hydroxyl- bzw. Carboxyl-terminierten Substraten konnten SURMOFs mit einer [001]- bzw. [110]-Orientierung aufgewachsen werden. Diese SURMOFs wurden erstmals mit OCD charakterisiert, die das eingestellte DCam-LCam-Verhältnis sowie die Ausrichtung der enantiomeren Moleküle bestätigt. Theoretische Berechnungen zeigen, dass die OCD-Bandenintensitäten der in verschiedenen Orientierungen gewachsene, enantiomerreine $[Cu_2(DCam)_2(dabco)]$ ein direktes Ergebnis der anisotropen Natur der chiralen SURMOFs sind. Schließlich wurden die enantiomerreinen $[Cu_2(DCam)_2(dabco)]$ (oder $[Cu_2(LCam)_2(dabco)]$) SURMOFs mit einem Enantiomerenpaar beladen. Beim Beladen des homochiralen Wirtsgerüsts aus einem racemischen Gemisch wurde mittels OCD eine enantio-selektive Anreicherung nachgewiesen.

Die Qualität der SURMOFs ist für viele Anwendungen entscheidend und die Verbesserung der SURMOF-Qualität ist eine wichtige Aufgabe. Im Rahmen dieser Arbeit wurde ein neuer Tauchroboter mit Ultraschallbad eingeführt, um die SURMOF-Qualität zu verbessern. Mittels Anwendung des Ultraschalls während des Spül-Schrittes wurde die Probenqualität deutlich verbessert. SURMOFs vom Typ HKUST-1 und SURMOF-2 wurden mit Reagenzlösungen verschiedener Konzentrationen hergestellt. Mittels optischer Mikroskopie, Rasterelektronen- und Rasterkraftmikroskopie wurde eine gute Probenqualität bestätigt, sowie eine Zunahme der Filmdicke mit zunehmender Reagenzkonzentration festgestellt.

1 INTRODUCTION – STATE OF THE ART

1.1 Metal-Organic Frameworks (MOFs)

1.1.1 General synthesis, properties, classification and applications

Metal-organic frameworks (MOFs), also known as porous coordination polymers (PCPs), are crystalline materials in which metal ions are connecte by organic ligands to form one, two or three dimensional frameworks (*Figure 1*).[1-4] The design and synthesis of MOFs have attracted great attention currently because of the possibility to obtain a large variety of
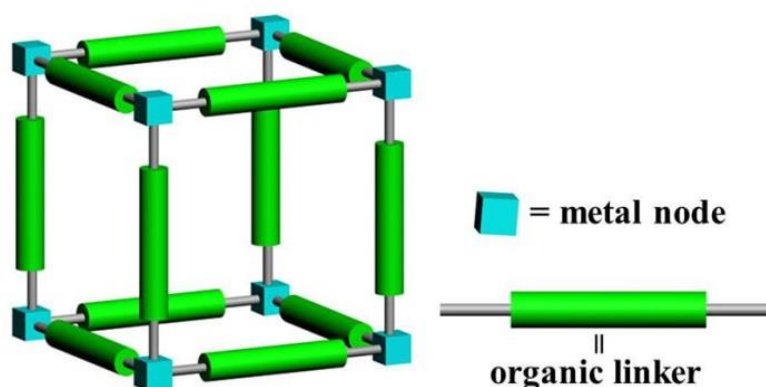
Figure 1. Connection of metal nodes and organic linkers leads to a metal organic framework (MOF). A simple cubic topology was employed as an example.

interesting topological networks. This is of great interest for the applications in a number of fields such as storage, separation and catalysis.[5-8] These are based on pore size and shape of MOFs and the interactions between host framework and guest molecules.[9-10] The fluorescence and magnetism applications depend on the choice of appropriate metal ions and ligands as well. In addition, biomedical applications and the sensor materials are also intensively investigated.[11-13]

MOFs are typically synthesized by combining metal salts and organic ligands in hydro/solvo-thermal reactions. The reactants are mixed into solvents such as water, ethanol, benzene, dimethylformamide (DMF) and dimethylsulfoxide (DMSO). The most fundamental determinants of MOF synthesis are the temperature, the concentrations of metal salts and ligands, the solubility of the reactants in the solvent and the pH of the solution. The characteristics of the ligand (bond angles, rigidity, ligand length and chirality.) also play a crucial role in the construction of the frameworks. Furthermore, the tendency of metal ions

can make different coordination numbers of metal, which can influence the geometric configuration of MOF structures.[14]

In addition to the conventional synthesis method, several other synthesis methodologies are described in the literatures including the electrochemical route,[15] microwave irradiation method[16] and chemical vapor deposition method.[17]

In terms of the description of the MOF structures, it is convenient to start with the secondary building units (SBUs). SBUs are essential for the design and construction of MOFs and dictate the final topology of the frameworks. So far, there are numerous well-known SBUs for MOFs, including the inorganic and organic SBUs.[1] In particular the inorganic SBUs are very important for the MOFs. For instance, metal ions are bridged by the coordinating oxygen atoms of the ligand resulting in a trigonal and a square planar (*Figure 2a* and *2b*) or a tetrahedral and a tetragonal paddlewheel SBUs (*Figure 2c* and *2d*).
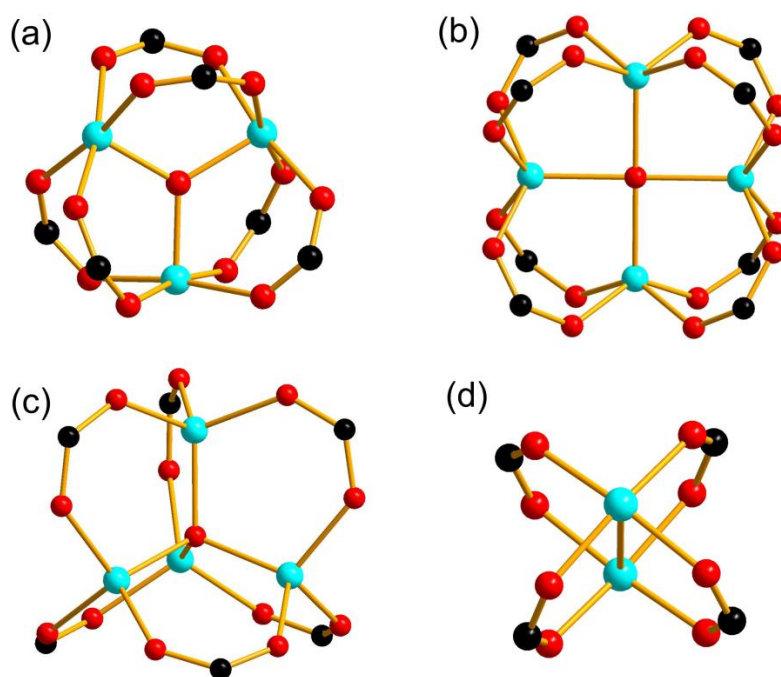
Figure 2. Structural representations of several SBUs, including (a) trigonal and (b) square planar, (c) tetrahedral and (d) tetragonal paddle wheel.

Kitagawa et al first classified MOFs into three categories: 1st, 2nd and 3rd generations (*Figure 3*).[18] The frameworks in these three classifications contain guest molecules inside their cavities or channels. The 1st generation compounds have a pore system which is stable only if the guest molecules are present. These frameworks collapse irreversibly when removing the guest molecules. The 2nd generation compounds have robust porous frameworks, which show permanent porosity also without guest molecules in the cavities,

pores or channels. The 3rd generation compounds have flexible and dynamic frameworks, responding to external stimulation, such as guest molecules, light, temperature, magnetic or electric field.
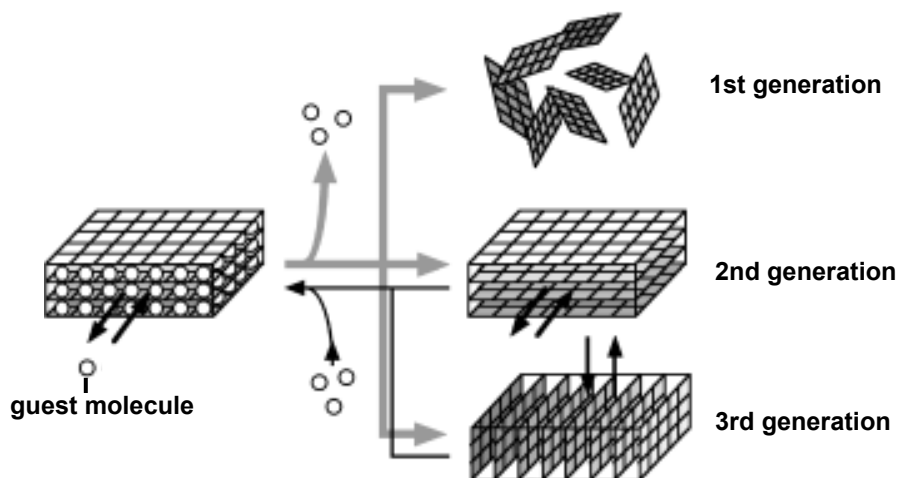
Figure 3. Classification of MOFs as 1st, 2nd and 3rd generation. (Figure taken from ref. [18])

MOFs have been investigated widely and are found to be applied in many fields. Applications in gas storage, size-, shape- and enantio-selective catalysis, luminescent and fluorescent materials and drug storage and delivery have been explored.[19-22]
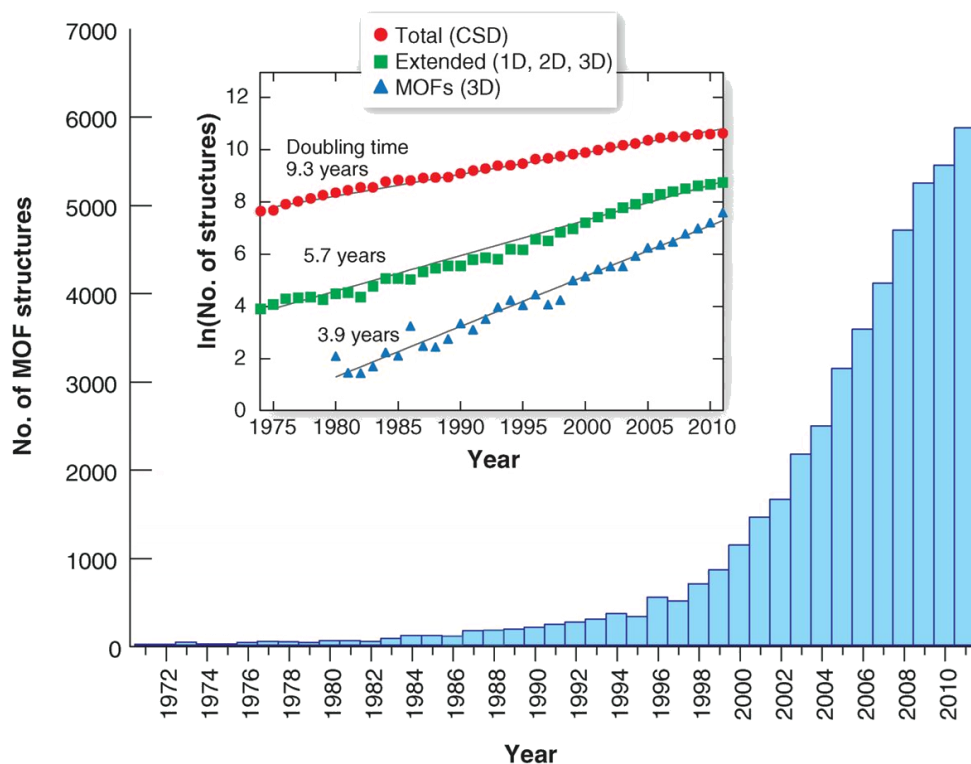
Figure 4. Metal-organic framework structures (1D, 2D and 3D) reported in the Cambridge Structural Database (CSD) each year from 1971 to 2011. (Figure taken from ref.[23])

In the past decade, there are more than 20,000 different MOFs being reported and studied (*Figure 4*).[23]

In the following, a few examples of typical MOFs will be introduced (*Figure 5*).

Yaghi et al reported a cubic zinc carboxylate MOF structure with a formula of $[Zn_4O(bdc)_3]$ (referred to as MOF-5 or IRMOF-1, where IRMOF-*n* stands for isoreticular MOFs with *n* as a series number, bdc = 1,4-benzenedicarboxylate).[24] MOF-5 exhibited an exceptionally rigid structure (stable up to 450 °C), high porosity (55%~61%), and high Langmuir surface area (2900 m^2g^{-1}), which attracts attention and triggers the extensive investigations of MOF materials.[24]

HKUST-1 (also named $Cu_3(btc)_2$ or MOF-199, btc = 1,3,5-benzenetricarboxylate), a copper-based MOFs with big pore channel about 10 Å in diameter, a Langmuir surface area of roughly 920 m^2g^{-1} and porosity of 40% was published.[25] HKUST-1 has attracted considerable interest and has been widely studied for gas adsorption, metal loading and catalyst.[26-28]

Yaghi et al introduced a new framework $[Zn_4O(btb)_2]$ (named MOF-177, btb = 1,3,5-benzenetribenzoate) which has a similar structure as HKUST-1, with a significantly increased Langmuir surface area of around 5300 m^2g^{-1} and a porosity of 83%.[29] The large pore of MOF-177 makes it possible to load large organic molecules such as polycyclic dye molecules or C60.[29-30]

Ferey et al published a chromium terephthalate framework, MIL-101 ($[Cr_3OX(H_2O)_2(bdc)_3]$, X=OH⁻/F⁻) with high Langmuir surface area of 5900 m^2g^{-1}. MIL-101 has pores with diameter of 29 and 34 Å, which provide big space for loading large molecules and lead to a well potential application of drug delivery and storage.[8]

The UMCM-2 structure, namely, $Zn_4O(T^2dc)(btb)_{4/3}$ (T^2dc = thieno[3,2-b]thiophene-2,5-dicarboxylate), exhibits a Langmuir surface area of around 6100 m^2g^{-1} and two different micropores from the structure.[31]

MOF-5   **HKUST-1**   **MIL-101**   **UMCM-2**   **[Zn₂(bdc)₂(dabco)]ₙ**
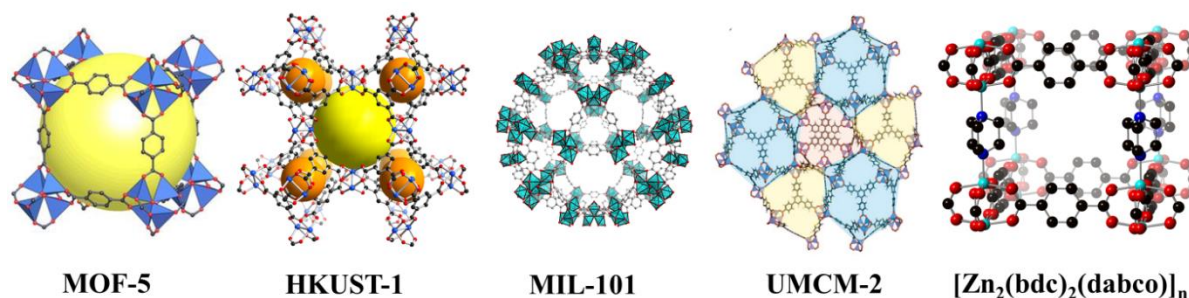
Figure 5. The structure of MOF-5 (Figure taken from ref.[24]), HKUST-1 (Figure taken from ref.[33]), MIL-101 (Figure taken from ref.[8]), UMCM-2 (Figure taken from ref.[31]) and [Zn₂(bdc)₂(dabco)].

The pillared-layer MOF [$Zn_2(bdc)_2(dabco)$] (dabco = 1,4-diazabicyclo[2.2.2]octane) was firstly reported by Kim et al in 2004.[32] The framework is composed of dinuclear Zn_2 paddle wheel unit. These units connect with bdc ligands to form an infinite 2D square-grid [$Zn_2(bdc)_2$] layer. The dabco are perpendicularly connected to paddle wheels dinuclear Zn_2 in the layers and as pillars to extend the 2D layers into a 3D structure. This highly porous pillared-layer MOF [$Zn_2(bdc)_2(dabco)$] has both properties: rigidity and flexibility. This means a stable framework with permanent porosity has a flexible dynamic behavior adjusted by switching guest molecule dimethylformamid (DMF) to benzene. The guest-free framework has a type I isotherm with a Brunauer-Emmett-Teller (BET) surface area of 1450 m^2g^{-1}. In contrast, the H_2 sorption of framework shows an unsaturated with a capacity of 225 cm^3g^{-1} at standard temperature and pressure.

1.1.2 Chiral Metal-Organic Frameworks (Chiral MOFs)

The interest in the synthesis of crystalline materials with characteristic structural chirality is rapidly expanding because of their potential applications in enantioselective processes, heterogeneous asymmetric catalysis and sensor technology in optoelectronics chemistry.[22, 34-37] Crystalline chiral metal-organic frameworks (chiral MOFs) have been prepared through four distinct strategies: (i) prepared from achiral linkers by self-assembly during crystal growth; (ii) synthesized from achiral metal complexes and bridging ligands under chiral influence; (iii) constructed by using chiral linkers as the building blocks; (iv) obtained by postsynthetic modification (PSM) method from pristine achiral MOFs.[38]

Kim et al reported the first example of asymmetric catalysis with a homochiral MOF L-POST-1 based on an enantiopure derived bridging ligand of tartaric acid and the $Zn_3(\mu_3$-O)-(carboxylate)$_6$ SBU.[39] In this structure, three zinc ions are connected by six carboxylate groups and a μ_3-oxygen to form the enantiopure trinuclears SBU (*Figure 6*). These SBUs are linked by the chiral ligands to generate 2D layers with a hexagonal topology. The resulting MOF has large chiral 1D channel with an estimated void space of around 47%. The remaining pyridine is exposed in the channels to endow the chiral MOF with catalytic properties.[39]
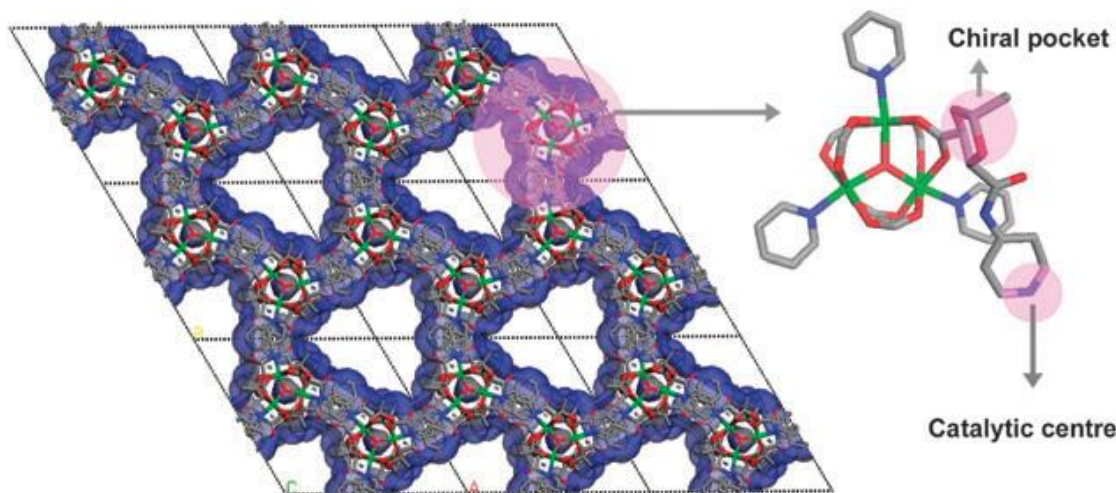
Figure 6. 1D equilateral triangular shape channel (left); coordination environment of zinc centers, showing the catalytic center and the chiral pocket (right) (Figure taken from ref.[22]).

The isoreticular homochiral pillared-layer MOFs were constructed by chiral ligand camphoric acid. These pillared-layer frameworks have the chiral, rigid layer $[Zn_2(cam)_2]$ and the pillar rigid N-donor linker dabco, bipy and bpe bridge to the layers (bipy = 4,4′-bipyridy, bpe = bis(4-pyridyl)-ethylene) (*Figure 7*). The structures of these frameworks are adjusted by the lengths of the pillar linkers, the length of the linker increase from dabco (4.5 Å) to bipy (8.0 Å) and bpe (10.5 Å). In this case, the pore sizes of the channels vary from 3×3.5 Å^2 for $[Zn_2(cam)_2(dabco)]$ to 5×7 Å^2 for $[Zn_2(cam)_2(bipy)]$ and 5×10 Å^2 for $[Zn_2(cam)_2(bpe)]$.[40] So the isoreticular homochiral MOFs are constructed by the different length of N-donor ligands.
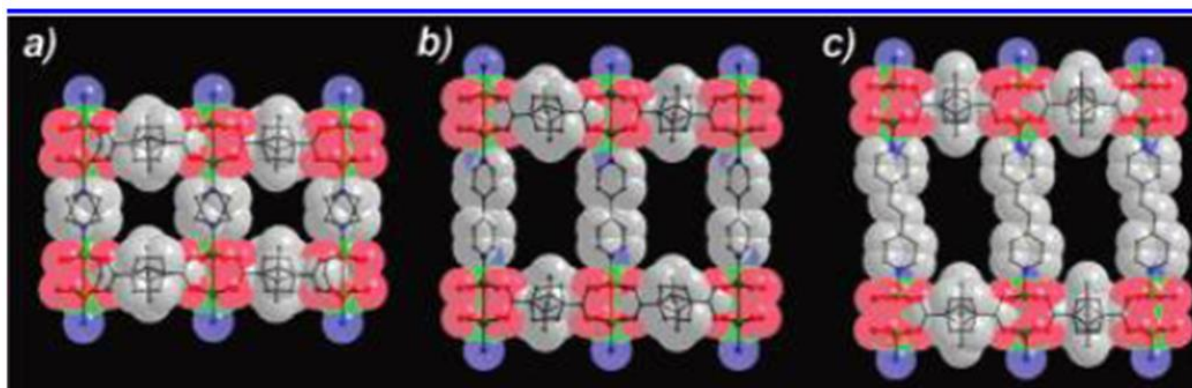
Figure 7. Side view of the MOFs $[Zn_2(cam)_2(dabco)]$ (a), $[Zn_2(cam)_2(bipy)]$ (b) and $[Zn_2(cam)_2(bpe)]$ (c). (Figure taken from ref.[40])

1.2 Surface Mounted Metal-Organic Frameworks (SURMOFs)

Metal-organic frameworks (MOFs) can be grown on functionalized substrates by liquid phase epitaxy (LPE), named SURMOFs. SURMOFs are highly porous and crystalline thin film materials.[41] The LPE approach of SURMOFs is a step by step fashion, which can control the thickness and homogeneity of the MOF thin film. So this method is suited for the fabrication of controllable layers with homo- or hetero-layers thin films. On other side, the orientation of MOF crystallinity can be depended by the functional groups on the modified substrate. The SURMOFs thin film prepared by the LPE method exhibit a homogenous, oriented, large flat surface material. These materials can be used for various storage, separation and sensor applications as well as for biologic applications.[42-43]

1.2.1 General description

The conventional hydro/solvothermal synthesis method of MOFs uses a one-pot reaction of mixed the metal salts and organic ligands. The functional groups of the ligands bind to the metal or metal-oxo clusters to form an ordered network.[44] In contrast, the SURMOFs are prepared by using a step by step LPE procedure, in which the metal salts and organic ligands solutions are separated. SURMOF is prepared by growing MOFs on the substrates with different functionalization, like -COOH, -OH and pyridyl functionalized surfaces. The LPE approach is based on the sequential immersion of SAMs modified substrate into the solutions of the metal salts and the organic ligands. Between each step the substrates were rinsed with solvent to remove the uncoordinated metal nodes or organic linkers. For starting the SURMOFs growth, the substrate should provide an organic template for stable MOF deposition, and also possibly enable epitaxial growth in a step by step fashion as shown in *Figure 11*. This results in this substrate supported, highly oriented and homogeneous SURMOF.

1.2.2 Self-assembled monolayers (SAMs)

The surfactant molecules spontaneously adsorb on surfaces to form a monomolecular layer, which is called self-assembled monolayers (SAMs). SAMs are widely used as nucleation-directing templates and adhesive surfaces for numerous applications.[45] The surfactant molecules possess a functionalized group which displays an affinity with the substrate and

can be anchored on the surface of substrate. As shown in *Figure 8*, SAMs could be depicted into a head group, tail and functional end groups. Usually, head groups can be thiols, silanes and phosphonates, tail or backbone groups are alkyl chains $(CH_2-CH_2)_n$, the functional end groups can be -OH, -COOH, $-NH_2$, $-CH_3$ and pyridyl to vary interfacial properties.
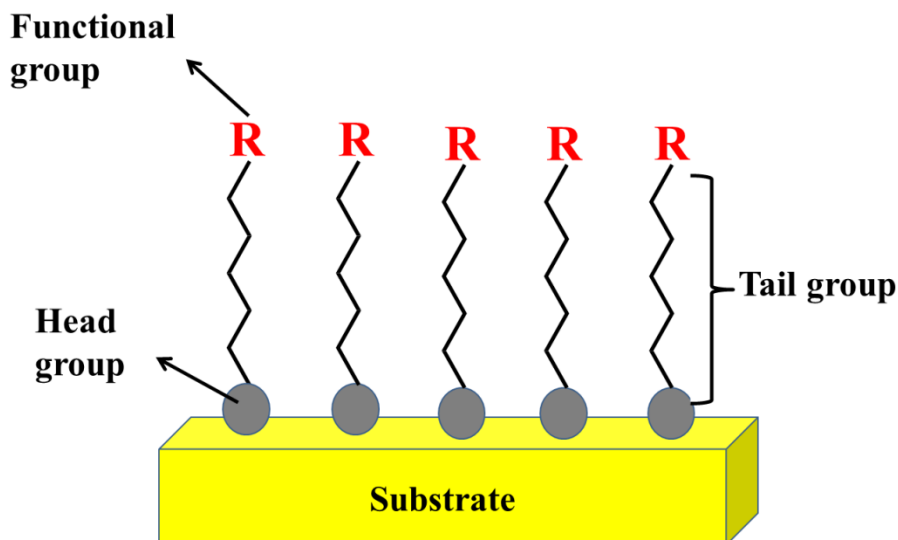
Figure 8. Representation of a SAMs substrate structure.

SAMs have been used in electroanalytical chemistry, molecular electronics and biochemistry.[45] In addition, SAMs can be also used for MOFs growth.[46] During the SURMOF growth, the Au substrate is used for SAMs preparations. The Au metals are oxidized by thiol or disulfide, which are then transferred into metal thiolates.[47] The chemical reaction between Au and thiol function group follows:

RSH + Au → RSAu + ½ H_2 ↑

For the SURMOFs growth, SAM molecules with -OH, -COOH or pyridyl functional groups are used.

1.2.3 Substrates

Different materials such as metal (i.e. Au, Ag, Cu, Pt or Pd) or semiconductor (i.e. SiO_2, Ai_2O_3, TiO_2 or ZnO),[48-50] can be used as substrate for the growth of MOFs.[42]

SAMs functionalized Au and quartz glass (SiO_2) are referred to as the substrates for SURMOF preparation in this work.

SAMs are fabricated by immersing 150 nm Au/2 nm Ti evaporated on Si wafers or commercially available Au coated quartz crystal microbalance (QCM) substrates for

SURMOF preparation in ethanolic solutions of MUD or MHDA (MUD=11-mercapto-1-undecanol, MHDA = 16-Mercaptohexadecanoic acid).[51] Because the method of the SAMs preparation is identical, only the process of MUD SAMs was described in detail as an example (*Figure 9*).The SAMs made from MUD molecules were prepared by immersing Au substrates into 1 mM ethanolic solutions of 11-mercapto-1-undecanol for 24 h and then rinsed with the ethanol and dried under nitrogen flux for the preparation.
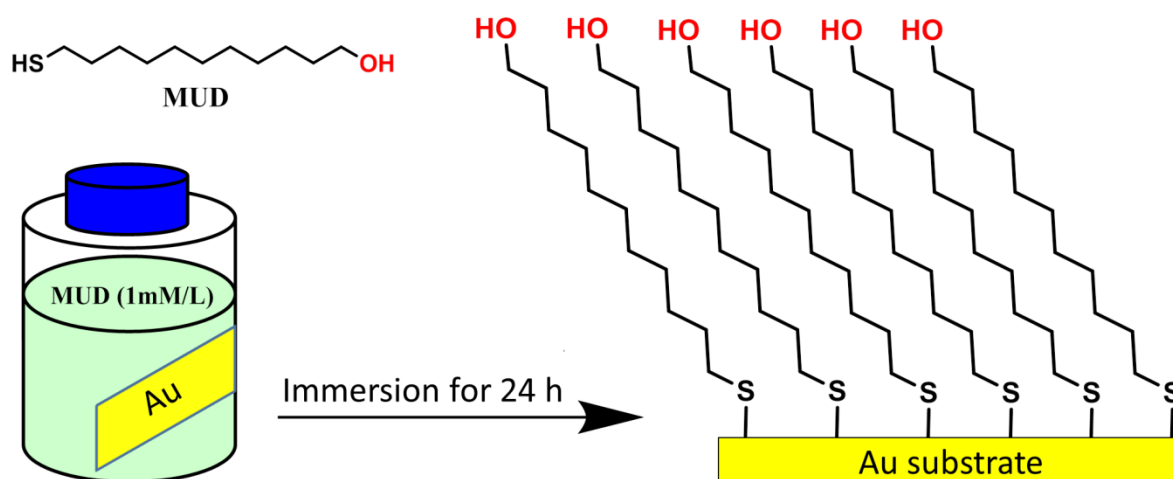
Figure 9. The process of MUD SAMs substrate preparation.

Commercially available round quartz glass plate (SQ1 (SUPRASIL), Hellma Jena) with a diameter of 20 mm and a thickness of 1.6±0.1 mm is used as a substrate for SURMOF preparation. After rinsing with water, the plates are subsequently immersed in a piranha solution consisting of 98% H_2SO_4/30% H_2O_2 (3:1) at 80 °C for 30 min, rinsed with water, dried, rinsed with ethanol and dried with nitrogen and then the -OH functionalized substrate was obtained (*Figure 10*).[52]
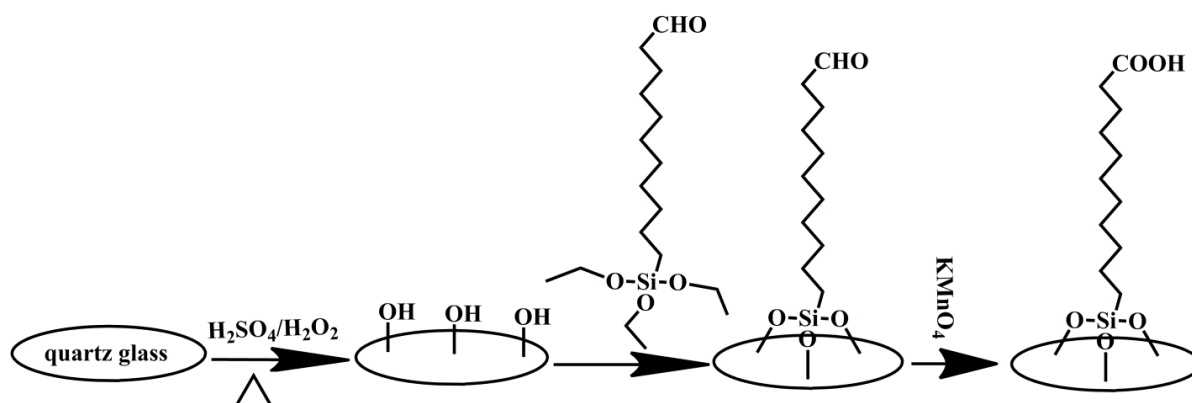
Figure 10. The preparation of -OH and -COOH functionalized groups on quartz glass.

The quartz glass functionalized by -OH groups was used 11-(triethoxysilyl)undecanal to modify aldehyde group on the substrate at room temperature for 3 h. Finally, the substrate

with aldehyde group was oxidized by potassium hypermanganate (0.1 mol/L) for 1 h to get the -COOH functionalized substrate (*Figure 10*).[53-54]

1.2.4   Liquid phase epitaxy (LPE)

Liquid phase epitaxy (LPE) is a widely used method to grow semiconductor crystal layers from the melt on a solid substrate. It has been applied to many compounds, but the main applications are compound semiconductors and magnetic rare-earth iron garnets.[55] Nelson at first used LPE grow thin layers for material studies and applications in the year 1963.[56]
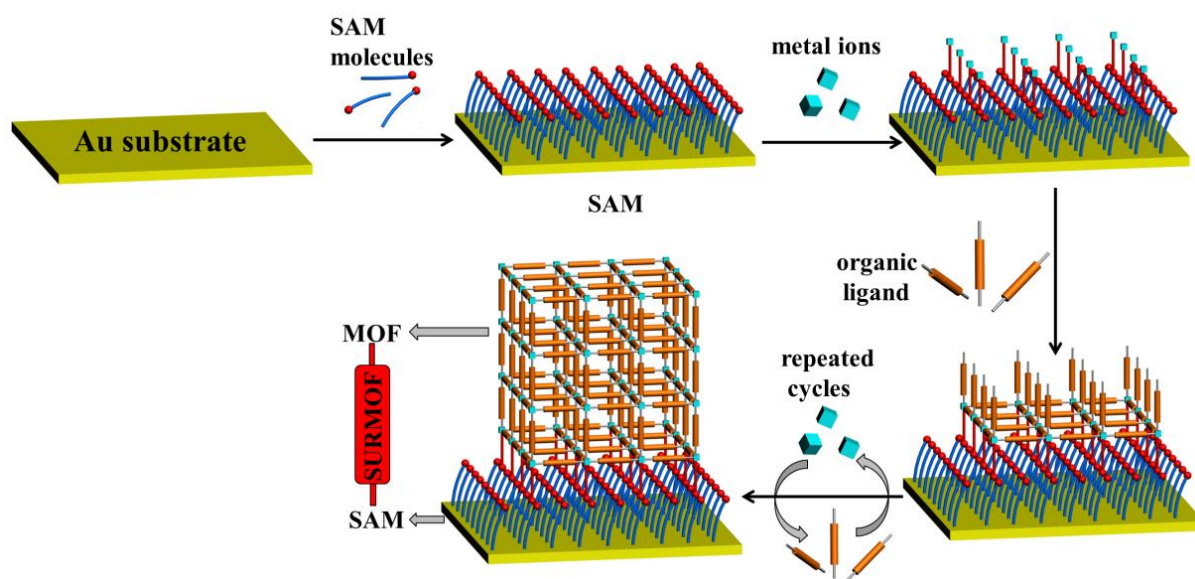
Figure 11. Illustration of the LPE growth of SURMOF on a SAMs functionalized gold coated substrate, the thickness of the SURMOF thin film depends on the number of coating cycles.

Currently, the LPE method is applied to grow MOF thin films (SURMOFs) on organic functionalized substrates (SURMOFs). The first SURMOF was reported by Wöll et al in 2007.[46] For preparation of SURMOF, at first, the organic SAMs with functional groups (-OH or -COOH) should be immobilized on the substrate, which provides an organic template for MOF deposition, as shown in *Figure 11*. After the SAMs are completely ordered on the substrate surfaces, the substrate is immersed into the metal salts solution for coordinating with the metal nodes. Then the substrate is rinsed with solvent and immersed in the organic ligands solution for the coordination of linker. After rinsing the sample with solvent again, the sequential immersion of metal salts and organic ligands solutions is done for a numerous cycles for the growth of the MOF thin film. So far, several techniques have been established for the SURMOFs preparation using LPE method, namely the pump, spray

and dipping methods.

1.2.4.1   Pump method

The pump method[57] is one of the standard techniques for SURMOF preparation. The setup of pump system (*Figure 12*) is controlled by a LabView program. There are four pumps for controlling the immersion time and volume of each step of solution. Three of them are responsible for the injection of metal salts, organic linkers and rinsing solvent solutions respectively into the reaction cell, in which the substrate is placed. The fourth one is responsible for pumping out the solution from the cell. The reaction temperature is controlled by a heating or cooling the pump system. Therefore, by using the pump method SURMOFs can be prepared in a temperature range of -20~150 °C (i.e. 20~70 °C for ethanol as solvent). The procedure for the SURMOFs preparation (e.g. HKUST-1) was done by using the following steps:

Firstly, the preparation of the pump system was set at 50 °C and then the SAMs modified substrate was placed into the clean reaction cell (*Figure 12*). The procedures are as follows:

- The substrates were firstly immersed in a 1 mM of copper acetate ($Cu(OAc)_2$) ethanolic solution for 15 min.

- The sample was subsequently rinsed with ethanol for 2 min.

- The sample was then immersed in a 0.2 mM of 1,3,5-benzyltricarboxylic acid (H_3btc) ethanolic solution for 30 min.

- The sample was then rinsed with ethanol for 2 min.

- These four steps are repeated for 40 cycles in order to grow a SURMOF (here: HKUST-1).

Usually, the pump method is used for thin SURMOFs preparation (less than 100 nm) because this method requires long immersion time. To obtain thick SURMOFs, it require therefore several days.
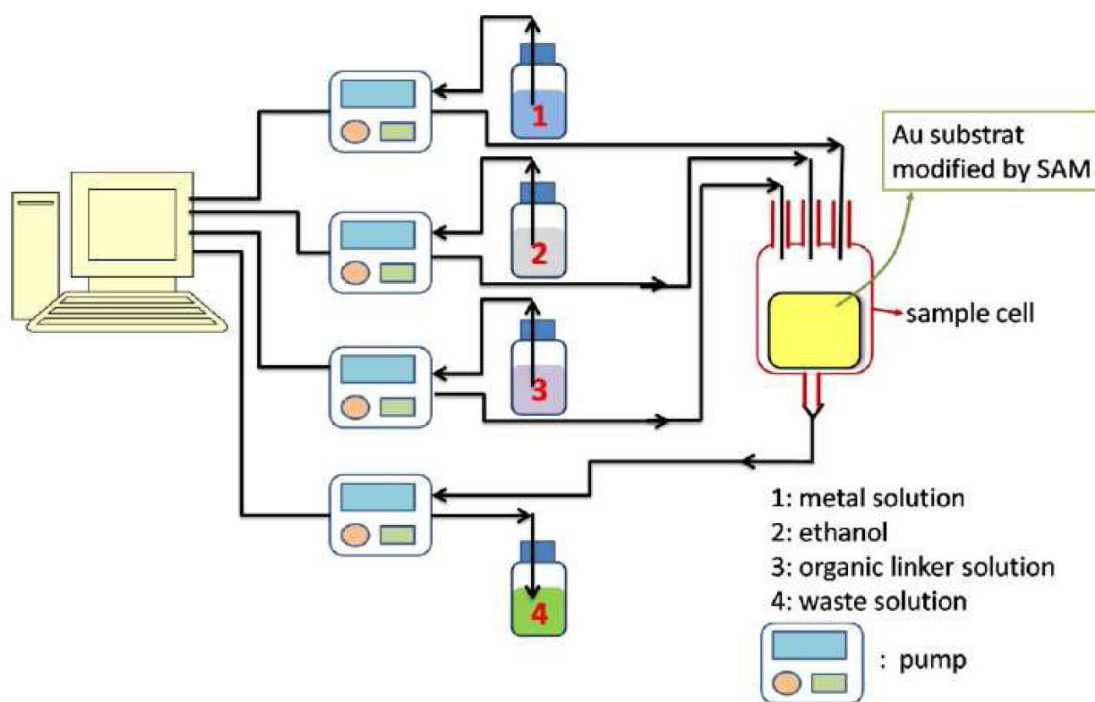
Figure 12. The diagram of the pump system for the automated layer by layer growth of SURMOFs. (Figure taken from ref.[57])

1.2.4.2   Spray method

The spray method is based on a nozzle spray system.[53] It has been successfully used in connection with other layer by layer techniques for coating substrates with two or more component thin layers. The spray method is based on a system in which an aerosol is produced by expanding solutions of the reactants through a small nozzle. The spray method includes hand spray and automatic spray methods. For the hand spray method, there are two nozzles for spraying the solutions (metal salts and organic ligands) and rinsing is performed by hand (squeeze bottle). For automatic spray method, there are three nozzles for spraying the solutions (metal source, organic ligands and rinsing solvent) and all the steps are executed by the program. When the droplets of the aerosol hit the substrate on the target, material is deposited at the solid-liquid interfaces (LPE process). The parameters of the spray procedure at room temperature are carrier gas pressure, flow rate, and distance between the nozzle and the target. Interestingly, spray method is less time-consuming, requires less solution and get thicker SURMOF than pump system. In addition, it has to be noted that the humility of the air is a parameter which can not be controlled.
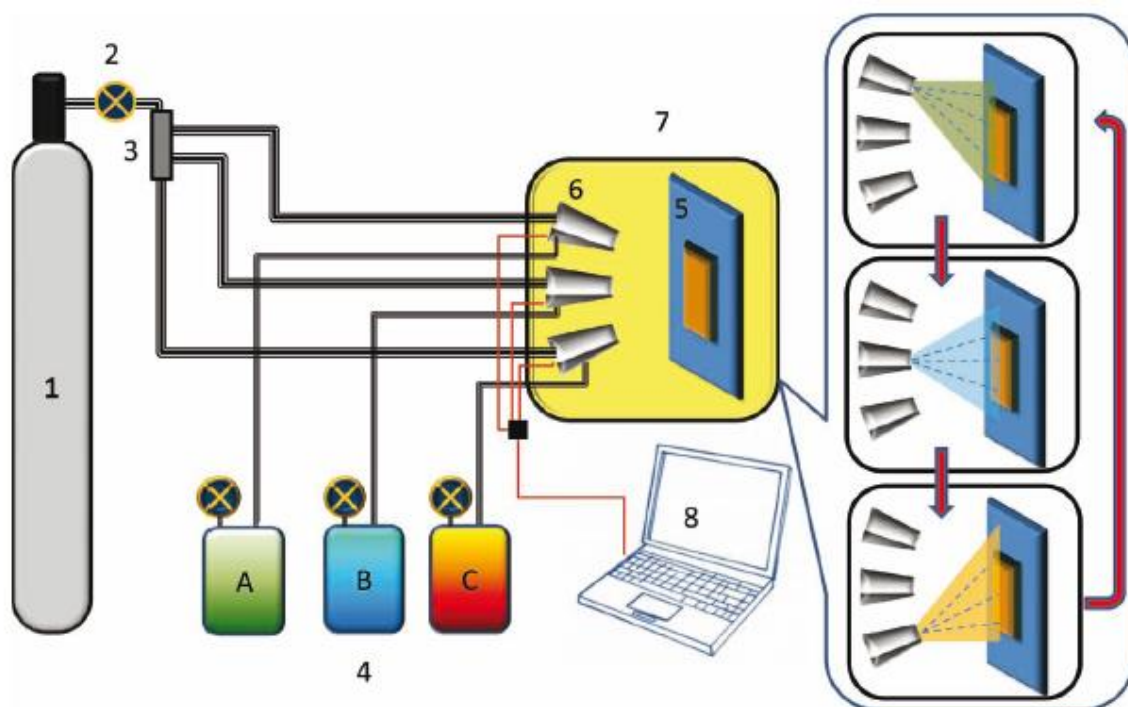
Figure 13. The diagram of the automatic spray method for LPE growth of SURMOF: (1) Gas supply, (2) gas flow controller (3) three-way valve gas distributor (4) (A, B and C) solutions storage containers (5) sample holder (6) dosing valves, (7) spray chamber, (8) PC. (Figure taken from ref.[53])

The procedure for the SURMOFs preparation (e.g. HKUST-1) investigated here was done using an automatic spray system using the following steps:

- Firstly, set up the automatic system (i.e. spray pressure or time), and then fix the substrate with functionalized SAMs on the target (*Figure 13*).
- The sample was subsequently sprayed with the 1 mM $Cu(OAc)_2$ ethanolic solution to the substrate for 10 s.
- After waiting 30 s, the sample was then sprayed with ethanol for 5 s.
- The sample was subsequently sprayed with the 0.2 mM H_3btc ethanolic solution for 15 s.
- After waiting 30 s, the sample was then subsequently sprayed with ethanol for 5 s.
- After waiting 30 s, one cycle of the SURMOF preparation is done.

In order to get a SURMOF HKUST-1 with ~100 nm thickness by this method, only 10 cycles need to be repeated.[53]

1.2.4.3   Synthesis in quartz crystal microbalance (QCM) cell

QCM is used to monitor the mass change in the materials coating on the QCM sensor. The growth of SURMOF also can be followed with *in-situ* synthesis in QCM cell. The changes of

the resonance frequency of the quartz sensor as a function of the deposition and removal of material have been monitored. The QCM with dissipation monitoring (QCM-D) with an autosampler is used in this thesis is shown *Figure 14*.
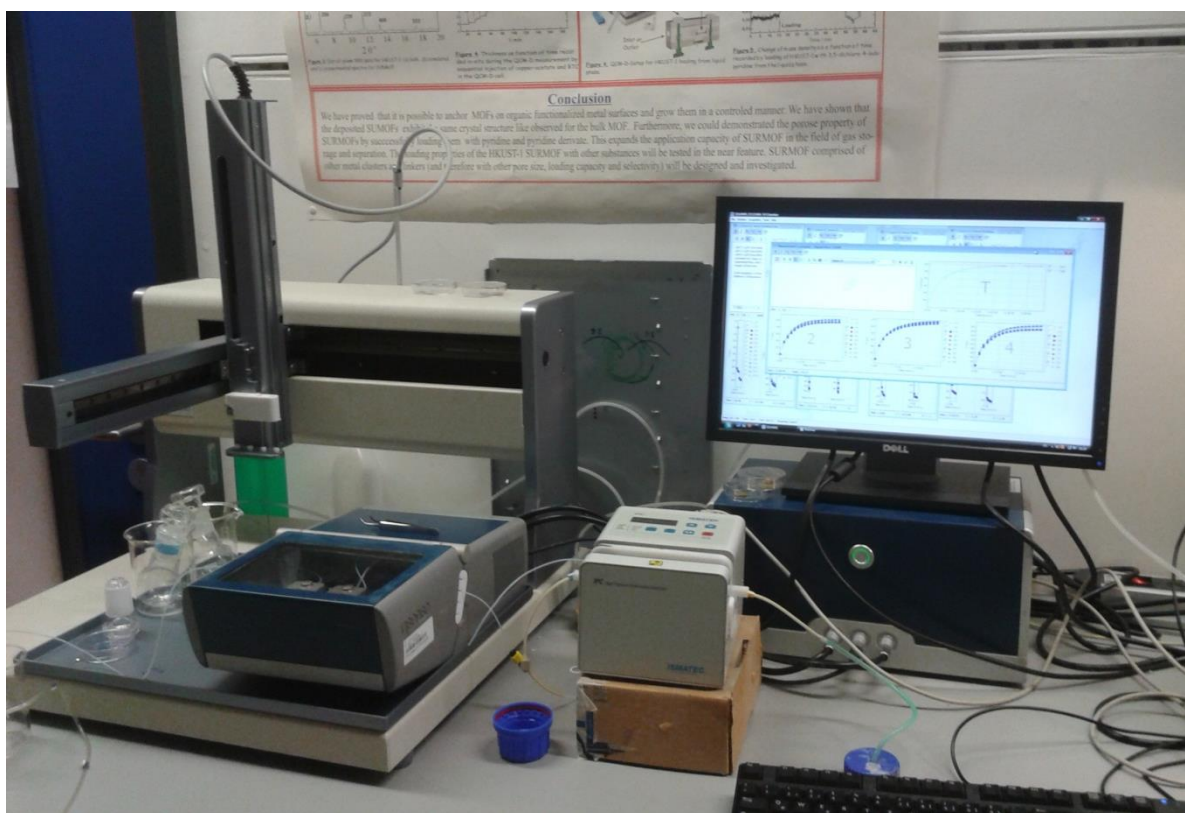
Figure 14. The setup of quartz crystal microbalance (QCM) method for SURMOFs preparation.

Taking the preparation of SURMOF HKUST-1 for example, at first the gold coated sensor with was functionalized by MHDA SAMs and then put in the sensor holder for experiment. Ethanol is flowed through QCM-D cell, resulting in a stable baseline at the beginning of the experiment. Then the autosampler is started by the program and then the pump can flow the liquid solution step by step with the setting time. The 1 mM $Cu(OAc)_2$ solution was flowed through the QCM sensor with MHDA SAMs, which causes binding of $Cu(OAc)_2$ on SAMs which can be detected by a frequency change directly until to the stable plateau for ~2 min.[58] The $Cu(OAc)_2$ connect with the -COOH group of the SAMs to cause the increasing the mass on the QCM sensor (*Figure 15*). Then the ethanol is flowed into the QCM sensor for cleaning after the frequency is stable. During this flowing step, the rest $Cu(OAc)_2$ is removed, which cause a slightly increasing frequency. When the frequency is stable again, the H_3btc solution is flowed into the QCM sensor, the 0.2 mM H_3btc coordinates $Cu(OAc)_2$ with covalent bonds, which make the frequency of QCM sensor is decreased. The related mass change takes ~5 min until the frequency is consistent. After the frequency is not changed, the

ethanol passes through the QCM sensor for rinsing again. This process is repeated for 40 times and a SURMOF HKUST-1 is otbatined in the end. Using the QCM-D to grow the SURMOF, it can monitor the mass change in each step and the growth environment can be protected against air in an effective way.
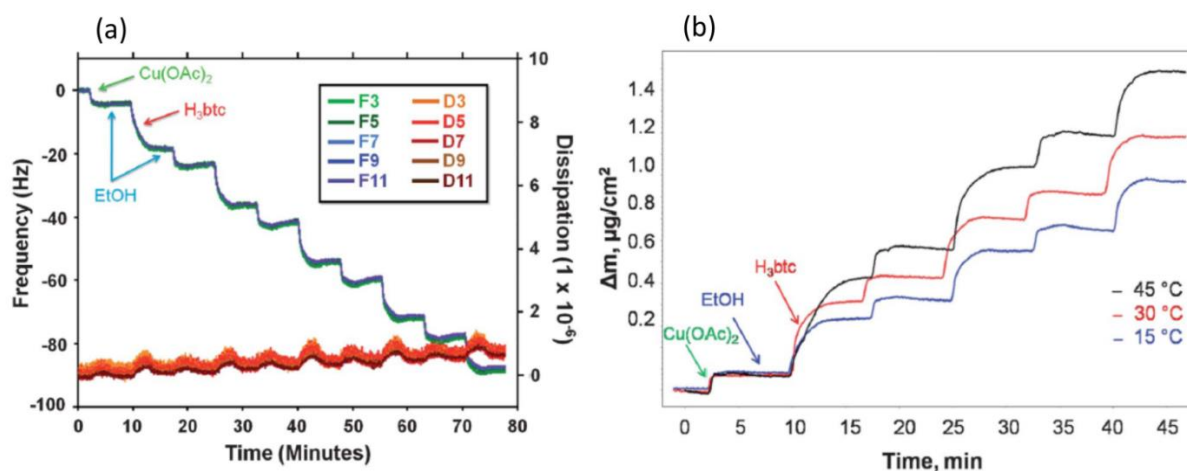
Figure 15. QCM-D results showing changes for various harmonics of the frequency, dissipation (a) Sauerbrey mass (b) change after Cu(OAc)$_2$ and H$_3$btc deposition cycles on SiO$_2$ coated electrodes. (Figures taken from ref.[58])

1.2.4.4 Dipping method

In the dipping system, there are three containers for different solution (metal salts, organic ligands and rinsing solutions) as shown in *Figure 16*. The functionalized substrate is immersed in each container sequentially. There are two kinds of dipping methods, one is dipping by hand method[46] and the other is dipping by an automatic robot method. For example, the process of dipping by hand method for HKUST-1 preparation was done using following steps,

- The gold substrate with functionalized MHDA SAMs is dipped in 1 mM Cu(OAc)$_2$ solution for 30 min, which causes the Cu-dimer ions to bind with the carboxylate groups at the substrate surface.
- The sample is rinsed with the ethanol for cleaning.
- Then the sample is put into the 0.2 mM ligand H$_3$btc ethanolic solution for 60 min.
- The sample is rinsed with ethanol.

By subsequently repeating and alternating the immersion of the substrate in 1 mM Cu(OAc)$_2$ and H$_3$btc solution, the SURMOF HKUST-1 is grown successfully by hand dipping method.
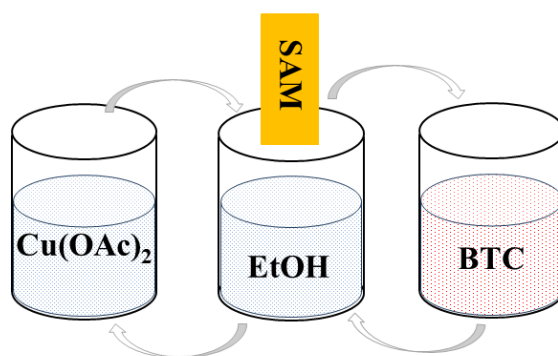
Figure 16. The diagram of dipping by hand method for SURMOFs preparation.

Dipping by robot method is an automated, computer controlled robot which is used for synthesizing SURMOFs by dipping the sample sequentially into the synthesis solutions. The setup is schematically shown in *Figure 17* and *Figure 18*. The main components are containers for immersion solutions (metal salts, organic ligands and rinsing solutions), position controller, holders (controller holder and sample holder), an ultrasonic bath and a pump system. In this setup, the position controller moves the sample holder to the immersion container in an accurate three-dimension position (x, y and z axis). The head of sample holder and container lids are made of iron and the controller holder is magnetic which can hold and lay down the sample holder or lids controlled by the software. There are seven positions for the containers (P1~P7). The central position of the working table is used for showering and other four positions for parking of the container lids. P0 is for sample placement at the beginning or end of the experiment. Usually P1, P2, P6, and P7 are used for metal salts or organic ligands solutions. The containers P3, P4 and P5 are used for the rinsing solutions, which are located in the ultrasonic bath. The ultrasonic treatment can be switched on by the program when the sample is immersed into the containers P3, P4 and P5 positions for rinsing. The ultrasonic bath will enhance the cleaning of sample and improve the sample quality. In addition, there is one showering step after each immersion step, where the rinsing solution from a container is spurted on the sample by a pump during this step to rinse the sample throughly. All the procedures are controlled by using software LabView.

Here, an example for synthesis for SURMOF HKUST-1 grown on MHDA SAMs is shown:

(1) P1 and P2 containers are filled with $Cu(OAc)_2$ solution (1 mM) and organic ligand H_3btc solution (0.2 mM), respectively. P3 and P4 containers are filled with ethanol. Ethanol is filled into the showering bottle, too.
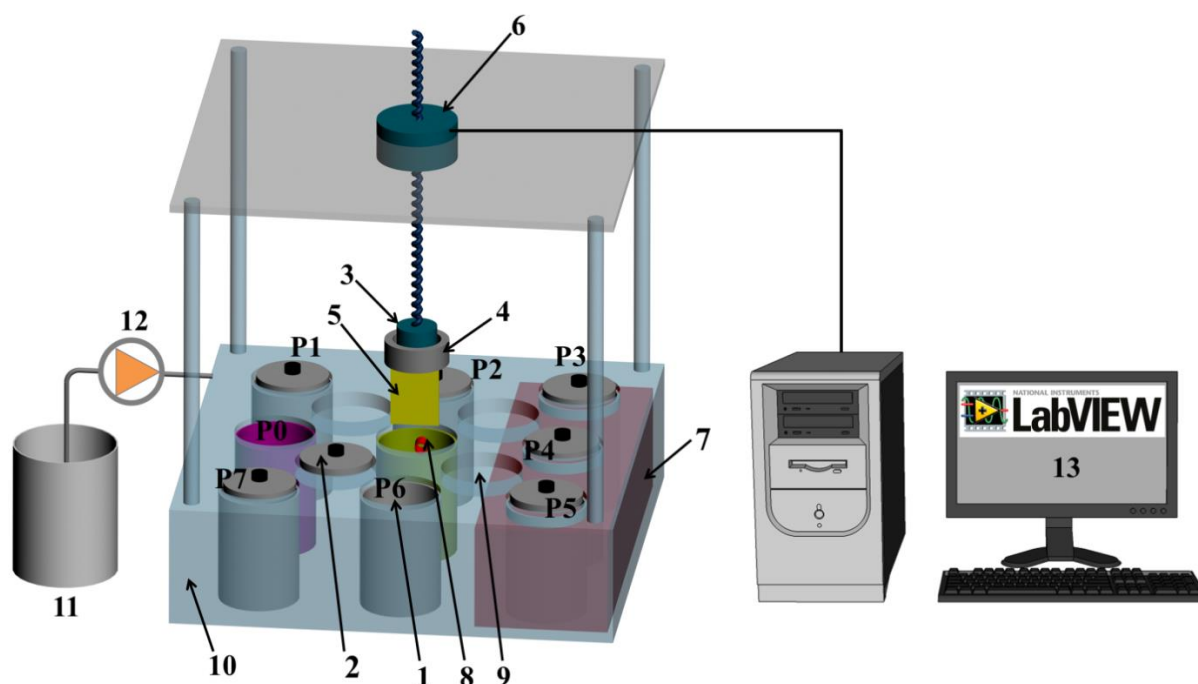
Figure 17. The setup of dipping robot system: (1) containers for immersion solutions or placement for sample (P1~P7); (2) container lid; (3) controller holder; (4) sample holder; (5) sample; (6) position controller; (7) ultrasonic bath; (8) shower; (9) parking position of container lid; (10) Teflon working table; (11) solution bottle for showering; (12) pump; (13) PC.

(2) The running order for SURMOF HKUST-1 preparation is set according to the step by step fashion.[46] The following order was set for the preparation: $P1(Cu(OAc)_2) \rightarrow P3(ethanol) \rightarrow P2(H_3btc) \rightarrow P4(ethanol)$. The immersion time and showering time are set to 600 s for $Cu(OAc)_2$ solution, 900 s for H_3btc solution, 100 s for rinsing ethanol solution and 3 s for showering. The ultrasonic treatment is switched on during immersion of the sample in P3(ethanol) and P4(ethanol).

(3) The Au substrate functionalized by MHDA SAMs is fixed on the sample holder in position P0.

(4) The running order and parameters are set in the program, which is done by the software LabView automatically. The process is started when the program in the software is turned on. After starting the preparation procedure, following steps are done:

(i) The controller holder moves to P1 and moves the container lid to the parking position of lid. Then the controller holder picks up the sample holder from P0 and puts it in $Cu(OAc)_2$ solution. The lid is taken back to P1 to avoid the evaporation of solutions.

(ii) After 600 s immersion of the sample in $Cu(OAc)_2$ solution, the lid in P3 is removed by controller holder. The sample is moved into the center position of the working table for

showering 3 s. The ethanol solution will remove the residual $Cu(OAc)_2$ and then the sample is moved into the P3 for immersion in ethanol solution. The lid is put back on the P3. During this time, the ultrasonic bath is also turned on.

(iii) After immersion of the sample in rinsing ethanol solution for 100 s, the controller holder removes the lid on P3 and P2, and then move the sample for showering 3 s and puts the sample to H_3btc solution (P2) for 900 s. Then the lid is put back in the P2.

(iv) After immersion of the sample in H_3btc solution for 900 s, the lid in P4 is removed by controller holder. The sample is moved to the center position for showering 3 s, then the sample is moved to the rinsing ethanol (P4) for cleaning. The lid is put back in the P3.

(v) After immersion of the sample in rinsing ethanol for 100 s using ultrasonic cleaning and then the sample is showered in the center position of the working table for 3 s. The first cycle of SURMOF HKUST-1 preparation is finished. The immersion process P1 ($Cu(OAc)_2$) → P3(ethanol) → P2(H_3btc) → P4(ethanol) is repeated for 40 cycles to obtain a SURMOF HKUST-1 thin film.
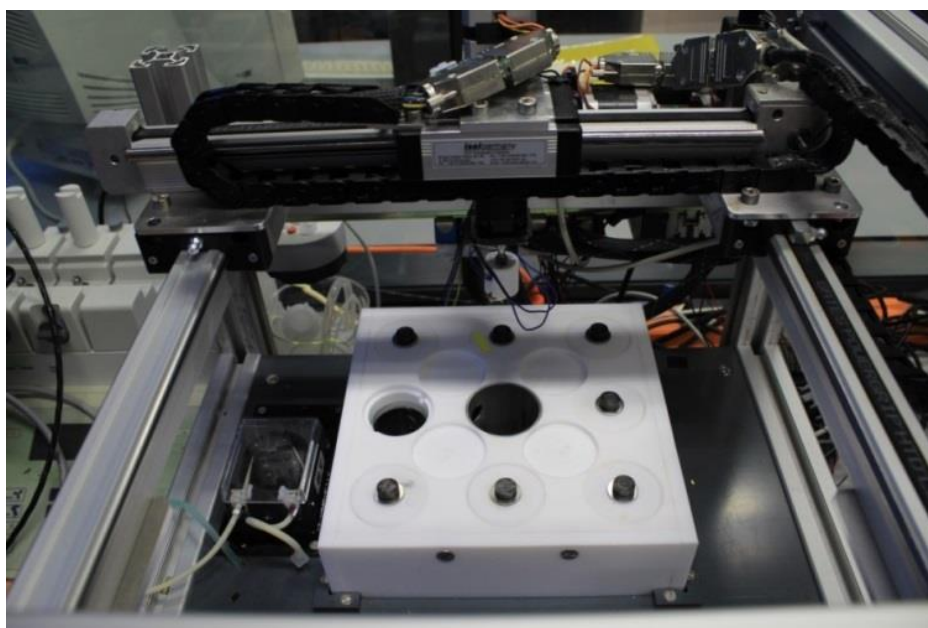
Figure 18. The setup of the dipping robot for SURMOF preparation.

1.2.5   Properties of SURMOFs

SURMOF is prepared by using LPE method, which can be resulted in oriented and homogenous thin film. The thickness of SURMOF is also can be well-controlled by the step by step fashion.

SURMOFs use SAMs as tailoring templates to control of the growth orientation. The growth

orientations of MOFs structure can be depended on location of -COOH, -OH and pyridyl groups or the density of functional groups at the surface.[51, 59] For example, the -OH groups of MUD SAMs at surface coordinate with the empty axial sites of paddlewheel copper dimer, therefore the MUD SAMs mimic the N-donor pillars and promote the [001] orientation. The -COOH groups at MHDA SAMs surface will fix the paddlewheel copper dimer and promote the [110] orientation.[60]

LPE method for SURMOF preparation is applied to control of the thickness of SURMOF thin film *via* adjusting the number of deposition cycles. The thickness of SURMOF is increased when the deposition cycle is increased.[53]

SURMOF can be prepared hetero-structures by changing the metal nodes and/or linker molecules in successive deposition cycles. For example, the case of MOF-on-MOF was prepared by employing step-by-step LPE process.[61] The $[Zn_2(ndc)_2(dabco)]$ was grown on $[Cu_2(ndc)_2(dabco)]$ to get the heteroepitaxial oriented hybrid MOF thin films (hetero-SURMOFs).

Based on the advantages of SURMOFs, SURMOFs can be applied to molecules storage and diffusion,[62-63] luminescence property[64] and biological application.[43]

1.3 Chirality

"The concept of 'chirality' has been known in chemistry since the 1870's although it would be nearly a hundred years before chemists began using this term."[65]

In simple terms, chirality is handedness, it means that the existence of left or right hand molecules, which are called "enantiomer", and the left and right hand are mirror images and can't be superimposed (*Figure 19*).
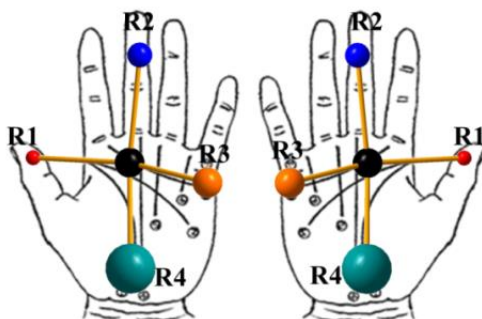
Figure 19. The model of chirality is "handedness".

In the modern pharmaceutical industry, chirality is an important concern for applications.

This interest can be attributed largely to an awareness that enantiomers of a racemic drug may have different pharmacological activities, different pharmacokinetic or pharmaceutical effects.[66-68] There are different chiral materials in the living organisms, such as amino acid, protein, DNA and RNA. Due to chirality, the living organisms can display different biological responses to different enantiomers in drugs, pesticides or waste compounds. This interacts with each chiral drug differently to give different pharmacological activity. Thus, one enantiomer may produce the desired therapeutic activities, while the other may be produced unwanted activity or inactivity. Therefore, the chiral separation is very important in the modern life. In nature, many biomolecules exist in only one of the two possible enantiomeric forms, e.g., amino acids in the L-form and sugars in the D-form.

1.3.1   Chiral SURMOFs

Surface mounted chiral metal-organic frameworks (chiral SURMOFs) are thin films of chiral MOFs grown on a substrate using LPE. The first chiral SURMOF has been prepared by Liu et al in 2011.[60] In this work, $[Zn_2(Dcam)_2(dabco)]$ (Dcam = (1R,3S)-(+)-camphoric acid, dabco = 1,4-diazabicyclo(2.2.2)octane) was prepared successfully and then the uptake of a pair of enantiomeric guest molecules, namely (2R,5R)-2,5-hexanediol (R-HDO) and (2S,5S)-2,5-hexanediol (S-HDO) was monitored by QCM. The difference of the absolute uptake for each of the chosen enantiomer was observed and it show that chiral SURMOF has significant enantioselectivity (*Figure 20*).
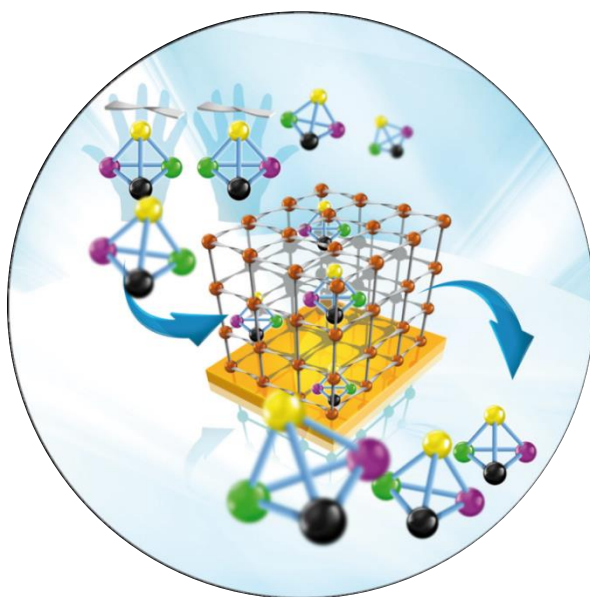
Figure 20. Enantioselectivity of chiral SURMOF. (Figure taken from ref.[60])

2 OBJECTIVES OF THESIS: CHIRAL SURMOFs AND OPTIMIZATION OF SURMOF PREPARATION

In this thesis, the major aims are preparation of surface mounted chiral metal-organic frameworks (SURMOFs) and the investigation of their enantioselectivities. These chiral SURMOFs are promising materials in the applications of enantioselective adsorption and separation. Another aim focuses on improving the SURMOF quality and optimizing the SURMOF preparation conditions by using a dipping robot.

SURMOF has been developed rapidly for several years since the first one was report in year 2007. However, synthesis and investigation of chiral SURMOF are limited currently. To date, there has only been one report about the chiral SURMOF reported in 2011. However the study of isoreticular chiral SURMOFs has not yet been reported. Therefore it's interesting to study the relationship between the enantioselectivity and the pore size in the isoreticular homochiral SURMOFs.

Oriented circular dichroism (OCD) has been observed for oriented chiral molecules and the orientated alignment of α-helical peptides reconstituted in such oriented biomembranes. However, so far there is no report about the chirality of SURMOFs. In addition, the circular dichroism (CD) is also used to characterize the chirality of MOFs, but by using CD to study the chirality of MOFs with different orientations and determine a racemic mixture of the enantiomers in MOFs has not been report. Therefore, it is important to explore the chirality of chiral SURMOF grown on different orientations since chiral SURMOFs can epitaxially grow on substrates with different orientations, as well as the CD technique is used to determine the racemic mixture of the enantiomers in chiral SURMOFs.

So far, several methods have been established to prepare the SURMOFs: pump method, spray method, *in-situ* QCM method and dipping by hand method. However the quality of the SURMOF with these methods is not enough and need to be improved. Therefore, the optimization of SURMOF preparation is important in the applications of SURMOF. In this thesis a new preparation technique: dipping robot method was introduced to get high quality SURMOF.

3 METHODS AND TECHNIQUES

3.1 X-ray diffraction (XRD)

X-ray diffraction (XRD) is an important tool for the study of crystal structures and atomic spacing. It is also used for phase identification of the crystalline materials (e.g. minerals, inorganic or organic compounds).[69]

X-ray diffractometer mainly consists of four parts: an X-ray tube, a sample holder, an X-ray detector and focusing elements (e.g. slits, etc). X-rays are generated in an X-ray tube by heating a filament to produce electrons, which are accelerated towards a metal target, i.e., Cu or Mo. When the electrons get enough energy to drive the shell electrons of the target material, part of the incident X-ray are transmitted from the crystalline material and the rest X-ray are recorded by the detector. Therefore, the characteristic X-ray spectra are produced (see *Figure 21*).
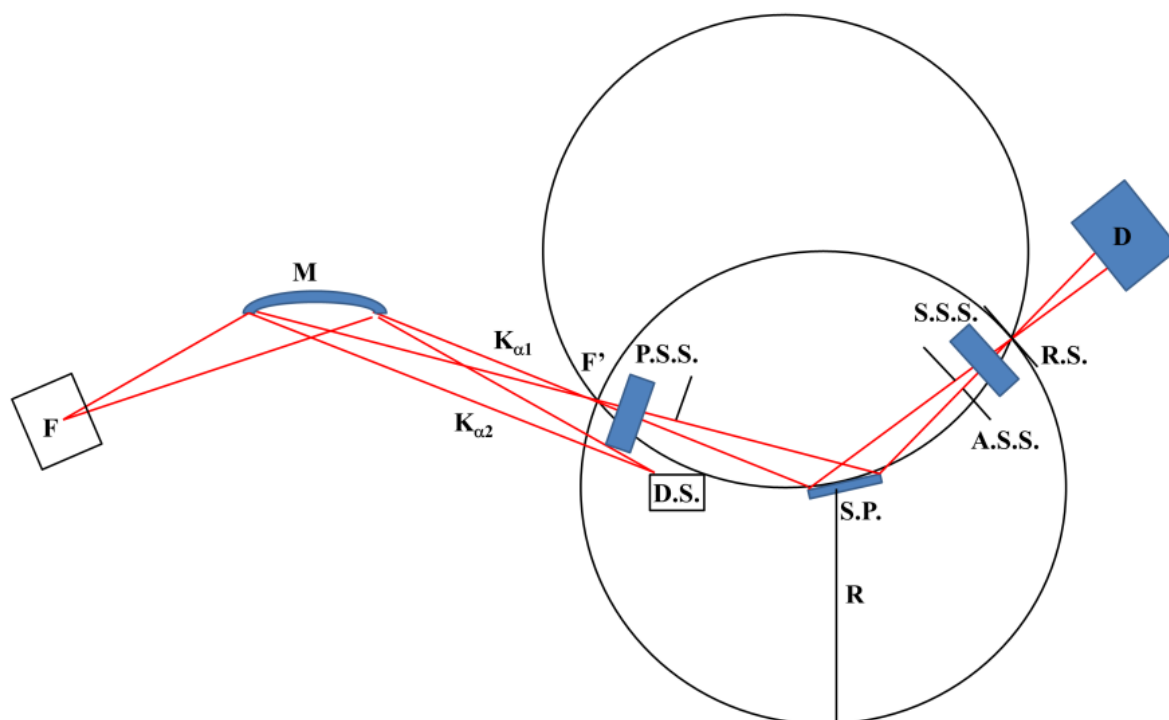
Figure 21. The schematic of modern Bragg-Brentano laboratory difrractometer in reflection geometry with bent (focusing) primary beam monochromator M, primary soller slit P.S.S., divergence slit D.S., scattering slit A.S.S., secondary soller slit S.S.S. and receiving slit R.S. (Figure adopted from ref.[70])

The X-ray spectra shows the intensity of X-ray, which is obtained by dispersion with a crystal or ruled grating. It is composed of a continuous "bremsstrahlung" spectrum on which the

characteristic X-ray spectrum is superimposed. The intensity of the "bremsstrahlung" spectra increases rapidly with the decreasing of bombarding particles mass. It can reach a significant value in the case of excitation by electrons. On the other hands, the resolution of diffraction pattern is defined by full-width at half-maximum (FWHM) of single peaks.[70]

The XRD peaks are directly related to the atomic distances. An inter-plane distance of lattice plane is given as d. The fundamental law for a peak to occur can be written as $2d\sin\theta = n\lambda$, which is known as the Bragg's law (*Figure 22*). In this equation, λ is the wavelength of the X-ray, 2θ is the scattering angle, and n is an integer of the order of the diffraction peak. For powder crystalline materials, all the possible diffraction orientations in the lattice are measured by scanning a range of 2θ angles of the sample. This law is one basic law for interpreting XRD peaks positions in crystalline materials.[71]
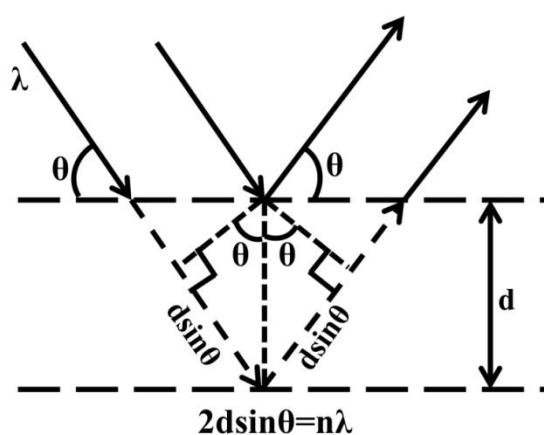
Figure 22. Description of Bragg's law: Two parallel beams with identical wavelength pass through a crystalline solid and then are scattered by two different atoms. The path of one beam is 2dsinθ longer than that of the other beam. Constructive interference occurs when the path length difference between these two waves is an integer multiple of the wavelength.

The XRD is also sensitive to crystalline thin films materials. With standard diffraction out of plane, such as the Bragg-Brentano geometry, lattice planes parallel to the sample surface are measured. For lattice planes perpendicular to the sample surface, the in-plane diffraction is used (see *Figure 23*).[72] Especially, in the crystalline and oriented SURMOFs materials, many XRD peaks are not appearing when only the out of plane XRD is carried out. Therefore the in plane XRD has to be measured for obtaining more XRD information.
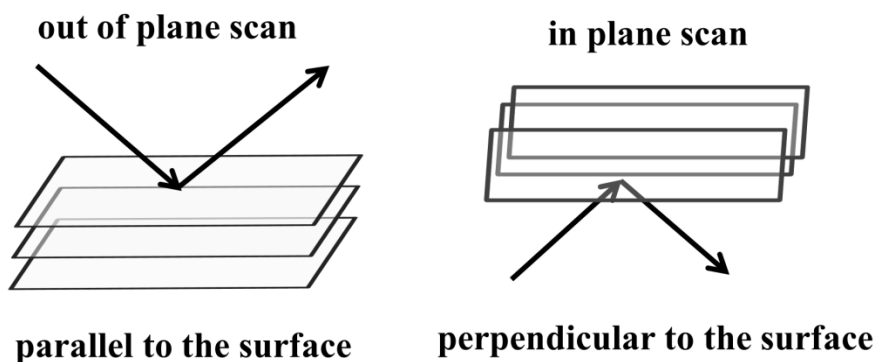
Figure 23. Two XRD diffraction modes of thin film, in-of-plane and out-plane.

In this work, out of plane was carried out with a Bruker D8 advance in θ-θ geometry equipped with a Si-strip detector (PSD Lynxeye) using Cu $K_{\alpha1,2}$ (λ = 0.15405 nm) radiation. On the tube side, a variable divergence slit was set to V12 (slit with 12 mm), and on the receiving side a 2.3° Soller slit was used.

Scans run typically from 5° to 20° (2θ with a step width of 0.025° and 6 s per step, which, due to the specific position sensitive detector (PDS) settings). Evaluation of data was done with Bruker evaluation software EVA 15.0. After background correction the peak position was calibrated by the gold (111) peak of the substrate at 38.2°. In addition, intensities of peaks are normalized by counts per second (cps).

3.2 Infrared spectroscopy (IR)

Absorption of electromagnetic energy in the infrared region causes changes in the vibration of molecules. The absorption of Infrared (IR) radiation can cause vibration of molecules. IR spectroscopy is widely used, primarily for the identification and structural analysis of inorganic and organic materials.[73-74]

A molecule can vibrate in many modes and each mode is called a vibration. Linear molecules have 3N-5 vibrational modes, while nonlinear molecules have 3N-6 vibrational modes (where N is number of atoms). For example nonlinear H_2O, has $3\times3-6$ = 3 vibrations. The number of fundamental modes includes bending and stretching vibrations (*Figure 24*).[75]
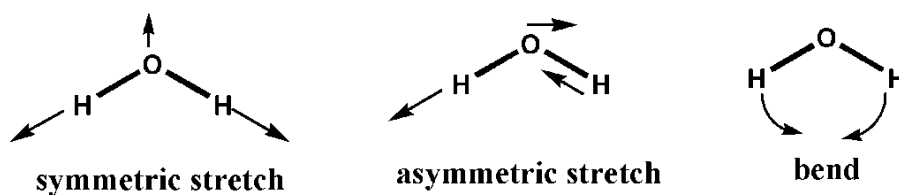
Figure 24. The important vibration types in nonlinear molecule H_2O.

Another illustration of normal vibration for methylene group (CH_2) introduces several terms. For a CH_2X_2 group (where X can represent any other atom), there are six vibrations in the CH_2 portion, including symmetric and antisymmetric stretching, scissoring, rocking, wagging and twisting as shown in *Figure 25*.
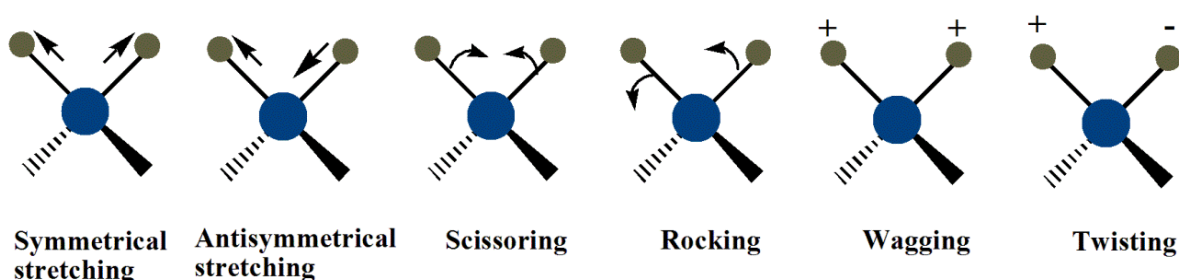
Figure 25. Six of the important vibration types in CH_2 portion in CH_2X_2 group.

For surface chemical compositional analysis, infrared reflection-absorption spectroscopy (IRRAS) can be applied. The gold substrate for the SAMs permits the use of reflectance methods, because of there is high reflectivity of IR light from the gold surface.[76] When the IR light induces vibrational transitions in the molecular bonds, the information such as identification of chemical environment, structure and functional group can be elucidated by measuring the frequency and intensity of the absorbed IR light. The photons interact with the surface molecules and then reflect from the gold substrate, where they are focused on the detector through another series of mirrors.[76]
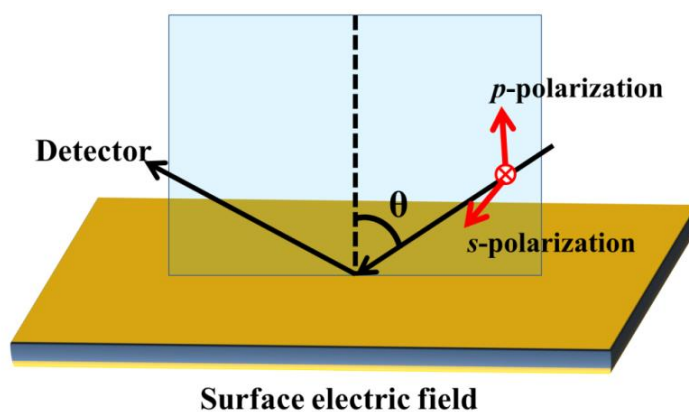
Figure 26. Principle of infrared reflection-absorption spectroscopy (IRRAS).

The polarized light is used for interpreting the vibrations of molecule on the surface. Linear polarized light can be separated into two different components: *s*- and *p*-polarized light (*Figure 26*). The *s*- polarized light is parallel to the surface and perpendicular to the plane of incidence, while the *p*-polarized is parallel to the plane of incidence. When the *s*-polarized light is reflected at the surface, it undergoes a 180° phase shift that results in a nearly total cancellation of the amplitude at the surface. The *p*-polarized light undergoes a 90° phase shift that results in amplitude addition. Installing a polarizer into the infrared beam path allows one to select only the *p*-polarized light. This results in a significant increase of the signal-to-noise ratio. Therefore, *p*-polarized light is used to take advantage of the surface selection rule.[77-78] This rule states that only absorption modes that have a component of vibration perpendicular to the surface will be excited. Modes that are completely parallel to the surface normally do not interact with *p*-polarized light. Therefore IRRAS can provide information on orientation of adsorbates in this case.

The SURMOFs were characterized with IRRAS. IRRAS data were recorded using a FTIR spectrometer (Bruker VERTEX 80) in this thesis. With a resolution of 2 cm^{-1} at an incidence angle of 80° relative to the surface normal is used. Liquid nitrogen is used for cooling the mercury cadmium telluride (MCT) narrow band (4000-400cm^{-1}) detector. Perdeuterated hexadecanethiol SAMs on Au substrate was used as reference for SURMOF grown on SAMs Au substrate. The quartz glass was used for the background of SURMOF grown on functionalized quartz glass. In both case 1024 scans were accumulated for the reference measurement. Dry air was purged continuously through the spectrometer and the sample compartment, which reduces the possibility of atmospheric water or CO_2 contamination of the spectra and samples. Samples were measured as long as the water absorption bands from ambient air disappeared (900-1300 scans). The data were processed using Bruker OPUS® software version 7.2.

3.3 Quartz crystal microbalance (QCM)

A quartz crystal microbalance (QCM) is an instrument that can monitor slight mass changes by measuring the resonance frequency change of the QCM sensor. The QCM with dissipation monitoring (QCM-D) is a special QCM, which is used in interfacial acoustic sensing. A common application is the determination of a film thickness in a liquid environment, such as the thickness measurement of a deposited protein film.

The application of an alternating potential to the crystal surface causes the crystal to oscillate.

When the thickness of the crystal (d_q) is double of the acoustical wavelength, a standing wave can be established where the inverse frequency of the applied potential during the period of the standing wave. This frequency is called a resonant frequency (f_0), and can be calculated the equation (1) and (2):

$$f_0 = \sqrt{\frac{\mu_q}{\rho_q}} / 2d_q \qquad (1),$$

$$\Delta f_n = -2n f_F^2 \frac{M_f}{v\rho_q} \qquad (2),$$

where d_q is the thickness of crystal, ρ_q is the density of crystal, μ_q is the ratio of sheer stress to shear strain and. n denotes the overtone order f_F is the frequency of the fundamental, v is the speed of sound. Given that f_F, ρ_q, and v are constants, one may write:

$$\Delta f_n = -nC\Delta M_f \qquad (3).$$

M_f is the mass of crystal, C the mass sensitivity constant is referred to the equation[62, 79]:

where the resonance frequency and dissipation are f_n and D_n and the bandwidth is Γ_n, $\omega_F = 2\pi f_F$ is the angular fundamental resonance frequency as shown in *Figure 27*.
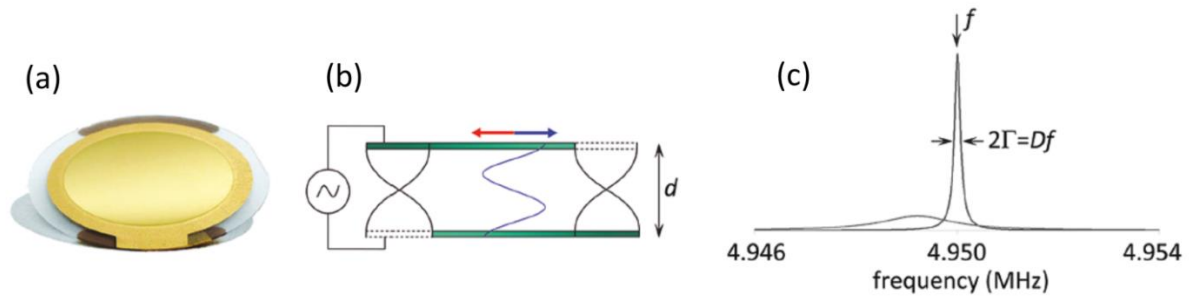
Figure 27. Schematics of QCM-D operation; (a) A photograph of a 4.95 MHz AT-cut quartz crystal (Q-Sense); (b) Side view of the crystal; (c) Resonances observed when a crystal is in air (blue) or liquid (red). Typical spectra obtained with impedance analysis. The excitation frequency is plotted on the x-axis. The y-axis represents the amplitude of the current passing through the crystal. Two parameters are used to characterize the resonance: frequency f and band width Γ. (Figures taken from ref.[79])

The experiments were carried out by using the automated QCM-D instrument Q-Sense E4 in this work. The QCM-D can be used in gas phase or liquid environments for monitoring the resonance frequency changes on the electrode thin film. A decrease of the resonance frequency is due to the increase of the mass on QCM sensor according to equ. (3). Typical QCM sensor has a gold electrode on the upper side where materials can be deposited on the surface (*Figure 27a*). The setup of gas phase QCM is schematically depicted in *Figure 28*, which includes mass flow controllers for controlling the flow rate of the carrier gas (e.g. Ar or N$_2$) and analyte storage container. The carrier gas is dosed by the gas flow controller into a

glass evaporator. The analyte vapour in the storage container is mixed with the carrier gas and then the mixture enters the sample in the QCM. In this case, the analyte will be loaded and then the mass of the QCM sensor will be increased. This increased mass lead to the frequency changes (Δf). When start the gas phase QCM experiment, the system is activated by the carrier gas at 65 °C for 20 h. The system is flushed with carrier gas at the setting temperature for about 10 min, which establish the baseline for the loading experiment. When the frequency is stable, the loading experiment is started by admitting analyte molecules to the storage container. From the recorded different frequencies, the mass of molecular loading is calculated. Furthermore, there is a pump for the flow rate of the solutions in the liquid QCM. When the liquid QCM experiment is started, the system is flushed the solvent for the baseline at the setting temperature. When the frequency is stable, which is used for the baseline, the experiment can be started for MOF growth or liquid loading. Then the mass changes can be observed from the frequency changes.
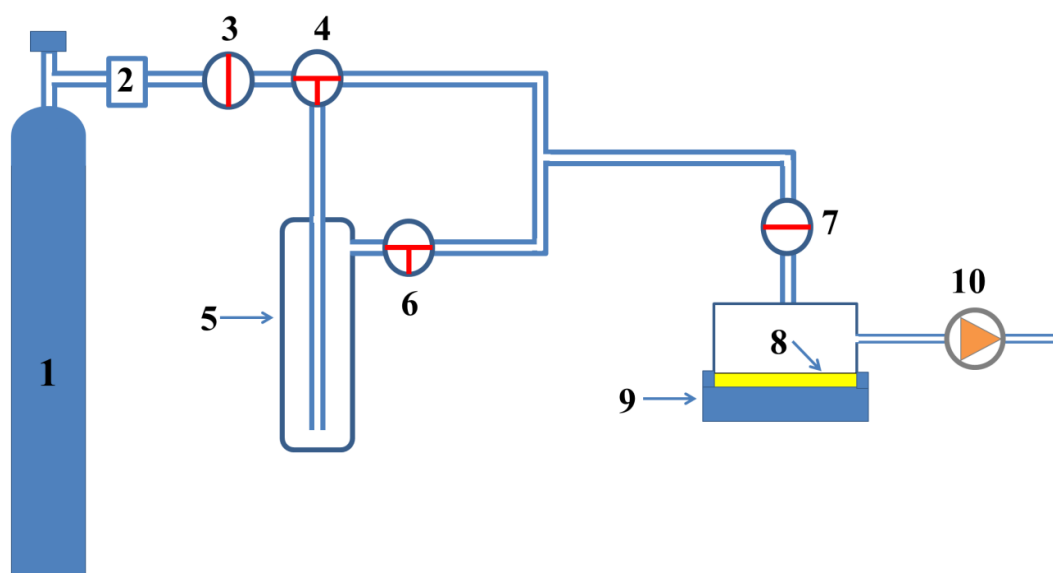
Figure 28. Setup employed for the sorption measurements: (1) gas (Ar or N₂) supply, (2) gas flow controller (FMD PR4000), (3) main valve, (4) three-way valve, (5) storage container with the loading substance, (6.7) outlet valves, (8) QCM sensor, (9) sample holder with electric feed through, (10) liquid pump.

3.4 Scanning electron microscopy (SEM)

Scanning electron microscopy (SEM) is a powerful technique in the examination of materials and it is used widely in detecting the information about the surface morphology and to some extent, the composition of the sample. High magnification images with a good depth of field

can be obtained and other features, such as individual crystals can also be analyzed. In a typical SEM, the main components are: electron column, scanning system, detector, vacuum system and electronics control as shown in *Figure 29*.
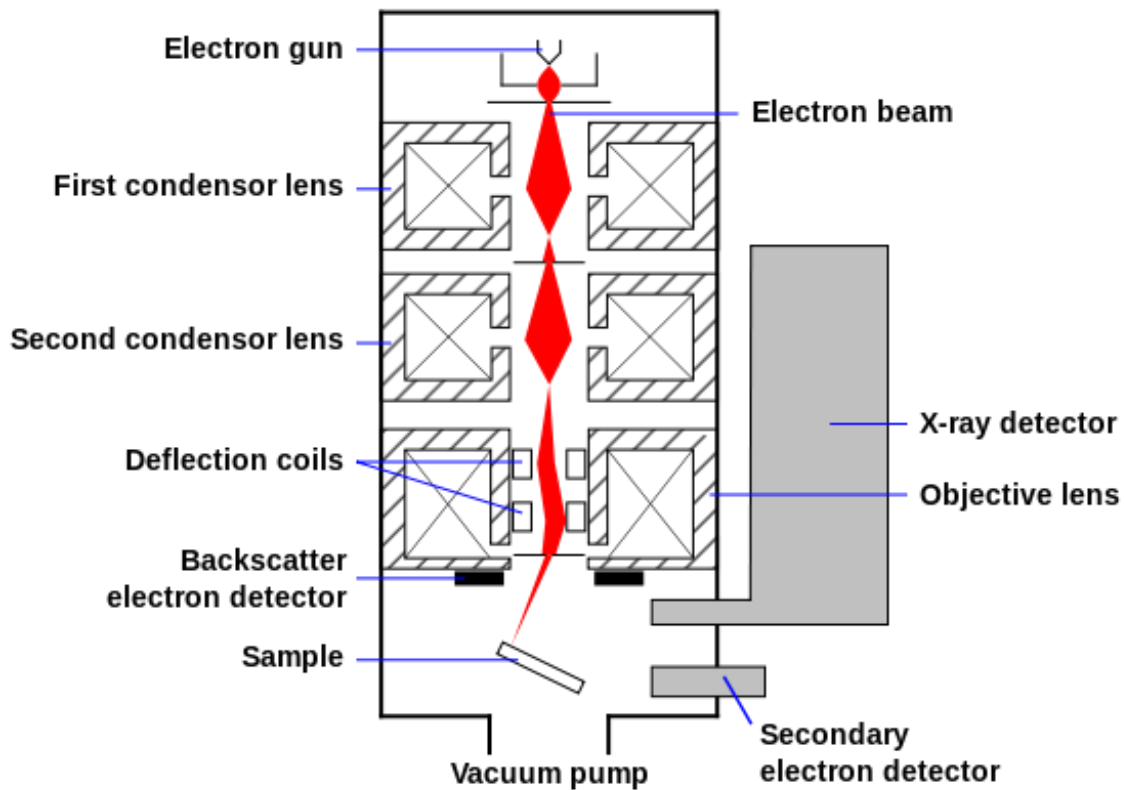
Figure 29. Schematic of an scanning electron microscopy (SEM). *(Figure taken from ref.[80])*

The electron column of the SEM consists of an electron gun and two or more electromagnetic lenses operating in vacuum. The electron beam is focused by one or two condenser lenses to a spot about 0.4 nm to 5 nm in diameter, which typically has an energy ranging from 0.2 keV up to 40 keV. The electron beam passes through pairs of deflector plates or scanning coils in the electron column, and then the final lens turn the beam to scan a rectangular area of the sample surface in a raster fashion.[81]

In this work, the morphology measurements are carried out in a FEI Philips XL 30 Field Emission Gun Environmental Scanning Electron Microscope (FEG-ESEM). To avoid charging, insulating materials have to be coated with a thin Gold/Palladium film. Then the specimen can be imaged under high vacuum conditions (10^{-5} Pa) using acceleration voltages between 5 and 20 kV.

3.5 Atomic force microscopy (AFM)

The atomic force microscopy (AFM) is a surface sensitive technique and has become a fundamental tool for nanotechnology in the field of nanomaterials and biochemistry, mainly in the surface morphology characterization with nanometric resolution. This means surface characteristics can be analyzed with very accurate resolution ranging from 100 μm to less than 1 nm. The AFM consists of a laser, a probe, a piezoelectric scanner and a detector. The MFP-3D-BIO-AFM was used for morphology (roughness and height) studies because this AFM provides high resolution images and accurate force measurement in air. There are two operating modes: contact mode and alternate current mode (AC mode, also named tapping mode) in MFP-3D-BIO-AFM.

The cantilever represents the probe with a sharp tip attached at one end, which is used to scan the samples surface. The cantilever (NSC-18) with resonant frequency of 75 kHz and spring constant of 3.5 N/m, is used in this thesis, which is typically made of silicon with a tip radius of nanometers (<10 nm). The cantilever displacement is important for reaching the good resolution of AFM images for an accurate measurement. Usually AFM are performed in AC mode, in which the cantilever vibrates near the natural resonant frequency of the cantilever, at relatively high amplitudes, and it is controlled with feedback loop on the amplitude channel. The advantage of AC mode is that, no lateral friction force is applied to the sample surface, which in turn, causes no damage on sample during the measurement.

The piezoelectric scanner is polycrystalline solid, and in this case, a X-Y piezo is used to move the sample in *x*- and *y*-axis, and a Z-piezo move the cantilever in *z*-axis (vertically) in AC mode.

The detector in AFM consists of a quadrilateral photodiode, which is used to receive the reflected laser beam. This laser beam tracks the sample surface as it is reflected up and down (from the back of the cantilever) due to a change in the normal force between the surface and the cantilever.

The principle of operation of the AFM is explained in *Figure 30*. The sample is placed on top of a scanner which is responsible to move the sample in X-Y directions. When the laser reaches to the back of the cantilever and then is reflected to a four-segment photodiode, the cantilever is shaken at its resonant frequency by a small Z-piezo in the cantilever holder. If the oscillation of the cantilever throughout the changes of topography causes a deflection signal, the laser hits the photodiode in the upper or lower field registering a difference in voltage. The signal can be simultaneously plotted by the PC program and a 3D representation

of the surface can be formed.
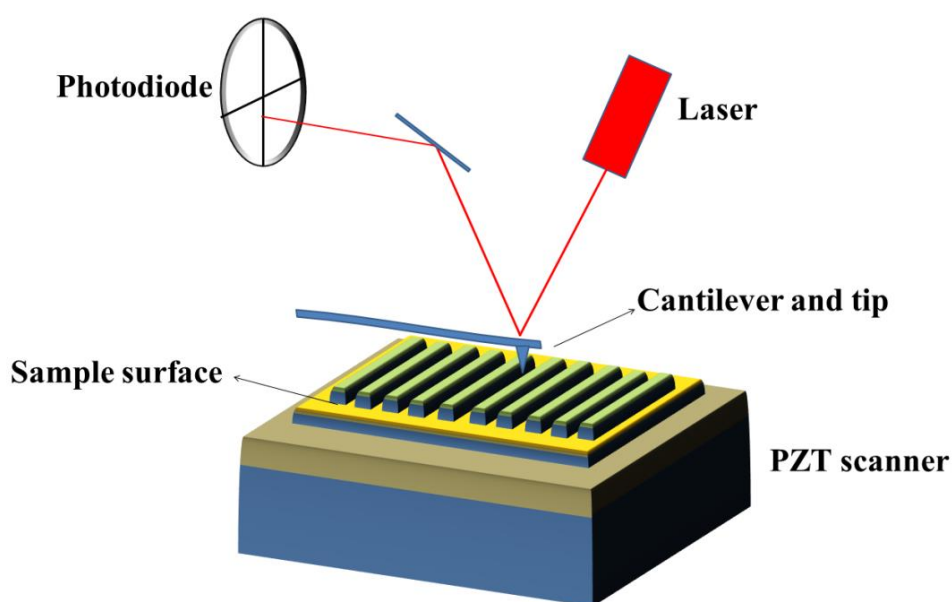
Figure 30.The instrument of atomic force microscopy (AFM).

3.6 Circular dichroism (CD) spectroscopy

Based on the differential absorption of right and left circularly polarized light in an optically active chiral medium, the circular dichroism (CD) spectroscopy is a widely useful technique to determine a chiral substance. CD spectra with 180-800 nm wavelengths can be analyzed for the different chiral compounds: organic molecules, metal complexes, protein and DNA, which is the optical signal and chirality information.[82] A number of excellent review articles report the technique and its application.[83-84] The principle behind CD spectroscopy is shown in *Figure 31*. The light (UV) passes through a photo elastic modulator (PEM) which can convert the linear polarized light into alternating left- and right-handed polarized light and they are perpendicular to each other. The two polarizations are differently absorbed when the beam passes the optically active sample. The difference in absorption is detected with a photo multiplier tube (PMT).

As a species of absorption spectroscopy, CD spectra are particularly powerful in monitoring conformational change of chiral substance and provide structural, kinetic and thermodynamic information about chiral medium. Currently, CD spectroscopy is mainly good for the determination and study of protein or peptides, such as: (a) determining whether a protein is folded, and if so, characterizing its secondary, tertiary structure or the structural family to which it belongs;[85-86] (b) comparing the structures of a protein obtained from different

sources (e.g. species or expression systems);[87-88] (c) studying the conformational stability of a protein under stress, thermal stability, pH stability or stability to denaturants.[89-91]
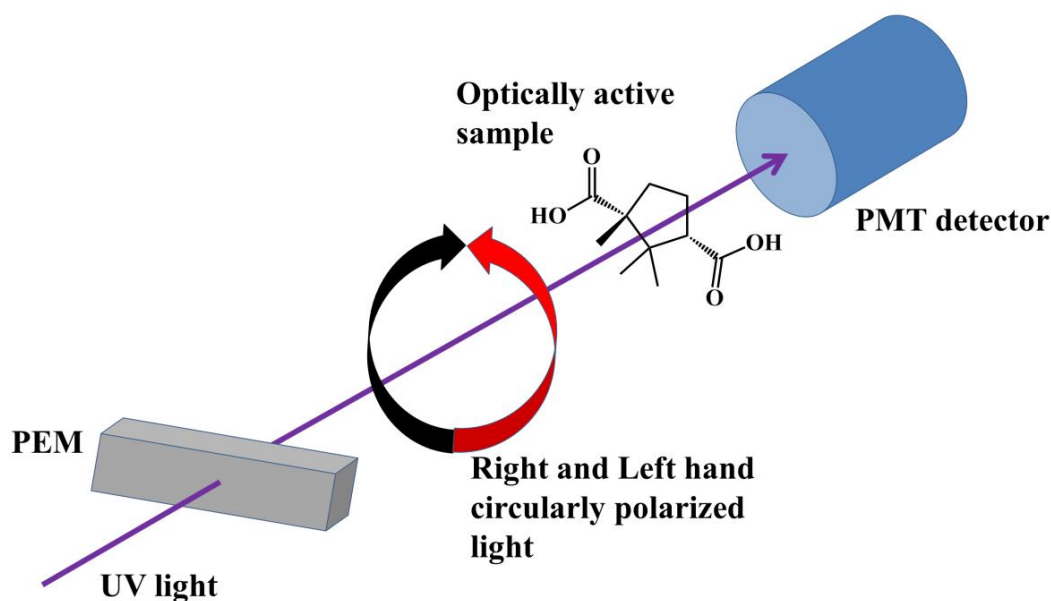
Figure 31. The principle of circular dichroism (CD) spectroscopy.

When circularly polarized light passes through an optically active medium, the speeds c of right circularly polarized light (R-CPL) and of left circularly polarized light (L-CPL) differ ($c_{\text{R-CPL}} \neq c_{\text{L-CPL}}$) as well as the extent to which they are absorbed ($\varepsilon_{\text{R-CPL}} \neq \varepsilon_{\text{L-CPL}}$). This effect, $\varepsilon_{\text{R-CPL}} \neq \varepsilon_{\text{L-CPL}}$, is called CD and the differential absorbance ($\Delta\varepsilon$) of right and left circularly polarized light is plotted against the wavelength λ to yield the CD spectrum. Usually the absorbance difference (ΔA), it is the difference between absorbance of R-CPL and L-CPL, is recorded by CD spectrometer. The ΔA is described by equ (4),

$$\Delta A(\lambda) = A(\lambda)_{\text{L-CPL}} - A(\lambda)_{\text{R-CPL}} \qquad (4),^{[92]}$$

where λ is the wavelength, $A(\lambda)_{\text{R-CPL}}$ is the absorbance of right circularly polarized light and $A(\lambda)_{\text{L-CPL}}$ is the absorbance of left circularly polarized light. Taking cell path length and compound concentration into account, a molar circular dichroism ($\Delta\varepsilon$) can be derived. Based on Beer's law, the equation can be expressed as equ. (5):

$$\Delta\varepsilon = \varepsilon_{\text{L-CPL}} - \varepsilon_{\text{R-CPL}} = \Delta A/(C \times l) \qquad (5),^{[93]}$$

where $\varepsilon_{\text{L-CPL}}$ and $\varepsilon_{\text{R-CPL}}$ are the molar extinction coefficients for L-CPL and R-CPL respectively, C is the molar concentration of the chiral substance, and l is the path length in centimeters.

In this work the CD and OCD experiments were recorded with a Jasco J-810 spectropolarimeter at room temperature. The spectra recorded for the pure quartz glass plate

(which was also used as the substrate for SURMOF thin film preparation) were used as a reference. Spectra were recorded from 350 to 180 nm in 0.1 nm steps using a 20 nm min^{-1} scan speed, an 8 s response time and a spectral bandwidth of 1 nm. The quartz glass plates were fixed perpendicular to the incident light beam on a rotation stage with a computer-controlled stepping motor. To reduce artefacts due to linear dichroism or birefringence arising from imperfections in the sample (slight vertical misalignment of the substrates, strain in the quartz glass windows) spectra were recorded every 45.0° of rotation of the sample at eight angles (0°, 45°, 90°, 135°, 180°, 225°, 270° and 315°) and averaged. Afterwards, the reference spectra recorded for the quartz glass plates were subtracted for background correction.

4 EXPERIMENTAL RESULTS AND DISCUSSIONS: CHIRAL SURMOFS

4.1 Used chemicals

The names, abbreviations and structures of chemicals which are used in this work are listed in *Table 1*.

Table 1. Names, abbreviations and structures of the chemicals.

names and abbreviations	structural formulas
self-assembled monolayers (SAMs)	
perdeuterated hexadecanethiol	
11-mercapto-1-undecanol (MUD)	
16-mercaptohexadecanoic acid (MHDA)	
11-(triethoxysilyl)undecanal (TESU)	
1-decanethiol	
organic ligands	
(1R,3S)-(+)-camphoric acid (Dcam)	
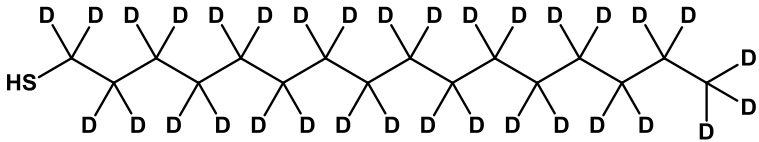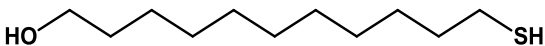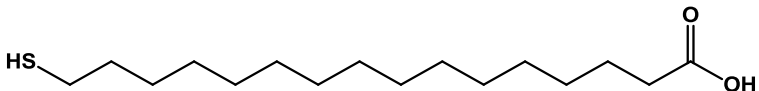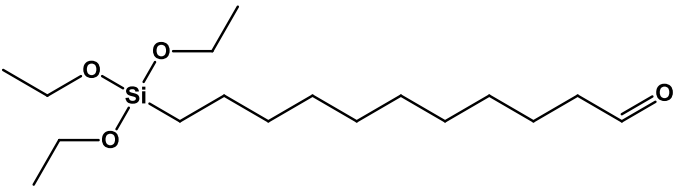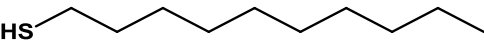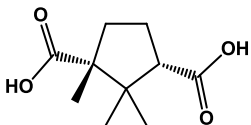
(1S,3R)-(-)-camphoric acid (Lcam)	
1,3,5-benzenetricarboxylic acid (H$_3$btc)	
terephthalic acid (H$_2$bdc)	
pillar linkers	
diazabicyclo[2.2.2]-octane (dabco)	
4,4'-bipyridyl (bipy)	
1,4-bis(4-pyridyl)benzene (bipyb)	
guest molecules	
(+)-Ethyl-D-lactate	
(-)-Ethyl-L-lactate	
R-(+)-Limonene	
S-(-)-Limonene	
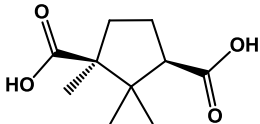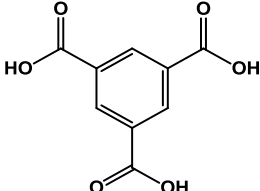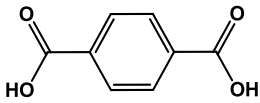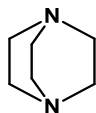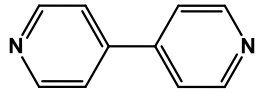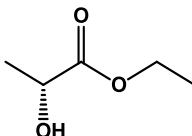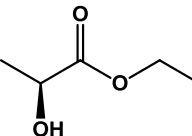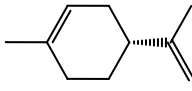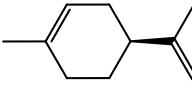
inorganic substance	
copper acetate (Cu(OAc)$_2$)	Cu(CH$_3$COO)$_2$·2H$_2$O
potassium permanganate (KMnO$_4$)	KMnO$_4$
sulfuric acid (98%)	H$_2$SO$_4$
hydrogen peroxide (30%)	H$_2$O$_2$
solvents	
ethanol (99.99%) (EtOH)	CH$_3$CH$_2$OH
deionized water (H$_2$O)	H$_2$O
toluene	(C$_7$H$_8$)
supplied gas	
nitrogen (99.9999%)	N$_2$
argon (99.9999%)	Ar
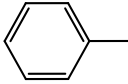
4.2   Isoreticular Homochiral SURMOFs with Tunable Pore Sizes

Since the first synthesis of homochiral MOFs in 1999,[94] the research field has rapidly developed.[38, 95] So far, many different chiral MOFs have been synthesized and the enantioselectivity has been studied.[96-98] So far, there has only been one report about the chiral SURMOF reported in 2011. However, a systematic study of isostructural homochiral SURMOFs have not been done and this is very important for understanding the enantioselectivity of chiral MOFs.

Here, we systematically investigate the influence of the pore size of isoreticular homochiral MOFs, i.e. of MOFs with the same topology and identical chiral centers but with tunable pore sizes, on the enantiomer separation. For this purpose, the enantioselectivity of the adsorption capacity of chiral probe molecules, R- and S-Limonene, by the isoreticular MOFs is studied. This means a series of homochiral, pillared-layer MOFs $[Cu_2(Dcam)_2(L)]$ (Dcam = (1R,3S)-(+)-camphoric acid)were prepared with identical chiral layer [Cu(Dcam)] and different pillar-linker L: diazabicyclo[2.2.2]-octane (dabco), 4,4′-bipyridine (bipy) and 1,4-bis(4-pyridyl)benzene (bipyb). The N-donor ligands (dabco, bipy and bipyb) are coordinated to the axial centers of the copper complexes forming pillars, which are perpendicular to the chiral $[Cu_2(Dcam)_2]$ layers. This results in isoreticular homochiral MOF with identical chiral centers and different pore sizes. The lattice distances are 0.95 nm in [100] and [110] direction and 0.95 nm, 1.4 nm and 1.8 nm in [001] direction for the $[Cu_2(Dcam)_2(dabco)]$, $[Cu_2(Dcam)_2(bipy)]$ and $[Cu_2(Dcam)_2(bipyb)]$, respectively (*Figure 32*).
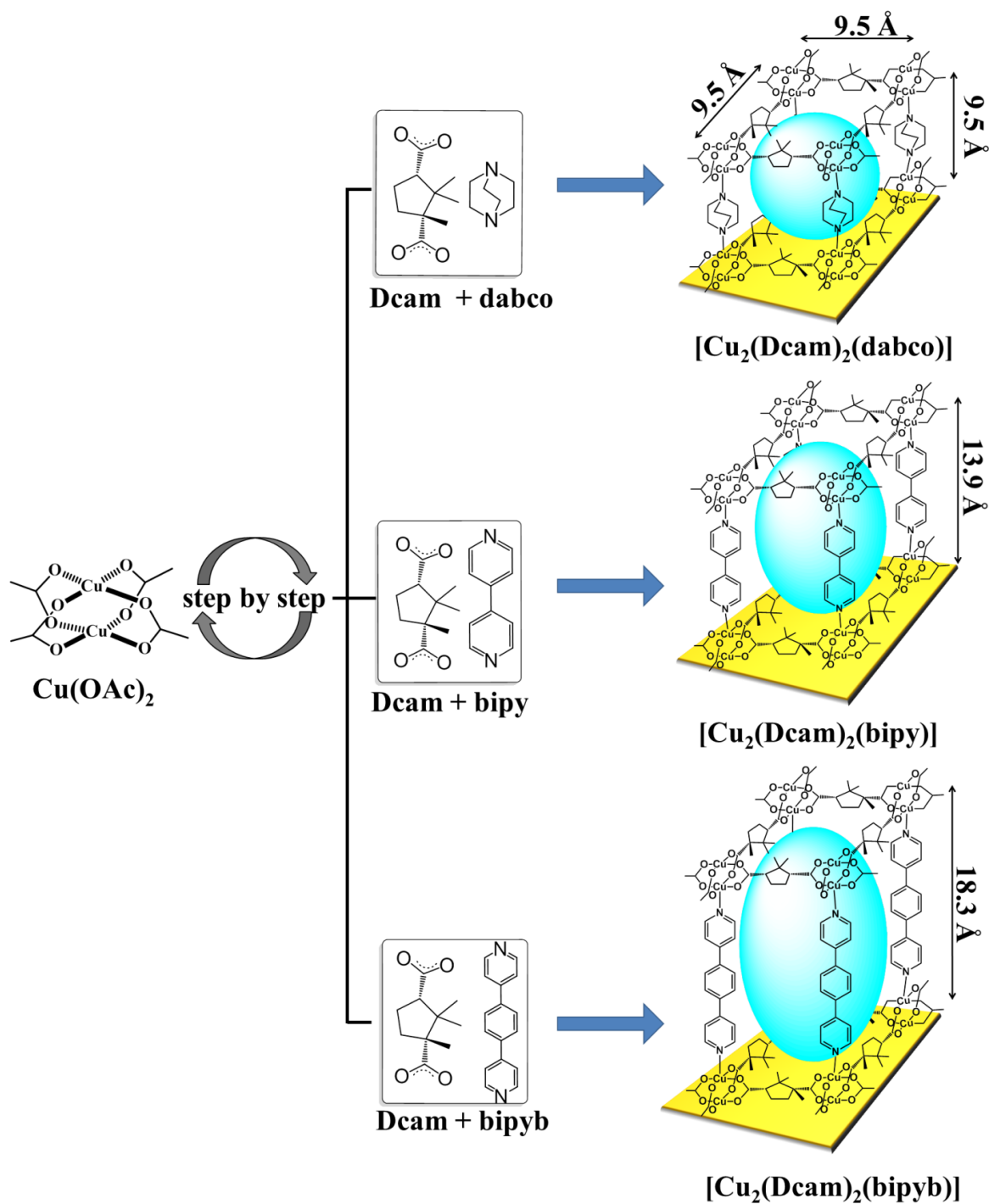
Figure 32. Isoreticular homochiral SURMOF [Cu₂(Dcam)₂(L)] with tunable pore sizes (L= dabco, bipy and bipyb).

4.2.1 Sample synthesis

Preparation of MUD SAMs

The preparation of self-assembled MUD substrate has been described in detail chapter 1.2.3.

Briefly, a polycrystalline Au film on Si wafer or QCM sensor were used. The substrate was immersed into a 1 mM MUD ethanolic solution for about 24 h. All the samples are rinsed with pure ethanol and dried under nitrogen flux before the preparation of SURMOF.

Preparation of SURMOFs

The [$Cu_2(Dcam)_2(L)$] SURMOF grown on MUD SAMs or functionalized quartz glass substrate are prepared using LPE approach with automatic pump system (L = dabco, bipy or bipyb). The substrates were immersed into 1 mM $Cu(OAc)_2$ ethanolic solution for 15 min. This first immersion is an important step and the growth orientation is dependent by the function group of the substrate (*Figure 33*). When the -OH functionalized group MUD SAMs substrate is used for SURMOF preparation, -OH groups at MUD SAMs has surface coordinate with the empty axial sites of paddlewheel $Cu(OAc)_2$, therefore the MUD SAMs mimic the pillar linkers (dabco, bipy and bipyb) and promote the [001] orientation. After 2 min rinsing with ethanol, the sample then was immersed subsequently into a 0.2 mM equimolar ethanolic solution of H_2Dcam/L mixture for 30 min at 50 $^{\circ}$C. The chiral ligands Dcam coordinate to Cu ions and to form the [$Cu_2(Dcam)_2$] chiral layers and the N-donor pillar linkers are perpendicular to chiral layers. The samples were rinsed with ethanol for 2 min. The procedure was repeated 50 cycles to obtain a 50 cycles [$Cu_2(Dcam)_2(L)$] SURMOF.
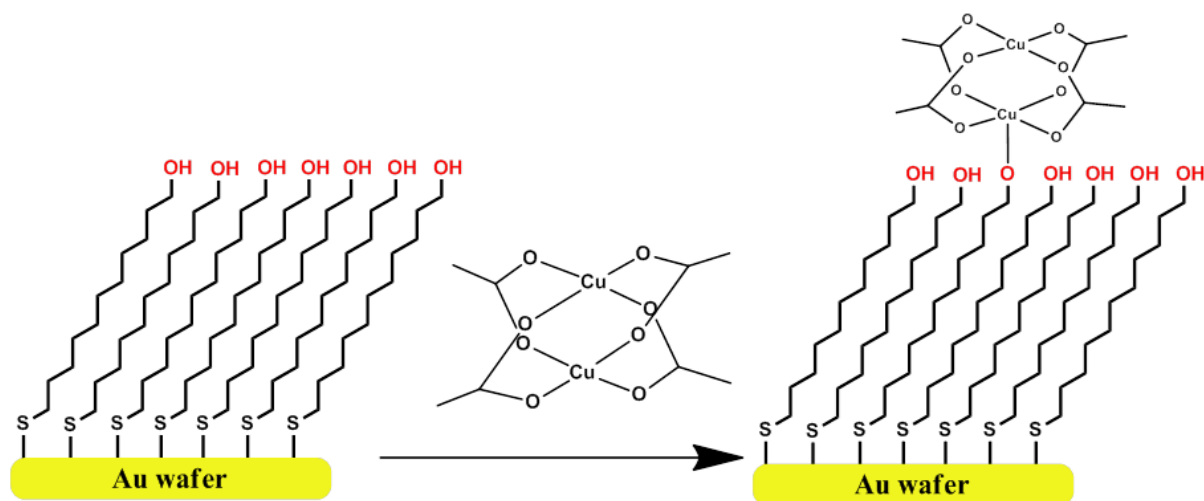
Figure 33. Growth mechanism of Cu(OAc)$_2$ in the first step of [Cu$_2$(Dcam)$_2$(L)] on MUD SAM (L = dabco, bipy or bipyb).

In order to monitor the SURMOF growth, typical experiments were also carried out by using *in-situ* QCM method to prepare the SURMOF on the QCM sensor.

4.2.2　Characterization

The out of plane and in plane XRD experiments were carried out using Cu $K_{\alpha1,2}$ (λ = 1.5405 Å) radiation in this work. This out of plane diffraction scan clearly demonstrates the presence of a highly ordered crystalline material.

Figure 34a shows that there are two reflexes at 9.3° and 18.4° correspond the (001) and (002) peaks in out-plane XRD of $[Cu_2(Dcam)_2(dabco)]$, respectively, which is accord with the calculated powder XRD well and display there are high oriented MOF thin film. The XRD peaks from in-plane shows (001), (200), (210), (002) and (310) that correspond with calculated data of $[Cu_2(Dcam)_2(dabco)]$.
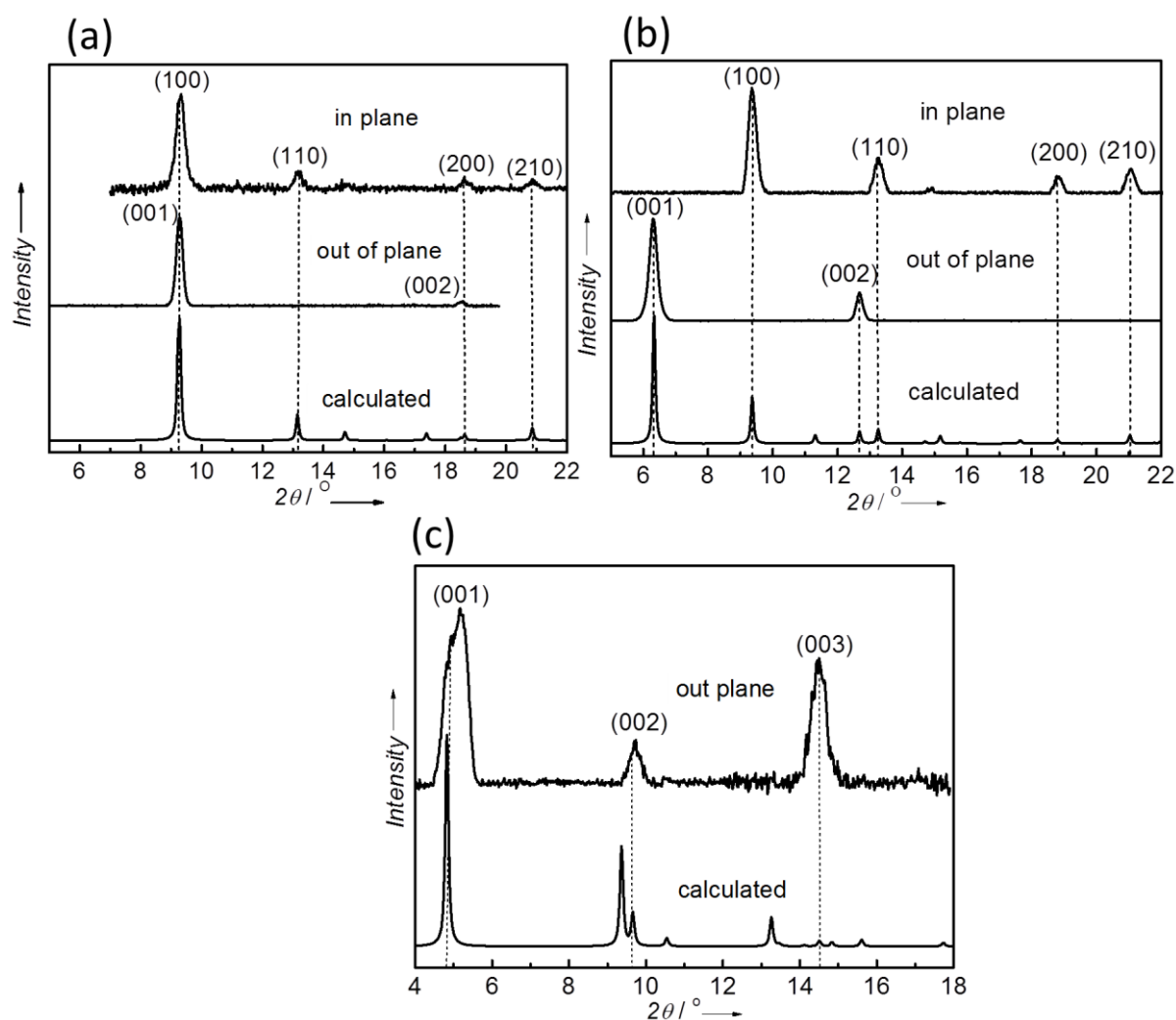
Figure 34. The XRD data of (a) $[Cu_2(Dcam)_2(dabco)]$; (b) $[Cu_2(Dcam)_2(bipy)]$ and (c) $[Cu_2(Dcam)_2(bipyb)]$ on MUD SAMs.

$[Cu_2(Dcam)_2(bipy)]$ thin film was nicely grown along [001] orientation as shown in *Figure 34b*. Two strong diffraction peaks at 6.3° and at 12.7° correspond the (001) and (002) planes,

respectively, which are in accordance with the diffraction peaks at (001) and (002) in simulated powder [Cu$_2$(Dcam)$_2$(bipy)] diffraction patterns. The out of plane XRD clearly demonstrates the SURMOF [Cu$_2$(Dcam)$_2$(bipy)] grown along [001] direction, the bipy pillars are perpendicular to the substrate. The in-plane data of [Cu$_2$(Dcam)$_2$(bipy)] on MUD SAMs show (110), (100), (110) and (310) diffraction peaks, which fit well to the bulk [Cu$_2$(Dcam)$_2$(bipy)] diffraction patterns.

The out of plane XRD shows that three diffraction peaks at 4.8º, 9.7º and at 14.5º correspond the (001), (002) and (003) peaks in simulated powder [Cu$_2$(Dcam)$_2$(bipyb)] diffraction patterns, respectively. It shows that the SURMOF [Cu$_2$(Dcam)$_2$(bipyb)] thin film was grown along [001] orientation, as shown in *Figure 34c*. Due to the linker length of bipyb, the growth of SURMOF [Cu$_2$(Dcam)$_2$(bipyb)] is significantly more difficult, which hinder the in plane XRD measurement.
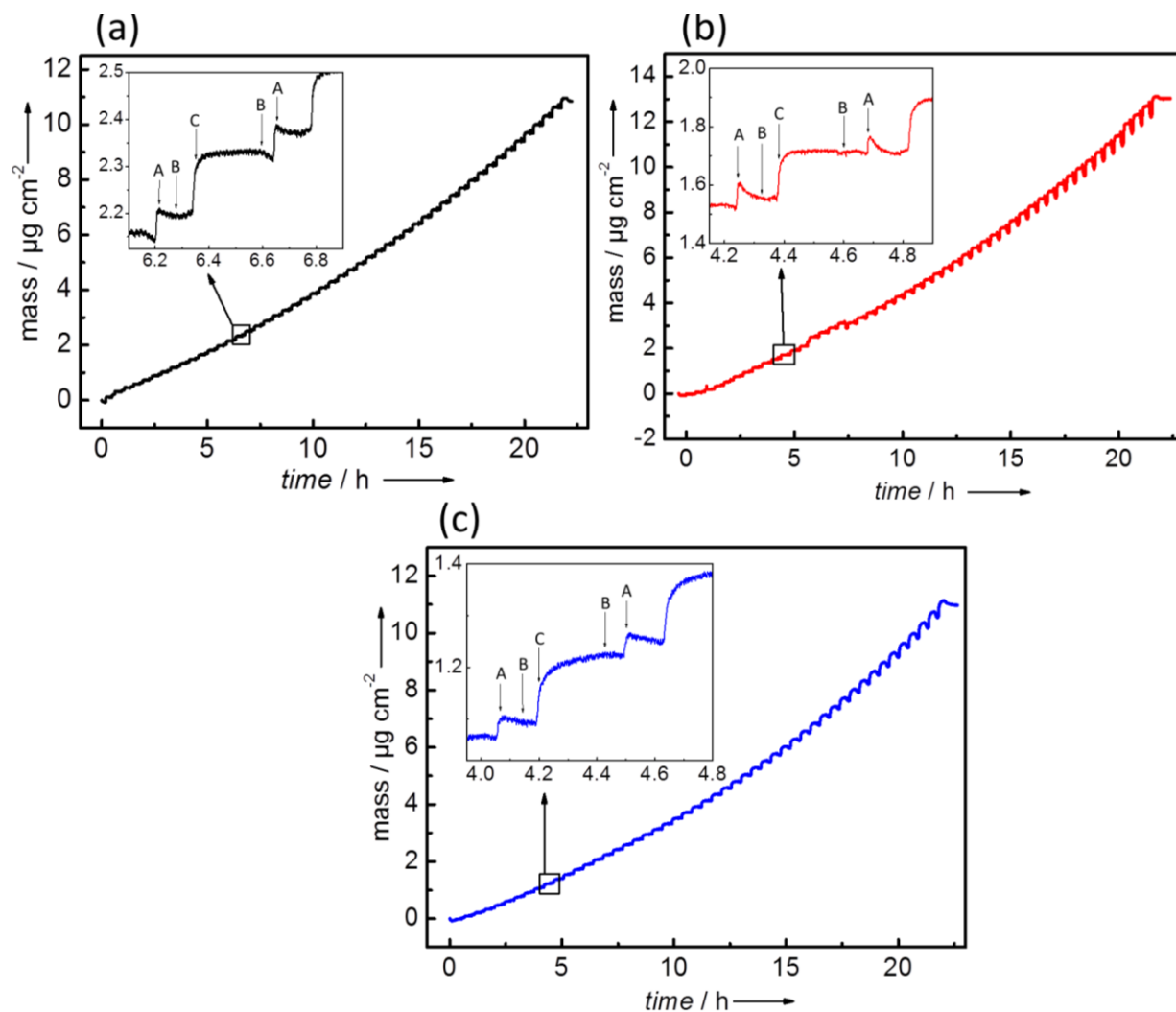
Figure 35. The step by step syntheses of the isoreticular homochiral SURMOFs; (a) [Cu$_2$(Dcam)$_2$(dabco)]; (b) [Cu$_2$(Dcam)$_2$(bipy)] and (c) [Cu$_2$(Dcam)$_2$(bipyb)] monitored in-situ by QCM. (A: Cu(OA)$_2$); B: ethanol; C: Dcam/L linkers).

The isoreticular homochiral SURMOFs were grown on gold-coated quartz crystal microbalance (QCM) sensors functionalized with MUD SAMs, resulting in a [001] crystal orientation of the SURMOF. The samples were synthesized *in-situ* in the QCM flow cell by pumping subsequently the ethanolic solution of 1 mM $Cu(OAC)_2$ and 0.2 mM equimolar H_2Dcam and L (L = dabco, bipy or bipyb) through the QCM cell. In between, the sample was purged with ethanol to remove unreacted, weakly absorbed reactants. In this way, the SURMOFs were synthesized in a step by step fashion in the QCM flow cell and the mass increases during the syntheses were monitored *in situ*, see *Figure 35*. The SURMOF masses were determined to 10.84 μgcm^{-2}, 13.04 μgcm^{-2} and 10.97 μgcm^{-2}, respectively.
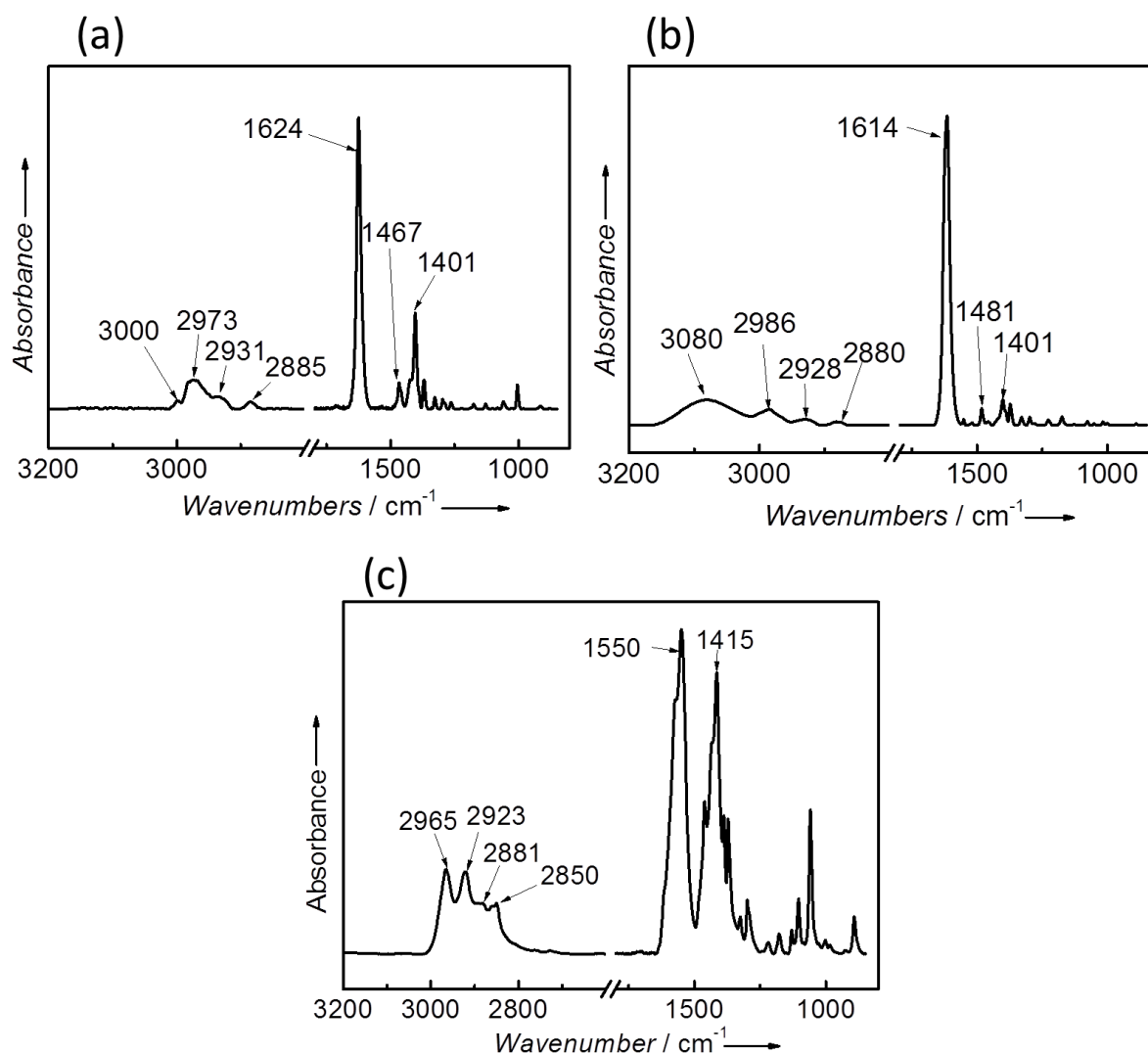
Figure 36. The IRRAS data of (a) [Cu₂(Dcam)₂(dabco)]; (b) [Cu₂(Dcam)₂(bipy)] and (c) [Cu₂(Dcam)₂(bipyb)] on MUD SAMs.

The IRRAS spectrum of SURMOF [Cu₂(Dcam)₂(dabco)] show than there are 3000~2973 cm^{-1} and 2931~2885 cm^{-1} absorption bands, which are assigned to the methyl and methylene, respectively (*Figure 36a*). The absorption bands 1624 cm^{-1} and 1467~1401 cm^{-1} is ascribed to

the ν_{as} and ν_s stretching bands of COO$^-$ groups. The same situation of IR absorption band in SURMOF [Cu$_2$(Dcam)$_2$(bipy)], and [Cu$_2$(Dcam)$_2$(bipyb)], the absorption bands 3080~2986 cm^{-1} in *Figure 36b*, and 2965 cm^{-1} in *Figure 36c* are ascribed to the methyl group. The assignment of bands 2928~2880 cm^{-1} in [Cu$_2$(Dcam)$_2$(bipy)] and 2923~2850 cm^{-1} in [Cu$_2$(Dcam)$_2$(bipyb)] are methylene group. The ν_{as} and ν_s stretching bands of COO$^-$ groups are 1614 and 14811~1401 cm^{-1} in *Figure 36b*, respectively. The ν_{as} and ν_s stretching bands of COO$^-$ groups are 1550 and 1415 cm^{-1} in *Figure 36c*, respectively.

4.2.3　Experimental results and discussion

A pair of chiral probe molecules, S- and R-Limonene, was chosen to systematically investigate the relationship between the degree of enantioselectivity and the pore size of the isoreticular homochiral SURMOFs. For this purpose, the uptake of the probe molecules by the different SURMOF samples was studied quantitatively by employing a QCM.[79] After activating the sample at 65 °C in a flow of argon (99.9999% purity, 100 ml min^{-1}) over night, the uptake of the enantiopure guest molecules into the SURMOFs was studied at a temperature of 303 K. Uptake was initiated by switching for a stream of pure argon to an argon flow which was enriched with R- or S-Limonene at room temperature (298 K) by passing over small amounts of the respective enantioamer. The uptakes by the three different SURMOFs are studied in parallel at the same time to ensure identical conditions during the experiments. The uptake of R- and S-Limonene was investigated subsequently five times to guarantee the reproducibility of the results. The experiments are performed at a temperature of 30 °C. Typical the uptake curves of the isoreticular chiral SURMOFs are shown in *Figure 37*.

The QCM uptake curves enable the determination of the adsorption concentration as shown *Figure 38a*. It is clearly visible that the adsorption capacity is different for the two different enantiomers. In addition, as expected, the total storage capacity increases with increasing pore size. For S-Limonene, compared to [Cu$_2$(Dcam)$_2$(dabco)], the MOF with the smallest pore size, the adsorption capacity is twice as large in [Cu$_2$(Dcam)$_2$(bipy)] and thrice as large in the [Cu$_2$(Dcam)$_2$(bipyb)]. The adsorption capacities of R-Limonene are smaller than that of S-Limonene, in particular in [Cu$_2$(Dcam)$_2$(bipy)], but also for this enantiomer adsorption capacity increases with increasing pore size.
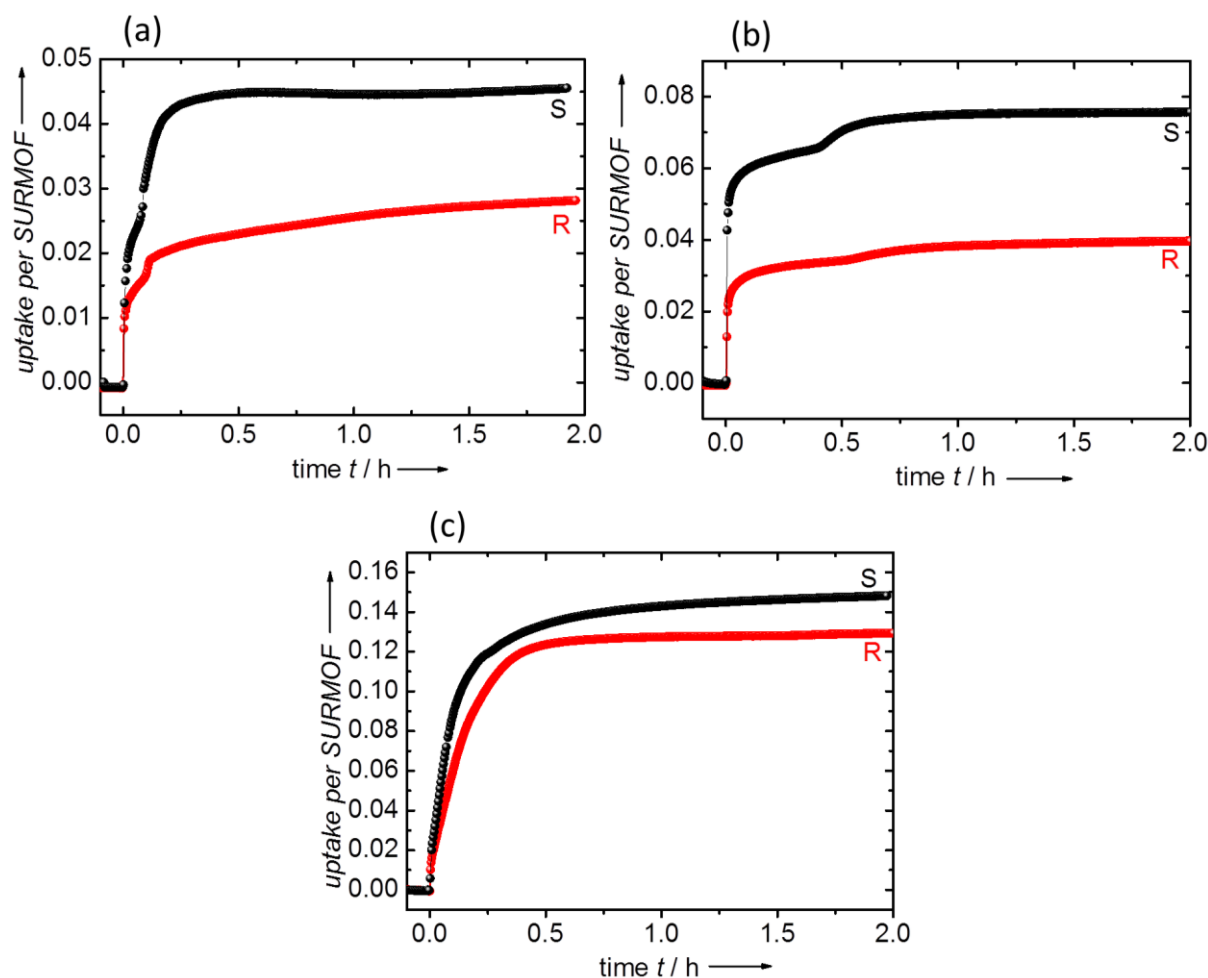
Figure 37. QCM curves of S-Limonene (black) and R-Limonene (red) uptake by the isoreticular SURMOFs; (a) [Cu₂(Dcam)₂(dabco)]; (b) [Cu₂(Dcam)₂(bipy)] and (c) [Cu₂(Dcam)₂(bipyb)].

The determined adsorption capacities allow the calculation of enantioselectivity of the adsorption as shown in *Figure 38b*. The enantiomeric excess (*ee*) of S-Limonene versus R-Limonene changes for the different MOF structures, with approximately 17% in [Cu₂(Dcam)₂(bipyb)], 40% in [Cu₂(Dcam)₂(dabco)] and about 106% in [Cu₂(Dcam)₂(bipy)]. This shows that the enantioselectivity does not only depend on the chiral center (the chiral ligand inside the MOF), also the pore size has a dramatic influence on enantioselectivity dramatically. Furthermore, the *ee* value does not follow such a simply trend as the adsorption capacity which increases with increasing pore size. The highest *ee* value was found for the medium pore size. It can be assumed that the differences of the adsorption capacities are caused by different alignment of the chiral guest molecules in the pores, where the chiral centers have different impact on the enantioselectivity.
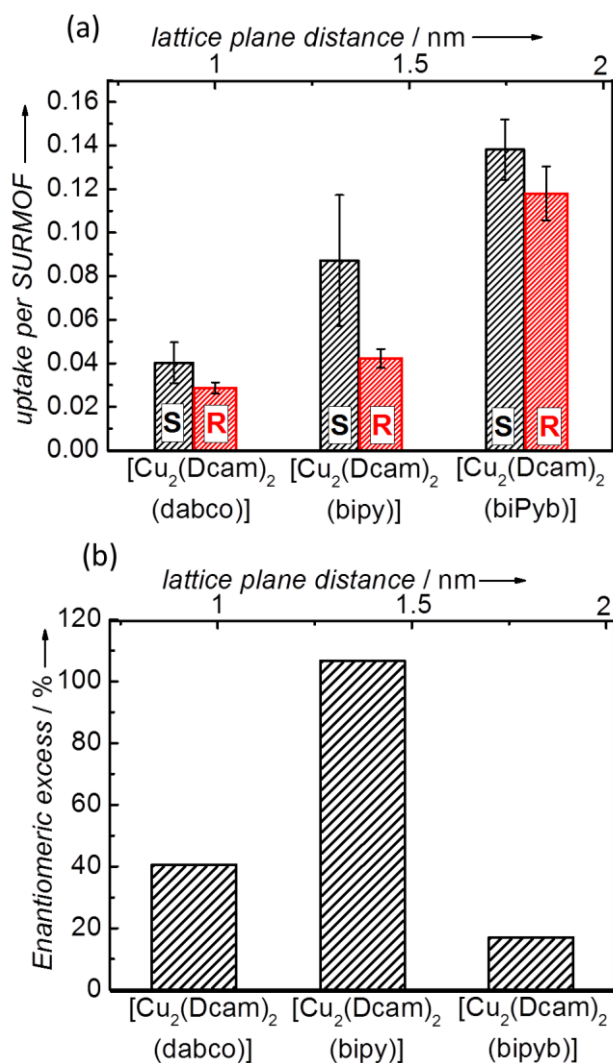
Figure 38. The S- and R-Limonene uptake (a) and enantiomeric excess (b) by the series of isoreticular homochiral SURMOFs [Cu₂(Dcam)₂(L)] with L = dabco, bipy or bipyb.

4.2.4 Conclusion

In conclusion, three isoreticular homochiral SURMOFs, [Cu$_2$(Dcam)$_2$(dabco)], [Cu$_2$(Dcam)$_2$(bipy)] and [Cu$_2$(Dcam)$_2$(bipyb)] can be grown on MUD SAMs substrate, which have the identical chiral centers and different pore sizes ($0.95 \times 0.95 \times 0.95$ nm^3, $0.95 \times 0.95 \times 1.4$ nm^3 and $0.95 \times 0.95 \times 1.8$ nm^3). A pair of chiral probe molecules, R- and S-Limonene were used to investigated the enantioselectivty of these three isoreticular homochiral SURMOFs. It was found that the adsorption capacity increases with increasing pore size of MOFs. For the enantiomer separation a more complex situation was found, where the highest *ee* value was found for SURMOF with the medium pore size while the enantiomeric excess for very small and large pores is significantly smaller. This study shows that an interplay of the chiral center and the pore size determine the enantioselectivity.

4.3 Oriented Circular Dichroism Investigation of Chiral SURMOF

The chirality of bulk MOFs has been reported and described in chapter 1.1.2. However, the chirality of MOFs on different orientations is still a challenge to investigate. Therefore, the chiral SURMOFs are good candidates for chirality investigation of MOFs with different orientations. Although CD measurements were carried out e.g. on surface-confined homochiral helices,[99] so far studies of highly oriented SURMOFs have not yet been reported. Such studies are interesting, since in addition to a conventional CD analysis of the guest compounds also the effect of highly oriented chiral ligands within the SURMOF lattice can be investigated. Oriented circular dichroism, or OCD, has been observed for oriented chiral molecules (e.g. embedded in liquid crystals), and is conveniently used in structural biology to characterize the conformation-in particular-the orientated alignment of α-helical peptides reconstituted in such oriented biomembranes.[100-102]

In this work, we focus on chiral pillared-layer SURMOFs of the type $[Cu_2(Dcam)_{2x}(Lcam)_{2-2x}(dabco)]$ ($0 \leq x \leq 1$), consisting of Cu^{2+} dimers, the enantiomeric linkers Dcam (Dcam = (1R,3S)-(+)-camphoric acid) and/or Lcam (Lcam = (1S,3R)-(-)-camphoric acid) and the pillar linker molecule dabco (*Figure 39*).[103-104]
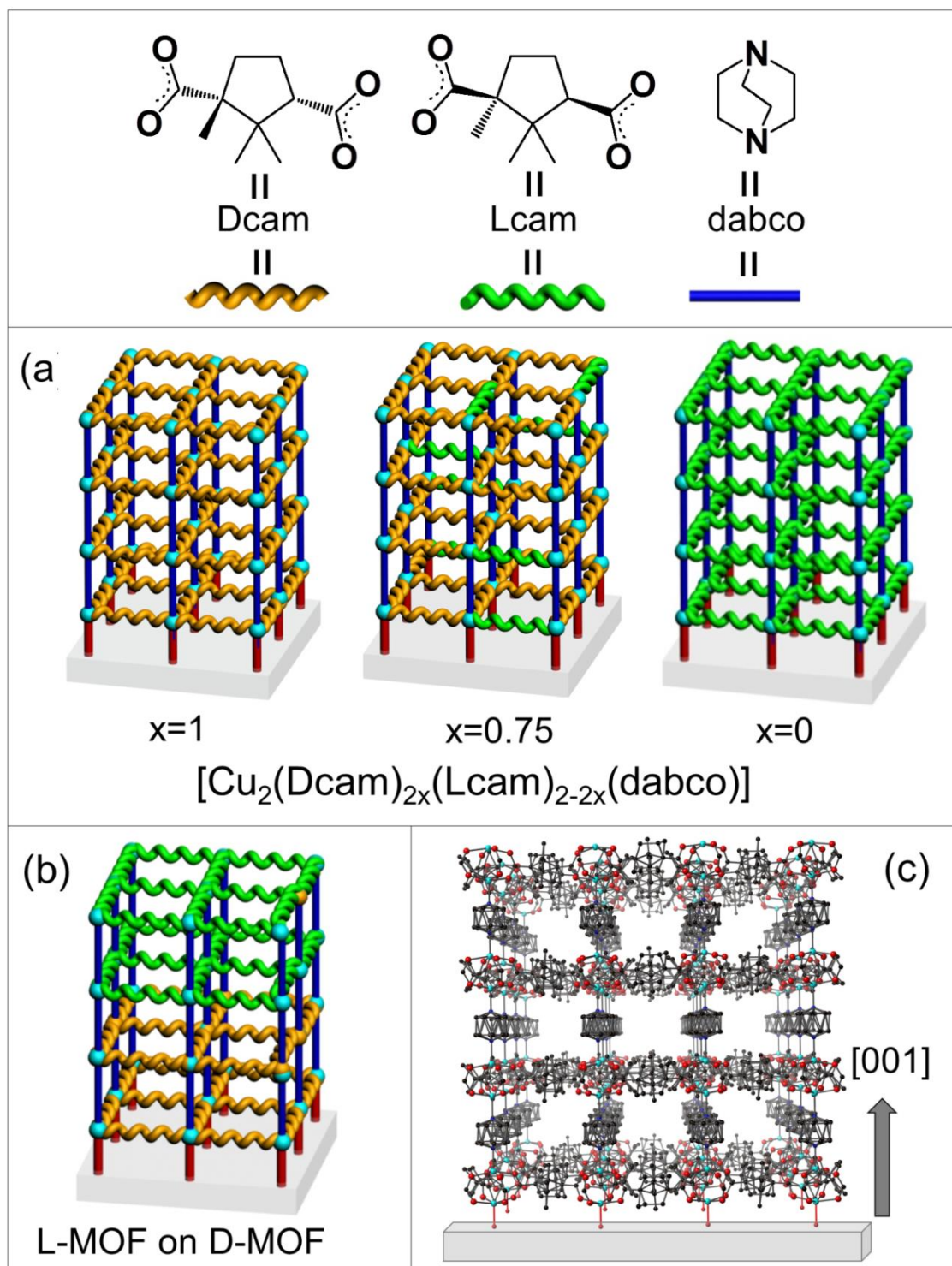
Figure 39. (a) Chiral [Cu₂(Dcam)₂ₓ(Lcam)₂₋₂ₓ(dabco)] for different x (0≤x≤1, x is the component of Dcam); (b) hetero-layered SURMOF [Cu₂(Lcam)₂(dabco)] (L-MOF) on [Cu₂(Dcam)₂(dabco)] (D-MOF); (c) [Cu₂(Dcam)₂(dabco)] structure.

4.3.1   Sample synthesis

Preparation of SURMOFs

The -OH functionalized quartz glass substrate was obtained by immersing the clear quartz glass into a piranha solution consisting of 98% H_2SO_4/30% H_2O_2 (3:1) at 80 °C for 30 min. The resulting substrates were used for SURMOF growth in [001] direction (*Figure 40a*). In order to obtain SURMOFs with a [110] growth direction, the -COOH functionalized quartz substrates were prepared by treating the OH-functionalized quartz glass with 11-(triethoxysilyl)undecanal (0.05 M toluene solution) for 3 h and potassium permanganate (1 mM aqueous solution) for 1 h, respectively.

After this cleaning procedure, the $[Cu_2(Dcam)_{2x}(Lcam)_{2-2x}(dabco)]$ (x = 0, 0.25, 0.5, 0.75 and 1) SURMOF films were grown on the quartz substrate by an LPE approach at 50 °C. The substrate was subsequently immersed in an ethanolic solution of copper acetate dihydrate (1 mM) for 15 min, in pure ethanol for 5 min, and in the ethanolic linker solution containing H_2Dcam/H_2Lcam with different ratios and dabco for 30 min. The ratios were 1/0, 3/1, 1/1, 1/3, and 0/1 with a total concentration of the Dcam and Lcam linkers of 0.2 mM and a concentration of dabco of 0.2 mM. As a final step, the sample was immersed again in pure ethanol for 5 min. The cycles were repeated 40 times to obtain a 40 cycles $[Cu_2(Dcam)_2(Lcam)_{2-2x}(dabco)]$ (x = 0, 0.25, 0.5, 0.75 and 1) SURMOF grown in the [001] direction.

Furthermore, films consisting of 20 cycles $[Cu_2(Lcam)_2(dabco)]$ (or $[Cu_2(Dcam)_2(dabco)]$) SURMOF were grown on top of 20 cycles $[Cu_2(Dcam)_2(dabco)]$ (or $[Cu_2(Lcam)_2(dabco)]$) SURMOF (and vice versa). They were prepared on cleaned quartz substrates using the LPE approach as described previously, with the difference that the linker solutions contain either Dcam or Lcam linker molecules. After growing 20 cycles of one SURMOF, the growth of 20 cycles of the other SURMOF was started.

Preparation of bulk MOF material

$[Cu_2(Dcam)_2(dabco)]$ bulk MOF was synthesized by a solvothermal method, one-pot reaction of 0.2 g (1 mol) copper acetate $(CH_3COO)_2Cu·H_2O$, 0.2 g (1 mol) (1R,3S)-(+)-camphoric acid (Dcam) and 0.056 g (0.5 mol) linear rigid N-donor dabco in a 2:2:1 ratio in ethanolic solution. The precipitated powder was washed with ethanol. XRD-patterns for $[Cu_2(Dcam)_2(dabco)]$ prepared at 350 K for 12 h are shown in *Figure 40b*. Calculation of the XRD pattern was done with Mercury CSD 2.4 version program applying the structural

information from the literature[15] with the space group #90 P42$_1$2.
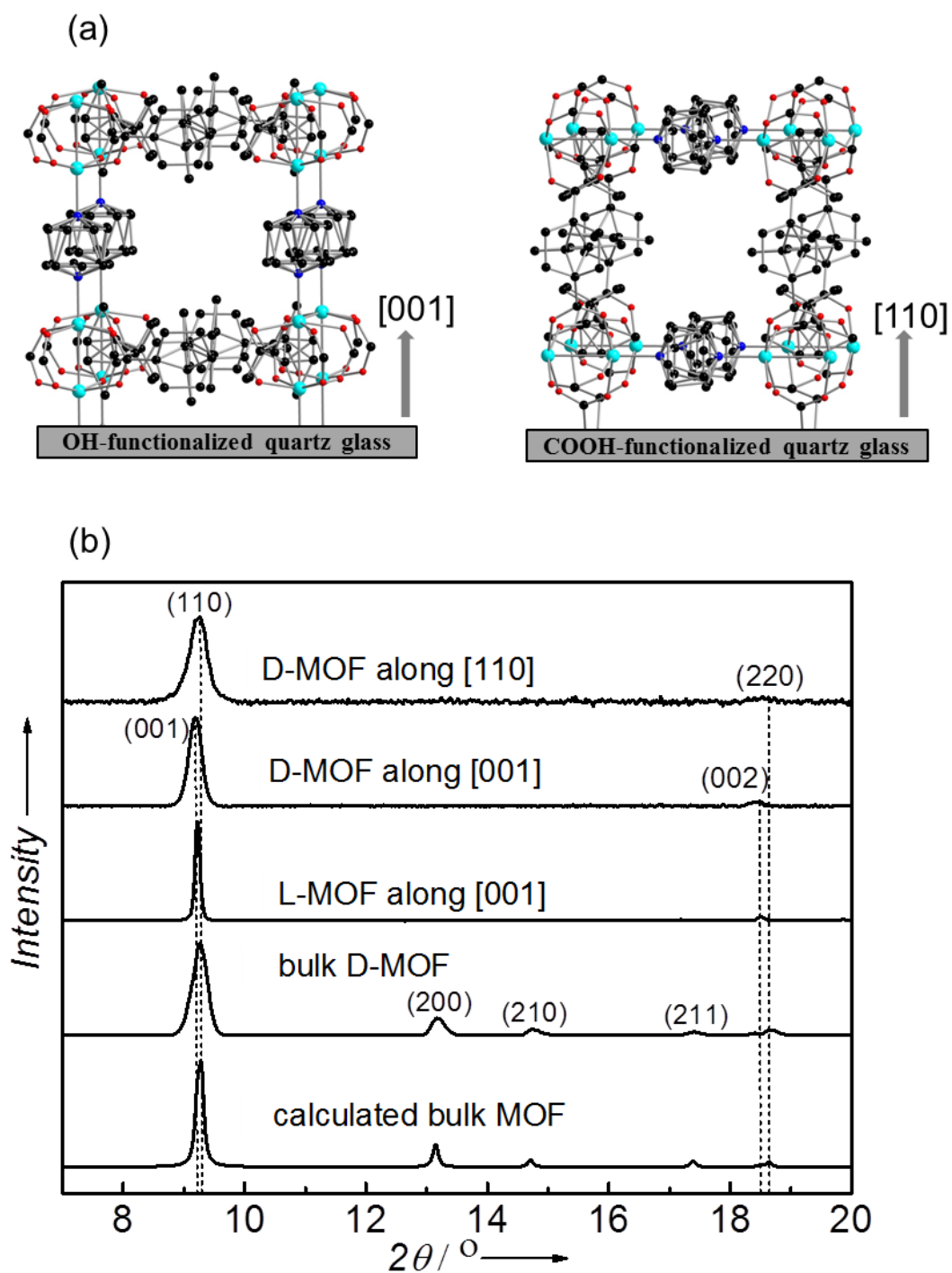
Figure 40. (a) Structures of the [Cu$_2$(Dcam)$_2$(dabco)] SURMOF grown in the [001] and [110] directions; (b) Experimentally obtained XRD of D-MOF grown in different directions, of L-MOF grown in the [001]-direction and of the powder MOF and the calculated bulk XRD.

4.3.2 Comparison of CD in SURMOF and bulk MOF

From the theory of OCD for proteins,[105] it is known that the intensity of the bands in the OCD spectrum of a chiral compound depends on the orientation of the transition dipole moment (TDM) of the chromophore (have COO$^-$ group) with respect to the plane of the rotating electric field vector (RE) of the incoming circular polarized light. According to *Figure 39a*, each of the chiral linker molecules in the [001]-oriented SURMOFs is oriented with its molecular axis perpendicular to the incoming light and hence parallel to the RE-plane. This results in a "net contribution" of each chiral linker to the OCD spectrum since the TMDs are all oriented perpendicular to the Dcam (or Lcam) molecular axis. This situation changes for SURMOFs with a different growth direction. To illustrate this relationship, the enantiopure SURMOF [Cu$_2$(Dcam)$_2$(dabco)] was grown along the [110] direction by using a - COOH functionalized SAM. When comparing the OCD spectra of a [001]-SURMOF with that obtained for a [110]-SURMOF (see *Figure 41*), significant changes are observed. This pronounced deviation can be rationalized by considering the different orientations of the chiral linkers within the two SURMOF structures. For the [001] orientation, the longitudinal axis of all chiral linkers is oriented parallel to the substrate (and thus parallel to the RE plane). On the other hand, in the case of the [110] oriented Cu$_2$(Dcam)$_2$(dabco)] SURMOF, for one half of the chiral linkers the molecular axis is oriented perpendicular to the surface (and thus perpendicular to the RE plane).
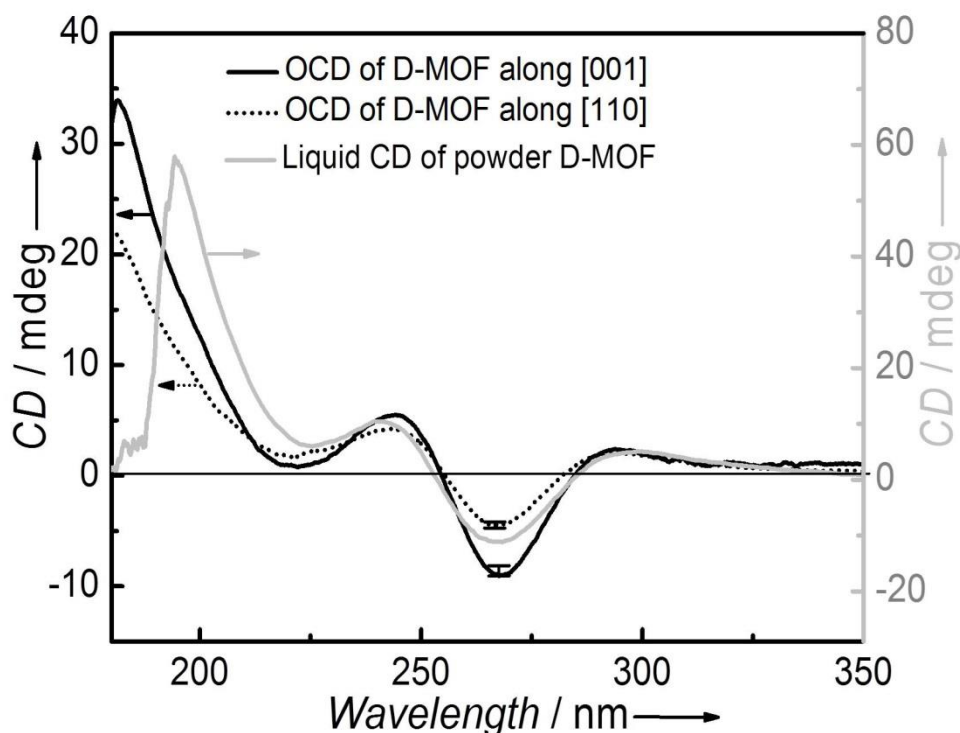
Figure 41. OCD spectra of [Cu₂(Dcam)₂(dabco)] grown in the two perpendicular orientations [001], [110] (left y-axis) and conventional CD spectrum of a suspension of the corresponding MOF powder (right y-axis).

The experimentally observed decrease in intensity of the OCD band at 267 nm when going from the [001] to the [110] orientation is fully consistent with quantum chemical TD-DFT computations of the D-MOF model system (*Figure 43a*).

A 0.2 mM ethanolic solution of the pure enantiomers and the racemate of EtLt were measured in the same way. The CD measurements of MOF powders were performed for a suspension of the powder particles in ethanol. The thickness of SURMOF films grown in the [001] and [110] directions was determined from the scanning electron microscope (SEM) images shown in *Figure 42*. Three places of the sample are chosen to measure the thickness of the SURMOF, displaying there are 143, 154 and 139 nm for SURMOF in the [001] direction while there are 139, 123 and 127 nm for SURMOF in the [110] direction. The thickness results show the SURMOF on different orientations have the identical thickness. The calculation of the error bars for CD spectra of SURMOF in the [001] and [110] directions is shown in *Table 2* and *Table 3*. It was taken into account that both sides of the quartz glass were coated with SURMOF.

All calculations of OCD spectra were carried out by Dr. Angela Bihlmeier in Prof. Dr. Wim Klopper group at Karlsruhe Institute of Technology (KIT). Several computations on a smaller

model system with various exchange-correlation functions showed qualitatively the same spectra, with larger absolute ellipticity for [001] than for [110], at least two times as large. This smaller model system was the $Dcam^{2-}$ anions, neutralized by two Na^+ ions, and the anion $NH_3(HCO_2)_3Cu_2Dcam^-$.
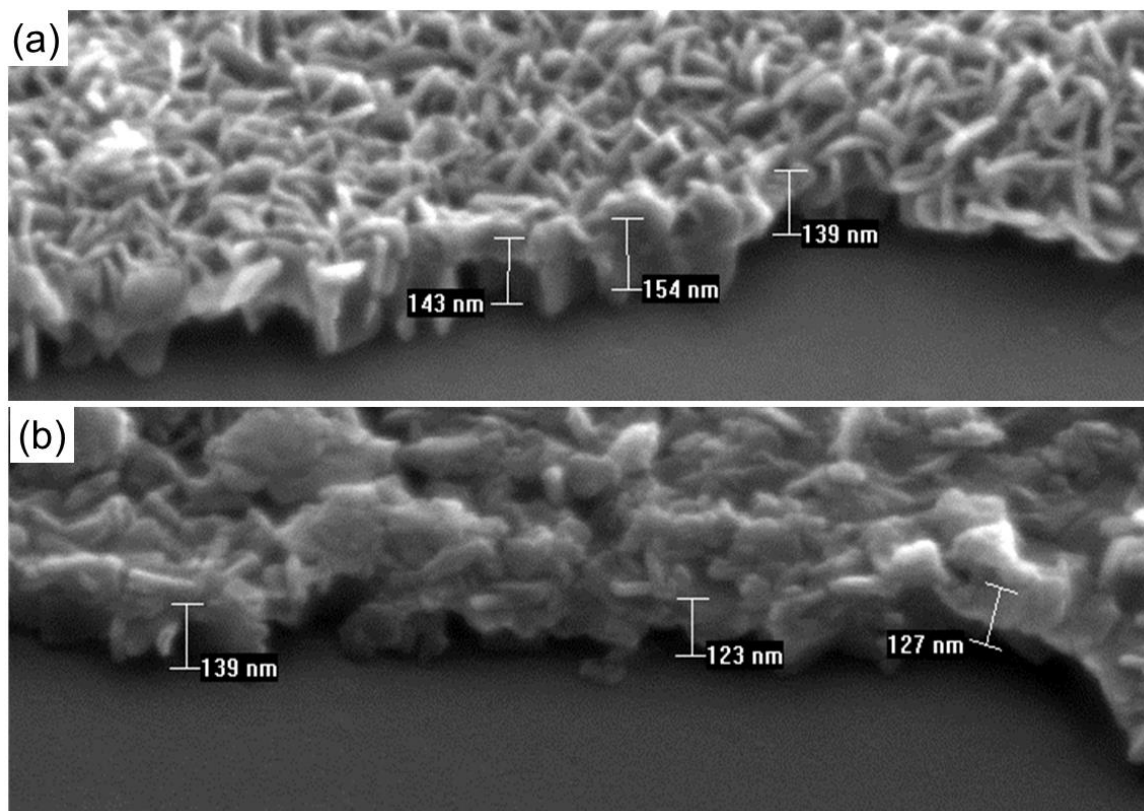
Figure 42. Scanning electron microscopy (SEM) was used to estimate the thickness of [Cu$_2$(Dcam)$_2$(dabco)] SURMOFs grown (a) in the [001] and (b) [110] direction on a quartz glass.

All quantum chemical computations were performed with the TURBOMOLE program package[106] in the def2-SVPD basis set for all atoms except H, for which the smaller def2-SV(P) basis set was used.[107-108] We shall refer to this basis set as "def2-SV(PD)". Computations were first performed for the anionic model system $NH_3(HCO_2)_3Cu_2Dcam^-$, whose equilibrium geometry was optimized in the framework of density-functional theory (DFT) with the functional B3LYP[109] and the conductor-like screening model COSMO[110] ($\varepsilon = \infty$). Then, a second $NH_3(HCO_2)_3Cu_2^+$ unit was added as a mirror image of the first unit to yield the final, neutral model system Dcam(NH$_3$(HCO$_2$)$_3$Cu$_2$)$_2$ (*Figure 43a*).

The large positive ellipticity at about 200 nm in the experimental spectra is not reproduced by the computations, however. Nonetheless, the theoretical results corroborate the explanation that the differences between the experimental spectra of the chiral SURMOF [Cu$_2$(Dcam)$_2$(dabco)] grown along [001] and [110] are due to the different orientation. The

conventional CD spectrum (not normalized) of a suspension of a powder Cu$_2$(Dcam)$_2$(dabco)] MOF is also shown in *Figure 41* for comparison. The difference between this spectrum and the superposition of the OCD spectra of the D-MOFs grown in [001] and [110] direction is explained by scattering contributions from the MOF powder particles.

Table 2. Calculation of error bars for [001] orientation at 267 nm in Figure 41:

Average thickness of SURMOF (according to *Figure 42a*) $(d_1 + d_2 + d_3)/3$	(143 nm + 154 nm + 139 nm)/3 = 145 nm
As both sides of the quartz glass are coated we assume an average overall thickness d'	d' = 2x145 nm = 290 nm
α'= average contribution of 1 nm of a SURMOF layer to the CD spectrum	α' = -9.6mdeg/290 nm = -0.03 mdeg/nm
Calculated α_n of a SURMOF with a thickness of d$_1$, d$_2$ or d$_3$	$\alpha_1 = \alpha' \times 2 \times 143$ nm = -9.5 mdeg $\alpha_2 = \alpha' \times 2 \times 154$ nm = -10. 2 mdeg $\alpha_3 = \alpha' \times 2 \times 139$ nm = -9.2 mdeg
Error bar max.	$\Delta\alpha_3$= -9.2 mdeg
Error bar min.	$\Delta\alpha_2$= -10.2 mdeg

Table 3. Calculation of error bars for [110] orientation at 267 nm in Figure 41:

Average thickness of SURMOF (according to *Figure 42b*) $(d_1 + d_2 + d_3)/3$	(139 nm + 123 nm + 127 nm)/3 = 130 nm
As both sides of the quartz glass are coated we assume an average overall thickness d'	d' = 2 × 130 nm = 260 nm
α'= average contribution of 1 nm of a SURMOF layer to the CD spectrum	α' = -4.5 mdeg/260 nm = -0.02mdeg/nm
Calculated α_n of a SURMOF with a thickness of d$_1$, d$_2$ or d$_3$	$\alpha_1 = \alpha' \times 2 \times 139$ nm = -4.8 mdeg $\alpha_2 = \alpha' \times 2 \times 123$ nm = -4.2 mdeg $\alpha_3 = \alpha' \times 2 \times 127$ nm = -4.4 mdeg
Error bar max.	$\Delta\alpha_2$ = -4.2 mdeg
Error bar min.	$\Delta\alpha_1$ = -4.8 mdeg
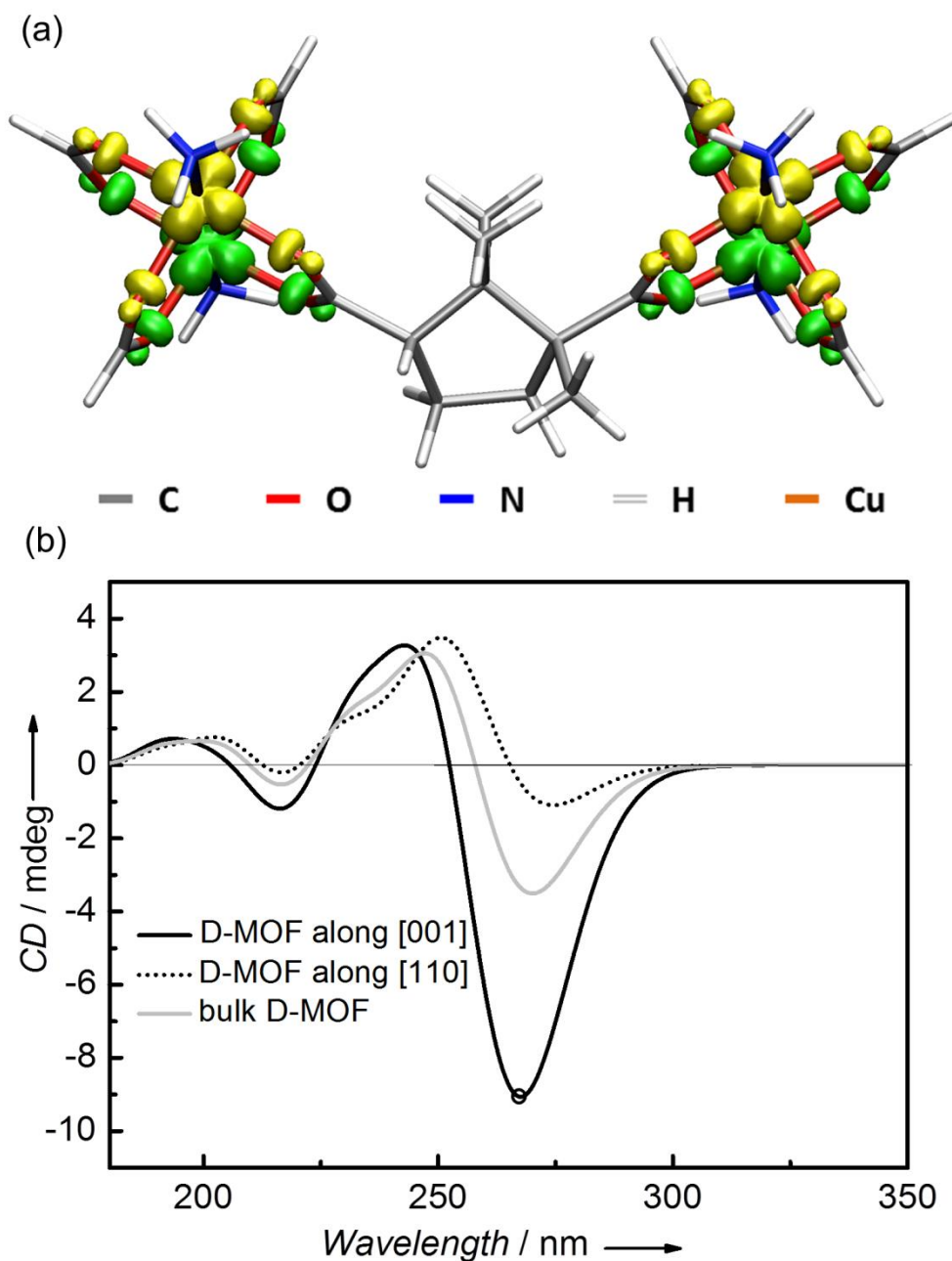
Figure 43. (a) D-MOF model system used for the computation of oriented circular dichroism. Also shown is an isosurface of the spin density at 0.01 a_0^{-3}, as obtained at the B3LYP(35%)/def2-SV(PD) level; (b) OCD spectrum of the D-MOF model system as computed at the B3LYP(0.35%)/def2-SV(PD) level. A scaling factor was applied such that the minimum of the OCD spectrum along [001] equals the corresponding experimental value (black open circle). Shifted by 0.31 eV and simulated with Gaussian broadening with a root-mean-square line width of 0.2 eV.

4.3.3 Experimental results and discussion

The preparation of the chiral SURMOF $[Cu_2(Dcam)_{2x}(Lcam)_{2-2x}(dabco)]$ (x = 0.75, 0.5, 0.25

and 0) on CD compatible quartz glass plates was carried out using the LPE process as reported previously.[111]

In case of the $[Cu_2(Dcam)_2(dabco)]$ and $[Cu_2(Lcam)_2(dabco)]$ SURMOF grown on -OH functionalized quartz glass the observation of sharp [001] diffraction peaks at 9.2° and 18.5° together with the absence of any diffraction peaks belonging to other crystallographic directions (See *Figure 44a*) reveals the presence of highly oriented SURMOFs with a [001] growth direction. The IRRAS data, which exhibited two characteristic bands centred at 1467 cm^{-1} and 1624 cm^{-1}, can be assigned to the symmetric and asymmetric -COO vibrations of the carboxylate groups of the camphorate linker, respectively, thus providing additional evidence for the successful growth of $[Cu_2(Dcam)_{2x}(Lcam)_{2-2x}(dabco)]_n$ SURMOFs (*Figure 44b*).
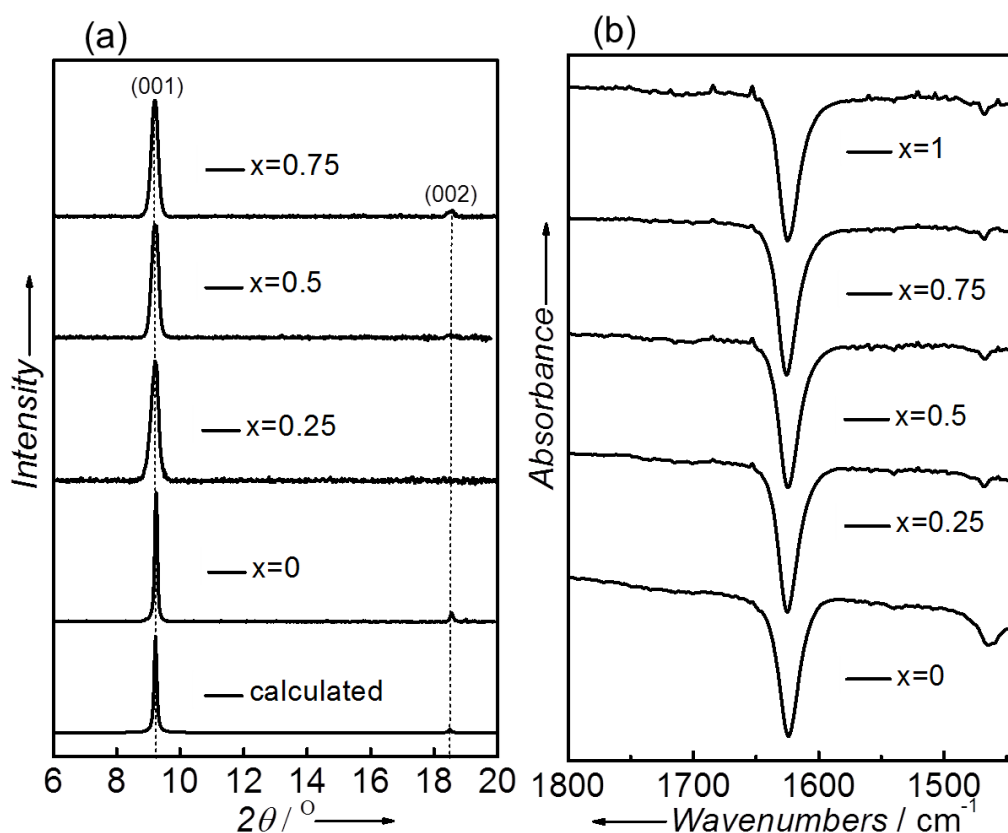
Figure 44. (a) XRD of $[Cu_2(Dcam)_{2x}(Lcam)_{2-2x}(dabco)]$ (x = 0.75, 0.5, 0.25 and 0) 40 cycles on a functionalized quartz glass substrate; (b) IRRAS of $[Cu_2(Dcam)_{2x}(Lcam)_{2-2x}(dabco)]$ (x = 1, 0.75, 0.5, 0.25 and 0) 40 cycles on a functionalized quartz glass substrate.

The OCD data recorded for a series of chiral SURMOFs $[Cu_2(Dcam)_{2x}(Lcam)_{2-2x}(dabco)]$ are depicted in *Figure 45*. For the SURMOF fabricated exclusively with Dcam (x = 1) or with Lcam (x = 0) the OCD spectra show two positive (negative) bands at 182 nm and 243 nm and a negative (positive) band at 267 nm, respectively. The intensities of all the corresponding

OCD bands are comparable in its values but exhibit opposite sign, as expected. The same mirror-inverted property can be observed for the two OCD spectra corresponding to the SURMOFs grown from mixtures of the chiral ligands (x = 0.75 and x = 0.25). For x = 0.5, the OCD spectrum only shows a flat line, because the contributions of the Dcam and Lcam linkers to the OCD spectrum cancel each other.
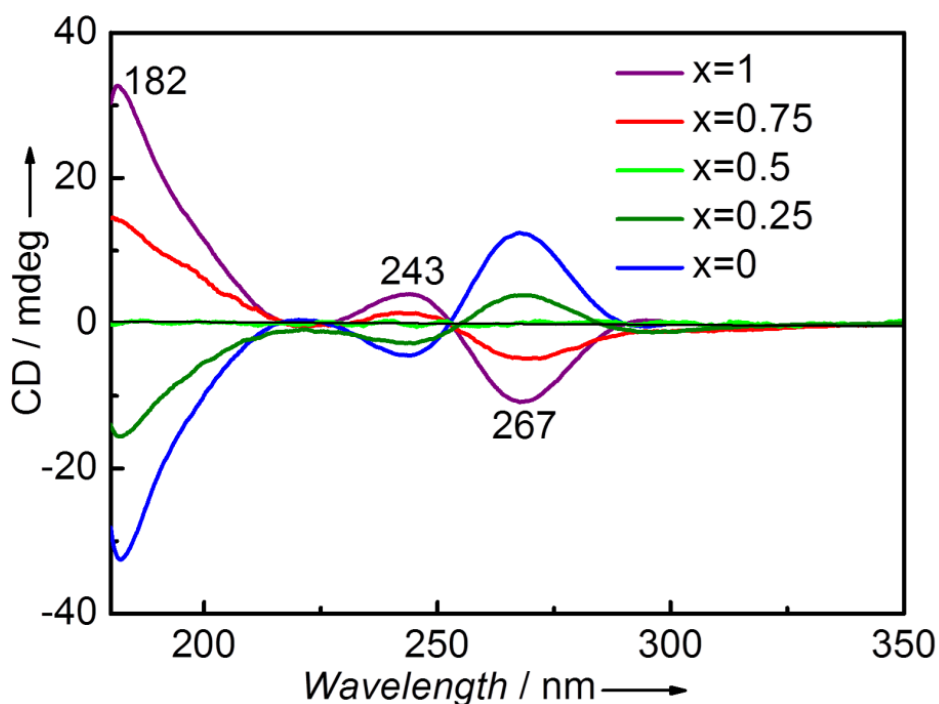
Figure 45. OCD spectra of [Cu$_2$(Dcam)$_{2x}$(Lcam)$_{2-2x}$(dabco)] grown on a functionalized quartz glass slide with x = 1, 0.75, 0.5, 0.25 and 0.

For comparison, the conventional (isotropic) CD data for liquid and solid camphoric acid (H$_2$cam) are shown in *Figure 46a* and *Figure 46b*, respectively. A positive band for H$_2$Dcam and a negative band for H$_2$Lcam at 211 nm are observed. For liquid-state CD measurements of the H$_2$DCam and H$_2$LCam enantiomers of camphoric acid a 5 mM solution in 2,2,2-trifluoroethanol was prepared and measured in a 1 mm quartz glass cuvette using the data acquisition parameters described above. Comparing with the CD between chiral MOFs and chiral linkers, two chromophores with strong electric-dipole are formed after metal and chiral organic linkers construct chiral MOF on substrate.
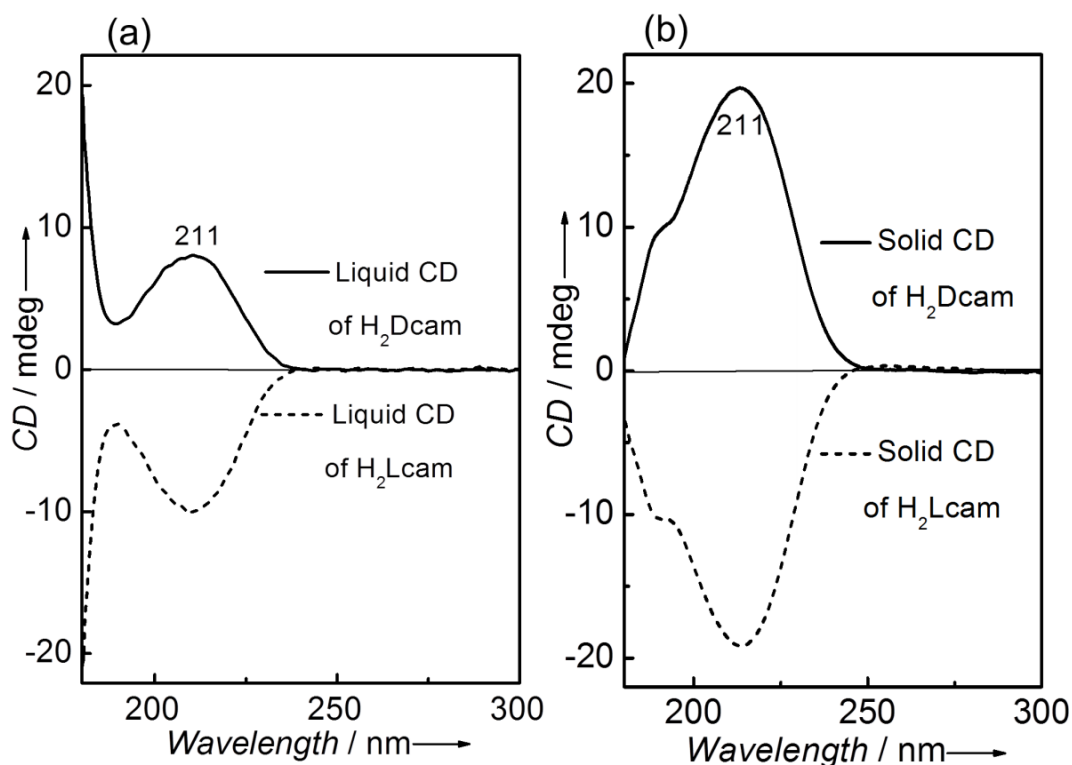
Figure 46. Conventional CD spectra of H$_2$Dcam and H$_2$Lcam (a) dissolved in a liquid (2,2,2-trifluoroethanol) and (b) as a solid powder sample.

The same result was obtained for a bilayer Dcam/Lcam hetero-SURMOF fabricated by first growing 20 cycles [Cu$_2$(Dcam)$_2$(dabco)] (or [Cu$_2$(Lcam)$_2$(dabco)]) SURMOF on the quartz glass substrate, followed by the deposition of [Cu$_2$(Lcam)$_2$(dabco)] (or [Cu$_2$(Dcam)$_2$(dabco)]) with the same number of cycles (*Figure 47* and *Figure 48*).

From the XRD result, there are strong (001) peak at 9.23° and (002) peak at 18.5° which display that the MOF grown on substrate and seeding layers along [001] orientation (*Figure 47b* and *Figure 48b*). We can see the MOF on MOF is available in the enantiomer linkers instead of different metal (change the metal source in the literature). There are two positive CD signal at 182 and 243 nm and a negative CD signal at 267 nm after 20 cycles [Cu$_2$(Dcam)$_2$(dabco)] on quartz glass substrate (seeding MOF layers) in *Figure 47a* (solid line). It is worth notice that there is no obvious CD signal after another 20 cycles [Cu$_2$(Lcam)$_2$(dabco)] on the seeding MOF layers and (dashed line in *Figure 47a*). With the same situation, with [Cu$_2$(Lcam)$_2$(dabco)] as seeding MOF layers, and then [Cu$_2$(Dcam)$_2$(dabco)] on the seeding MOF layers, there is also no CD signal in this case and both cases show that the counter chiral MOF will offset chirality of chiral MOF that locate the seeding layers (see *Figure 48a*). In this way, we can use the MOF-on-MOF method to achieve chirality conversion in MOF thin film.
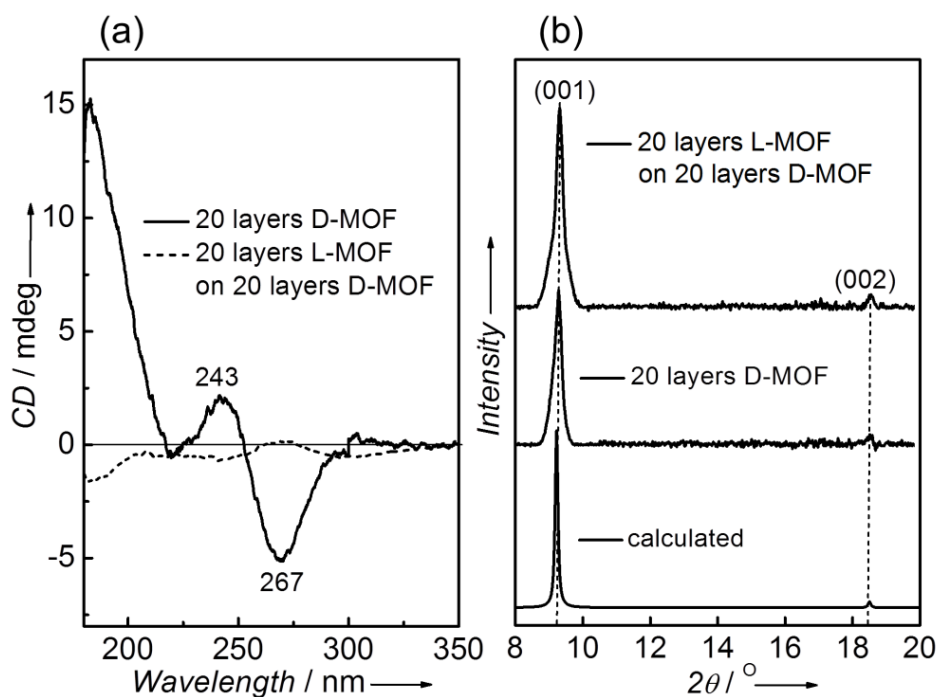
Figure 47. (a) OCD spectra of 20 cycles [Cu$_2$(Dcam)$_2$(dabco)] and of 20 additional cycles of [Cu$_2$(Lcam)$_2$(dabco)] on top of the initial 20 layers of [Cu$_2$(Dcam)$_2$(dabco)]; (b) Corresponding out-of-plane XRD, compared with the calculated diffractogram of a SURMOF in the [001] direction. All SURMOFs are grown in the [001] direction on quartz glass.
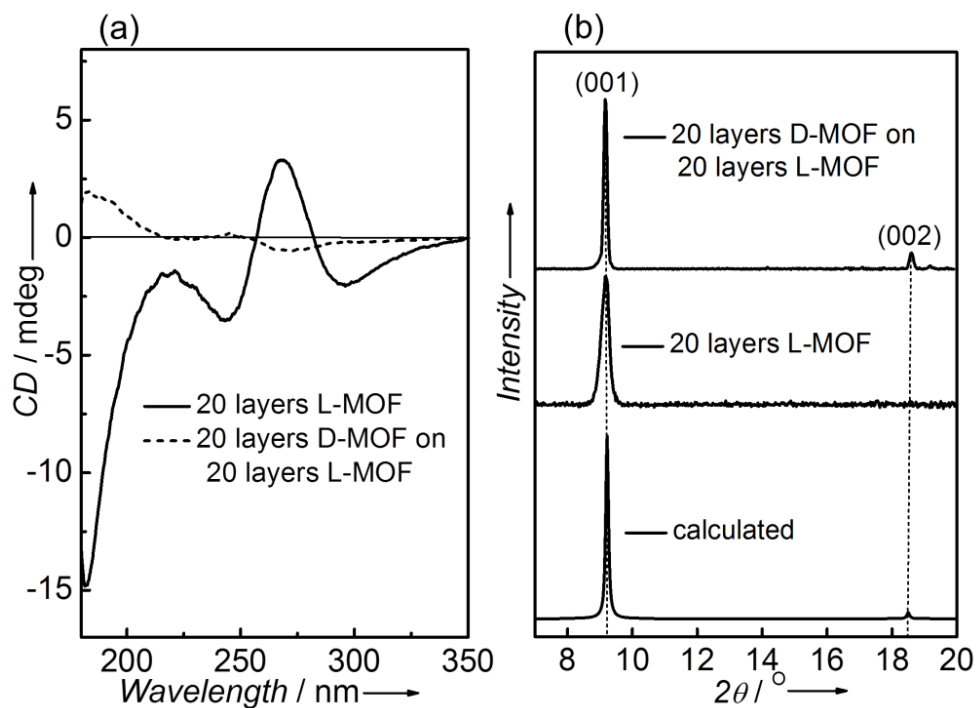
Figure 48. (a) OCD data and (b) out-of-plane XRD of 20 cycles enantiopure [Cu$_2$(Lcam)$_2$(dabco)], and of 20 cycles [Cu$_2$(Dcam)$_2$(dabco)] grown on top of 20 cycles [Cu$_2$(Lcam)$_2$(dabco)]. For comparison the calculated diffractogram is shown in (b).

The application of OCD for investigation the loading of SURMOFs with chiral guest molecules is demonstrated for (+)-ethyl-D-lactate [(+)EtLt] and (-)-ethyl-L-lactate [(-)EtLt]. The pure (-)EtLt and (+)EtLt compounds display a strong and characteristic CD band at 211 nm (*Figure 49a and Figure 50a*) shows the resulting OCD spectra for the case of [Cu_2(Dcam)$_2$(dabco)], before (red curve) and after loading with (-)EtLt and with (+)EtLt from the gas phase (solid black and blue curves, respectively). By subtracting the spectrum of the pristine SURMOF from the corresponding spectrum after loading, the OCD spectra of the loaded guest compounds (-)EtLt and (+)EtLt were obtained (*Figure 49*b, dotted black and blue curves, respectively). The resulting broad bands at 211 nm have opposite signs and can be assigned to the contribution of (-)EtLt and (+)EtLt to the CD spectrum. The relative amount of the loaded species was quantified by integrating the areas below the curves [A_+ for (+)EtLt and A_- for (-)EtLt] (shaded areas in *Figure 49*b), yielding $A_+ = \lvert$ -159 $\rvert$ mdeg•nm for (+)EtLt and $A_- = \lvert$ +158 $\rvert$ mdeg•nm for (-)EtLt.

In the next step, a racemic mixture of (-)EtLt and (+)EtLt was used for loading [Cu_2(Dcam)$_2$(dabco)] (*Figure 49*c, green curve). After subtracting the corresponding OCD data for the empty host lattice, the difference spectrum yields an integrated area A_{rac} of $\lvert$ -45 $\rvert$ mdeg•nm (green shaded area in Figure *Figure 49c*), demonstrating a pronounced enrichment of (+)EtLt. Considering the value of 158.5 mdeg•nm [(A_++A_-)/2] obtained for a 100% loading with ethyl lactate (see above), the corresponding enantiomeric excess of *ee* = A_{rac} / [(A_++A_-)/2] = 28% implies that the [Cu_2(Dcam)$_2$(dabco)] exposed to the racemate contains 64% (+)EtLt and 36% (-)EtLt.

The OCD spectra of [Cu_2(Lcam)$_2$(dabco)] SURMOF before (*Figure 50b*, red curve) and after the adsorption of (+)EtLt and (-)EtLt (*Figure 50b*, solid blue and black curves, respectively), exhibit similar amounts of loaded enantiomers when compared to the 40 cycles [Cu_2(Dcam)$_2$(dabco)] SURMOF with $A_- = \lvert$ +167 $\rvert$ mdeg•nm for (-)EtLt and $A_+ = \lvert$ -170 $\rvert$ mdeg•nm for (+)EtLt (black and blue shaded areas in *Figure 50*, respectively). The appearance of a positive broad band at 211 nm after loading the racemate ($\lvert$ +43 $\rvert$ mdeg•nm) reveals a preferential loading of the (-)EtLt enantiomer (*Figure 50c*). Determining a peak area of 168.5 mdeg•nm [(A_++A_-)/2] for 100% loading with ethyl lactate, one gets an enatiomeric excess *ee* = A_{rac} / [(A_++A_-)/2] ×100% = 26%, which means 63% (-)EtLt and 37% (+)EtLt were taken up by the 40 cycles [Cu_2(Lcam)$_2$(dabco)] SURMOF.
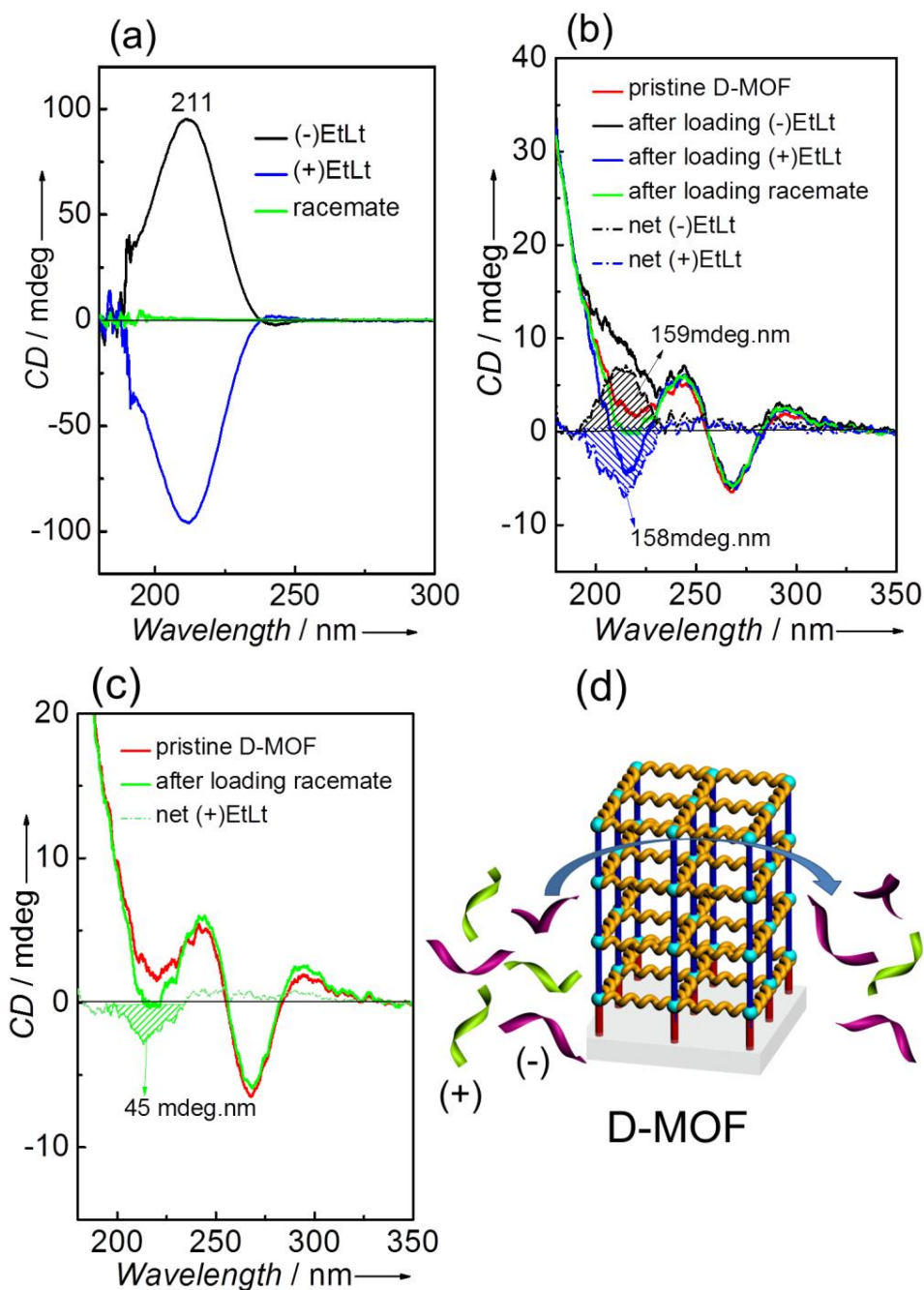
Figure 49. (a) CD spectra of the pure enantiomers (-)EtLt (black curve) and (+)EtLt (blue curve);(b) OCD spectra of [Cu₂(Lcam)₂(dabco)] SURMOF before (red curve) and after (black and blue solid curves) loading with the enantiomers and with a racemic mixture (green curve) of EtLt. The dotted curves represent the difference between the OCD spectrum of the pristine SURMOF and the SURMOF after loading with (+)EtLt (blue) and (-)EtLt (black). The shaded areas represent the relative net amount of the loaded enantiomer; (c) OCD spectra of [Cu₂(Dcam)₂(dabco)] SURMOF before (red curve) and after (green curve) loading with a racemic mixture of EtLt. The shaded green area represents the relative net amount of the adsorbed (-)EtLt enantiomer; (d) Schematic illustration of an enantioselective separation of a racemic EtLt mixture by enantiopure chiral [Cu₂(Dcam)₂(dabco)] SURMOF.
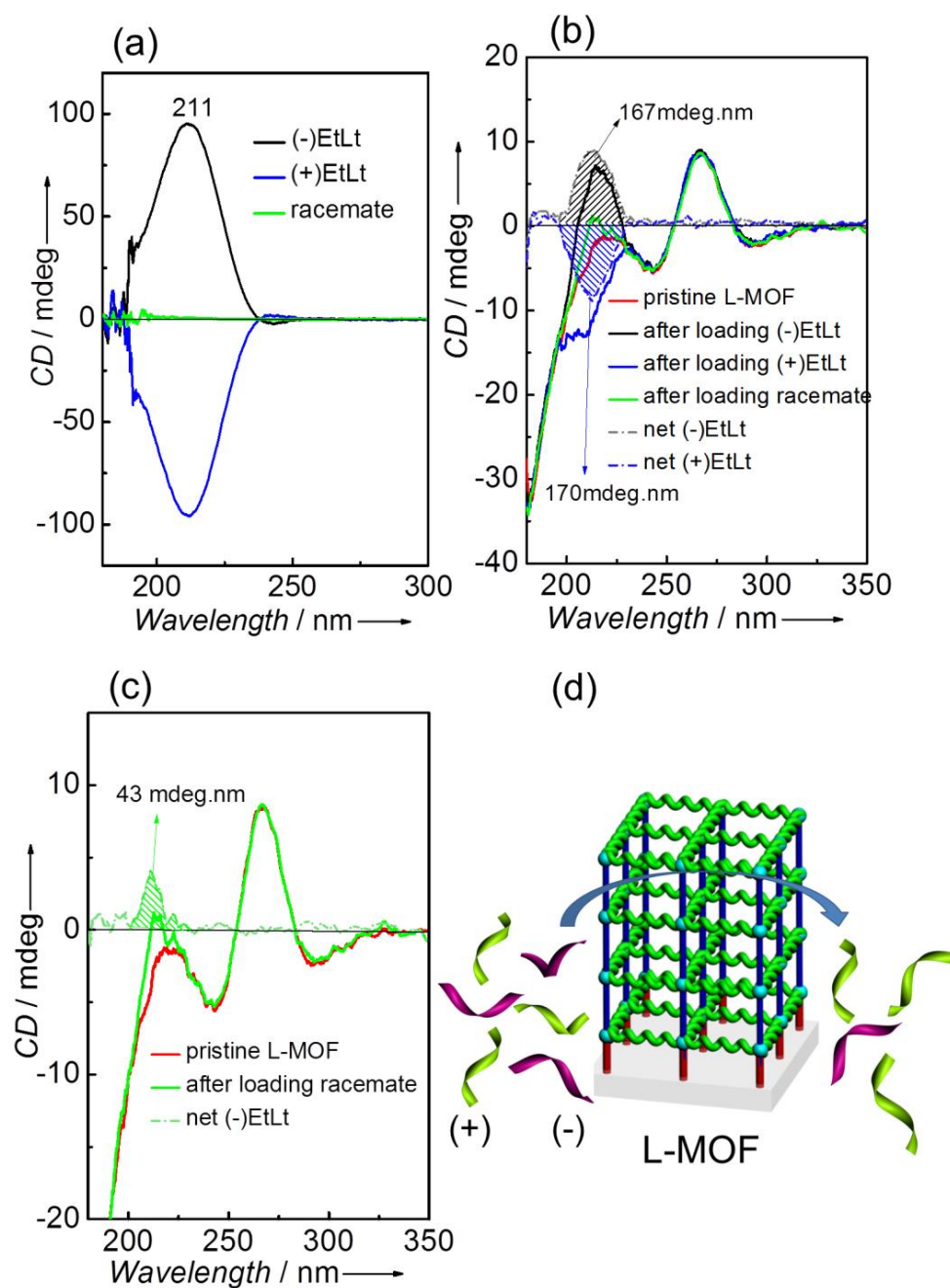
Figure 50 (a) Conventional CD spectra of both enantiomers and of the racemic mixture of EtLt in 0.2 mM ethanolic solution; (b) OCD spectra of [Cu$_2$(Dcam)$_2$(dabco)] SURMOF before (red curve) and after (black and blue solid curves) loading with the enantiomers and with a racemic mixture (green curve) of EtLt. The dotted curves represent the difference between the OCD spectrum of the pristine SURMOF and the the SURMOF after loading with (+)EtLt (blue) and (-)EtLt (black). The shaded areas represent the relative net amount of the loaded enantiomer; (c) OCD spectra of [Cu$_2$(Dcam)$_2$(dabco)] SURMOF before (red curve) and after (green curve) loading with a racemic mixture of EtLt. The shaded green area represents the relative net amount of the adsorbed (+)EtLt enantiomer; (d) Schematic illustration of an enantioselective separation of a racemic EtLt mixture by enantiopure chiral SURMOFs.

For comparison of the CD spectra for pure (-)EtLt and (+)EtLt are shown in *Figure 49a* and *Figure 50a*, which show that the CD bands (211 nm) of the enantiomers locate the different CD bands of the chiral SURMOFs (182, 243 and 267 nm). This means that the (-)EtLt and (+)EtLt molecules are good candidates for the determine experiments of SURMOFs [Cu$_2$(Dcam)$_2$(dabco)] or [Cu$_2$(Lcam)$_2$(dabco)] using by CD technique.

4.3.4   Conclusion

In conclusion, the OCD can be applied to characterize chiral SURMOFs in a straightforward fashion. The observed decrease in the intensity of OCD band going from a [001] to a [110] growth orientation of the D-MOF demonstrates that the OCD method can be used to determine indirectly the orientation of the chiral linkers molecules of a hierarchically grown structure with respect to the substrate surface. In addition to this demonstration of the huge potential of empty SURMOF lattices for OCD investigations, OCD was also used to study the enantioselective loading of the enantiopure SURMOFs [Cu$_2$(Dcam)$_2$(dabco)] and [Cu$_2$(Lcam)$_2$(dabco)] with (+)-ethyl-D-lactate and with (-)-ethyl-L-lactate. When exposing the homochiral SURMOFs to a racemic mixture of the ethyl lactate enantiomers, the OCD data directly demonstrated the selective enrichment of one of the enantiomers. A quantitative analysis of these data is allowed to determine the relative amounts of adsorbed guest molecules with different chirality. We conclude that the combination of SURMOFs with circular dichrosim spectroscopy carries a huge potential for investigations of the interactions of chiral host with enantiopure MOF materials with regard to applications as filter and membrane materials, which might contribute to the highly topical filed of enantiomer separation.

5 Experimental Results and Discussions: Optimization of SURMOF Growth Using A Dipping Robot

5.1 Improvement of the SURMOF prepared by immersing into ultrasonic bath

Ultrasonic in the dipping robot is applied during the SURMOFs preparation with the aim of understanding their influence and improving the SURMOFs quality. For this purpose, SURMOFs HKUST-1 are prepared at different ultrasonic treatment conditions under the same conditions (i.e. the same concentrations of metal salts and ligands and immersion time). Metal salts and organic ligand solutions, rinsing ethanol solution and all the solutions (metal salts, organic ligand and rinsing ethanol solutions) are put in the ultrasonic bath, respectively. The immersion time are 600, 900 and 100 s for $Cu(OAc)_2$ (1 mM), H_3btc (0.2 mM) and ethanol solution, respectively. In addition, there has 3 s showering time with ethanol between each immersion step. Thus process are repeated for 40 cycles, the SURMOFs samples are prepared at different ultrasonic treatment conditions under the same conditions, The XRD data shows all samples have similar crystallinity. Two strong peaks at 6.7° and 13.4° correspond to (200) and (400) peaks, which fit well with its corresponding calculated bulk XRD pattern (*Figure 51a*), indicating that the highly oriented HKUST-1 thin film can be obtained under ultrasonic treatment condition during the synthesis (*Figure 51b*).
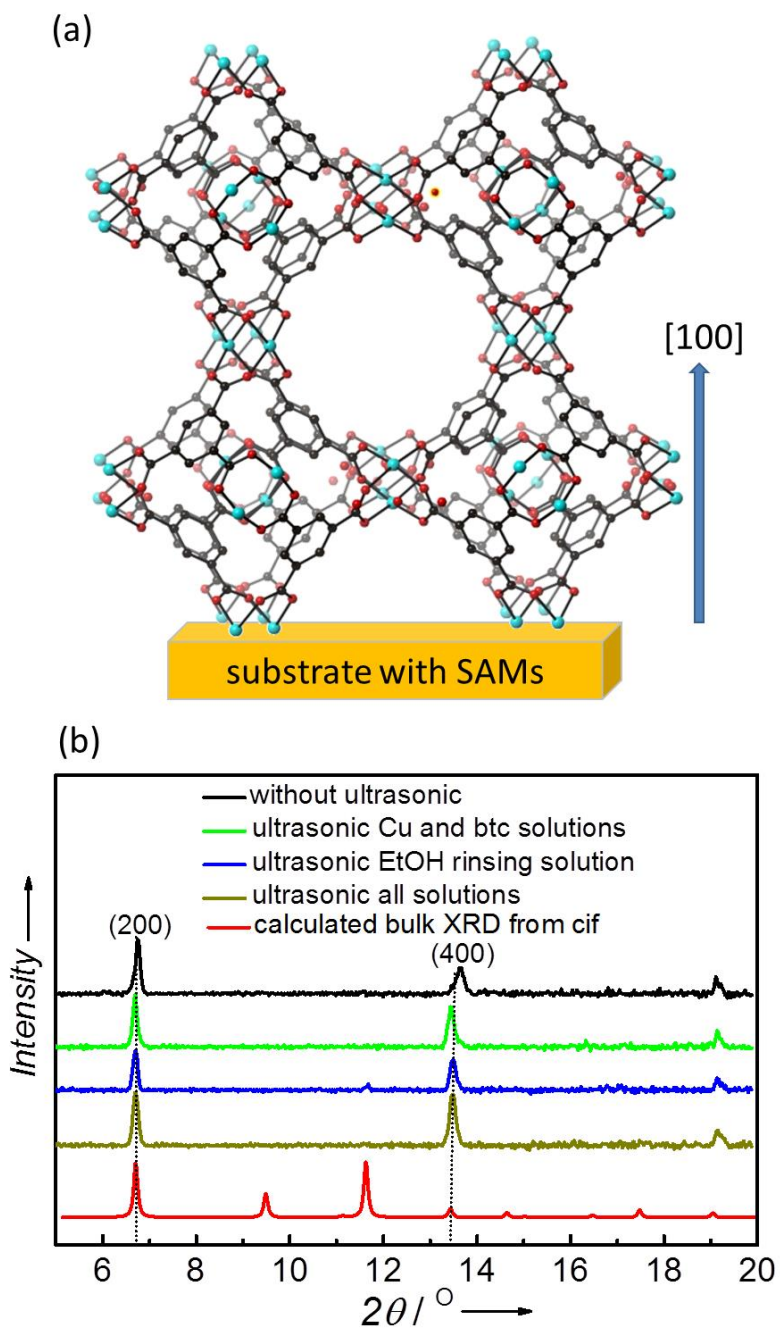
Figure 51. (a) The structure model of SURMOF HKUST-1 grown on MHDA SAM along [100] direction using LPE fashion; (b) The out of plane XRD of SURMOF HKUST-1 synthesized by using ultrasonic bath in the dipping robot system and calculated bulk XRD.
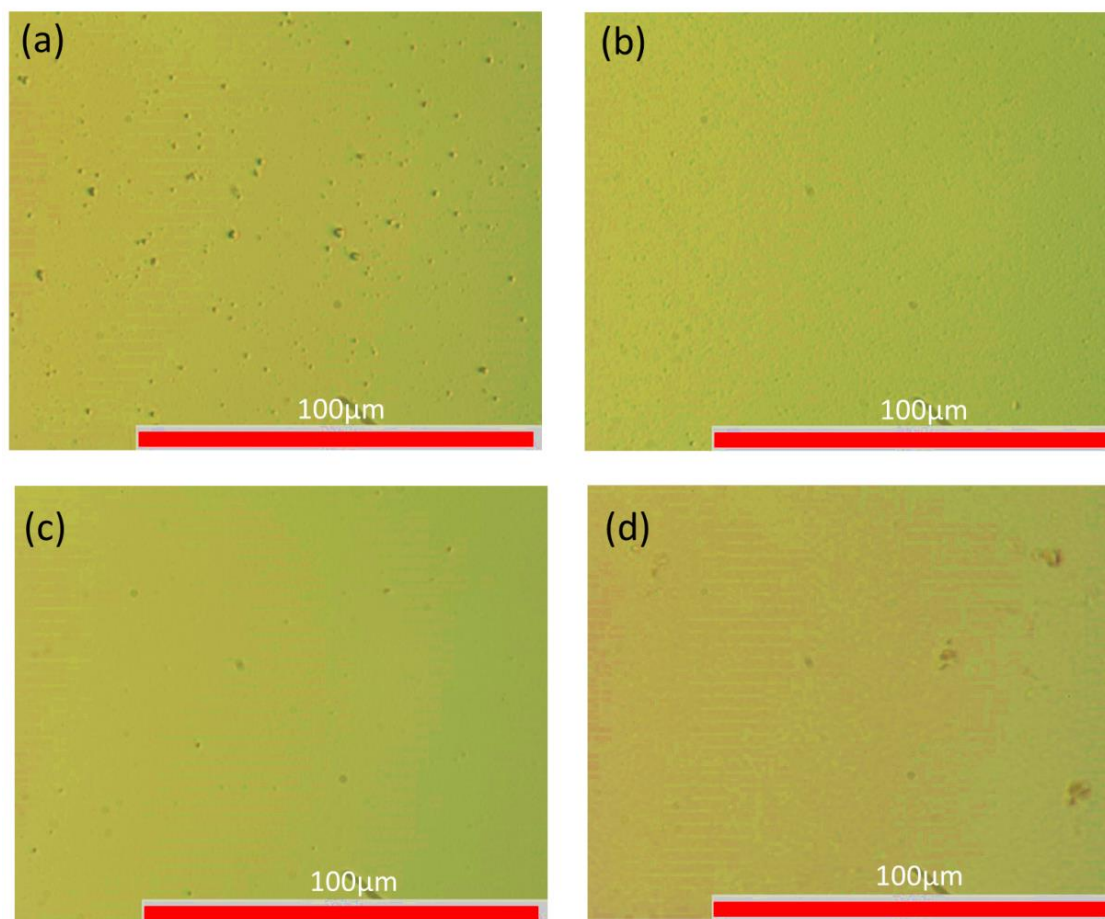
Figure 52. Optical microscopy images of HKUST-1 prepared without ultrasonic (a) and with ultrasonic treatment during immersion in rinsing ethanol (b), in metal salts and ligands solution (c) or in all solutions (metal ions, ligands and rinsing solutions) (d).
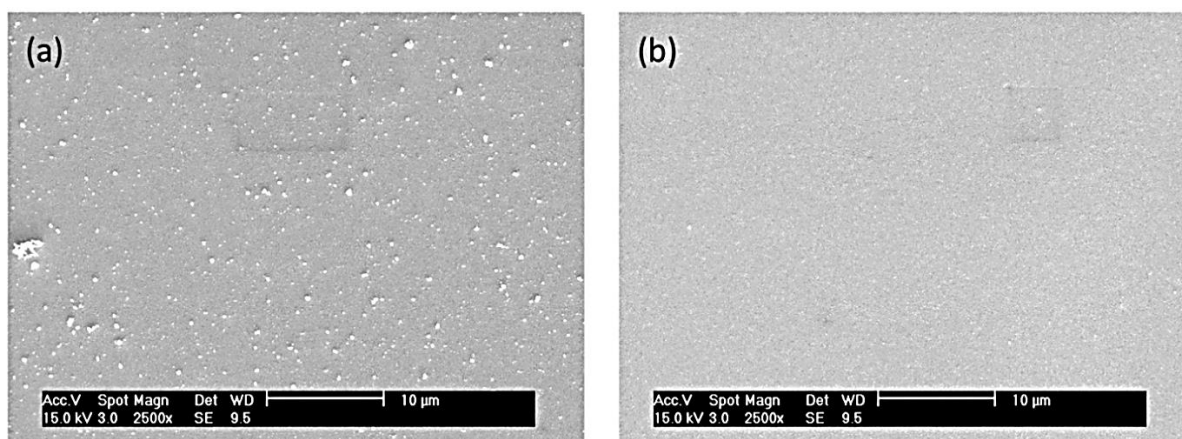
Figure 53. SEM images of SURMOF HKUST-1 prepared without ultrasonic (a) and with ultrasonic treatment during immersion in rinsing ethanol (b).

In this work, the morphologies of these HKUST-1 samples are investigated by optical microscopy, SEM and AFM. The optical microscopy, SEM and AFM images of SURMOF

HKUST-1 sample prepared without ultrasonic and with ultrasonic treatment during immersion in metal salts and ligand solution, in rinsing ethanol or in all solutions (metal salts, ligands and rinsing solutions) are shown in *Figure 52*, *Figure 53* and *Figure 54*, respectively. The Leica DM2500 M optical microscope was used to study the samples in transmission light bright filed and reflected light mode in this work. In the images of *Figure 52a*, many particles remain on the sample surface prepared without ultrasonic treatment during the synthesis. In contrast, the sample prepared with ultrasonic treatment is much smoother and more homogenous (*Figure 52b, c, d* and *Figure 54b, c, d*). The same phenomena are also observed in SEM images by comparison of the SURMOF HKUST-1 samples prepared without and with ultrasonic treatment during in the rinsing step (*Figure 53*). The SEM images show that the SURMOF prepared with ultrasonic treatment is much more homogeneous than the sample prepared without ultrasonic treatment. In addition, the height histogram in the four AFM images of SURMOF HKUST-1 prepared under different conditions shows that the SURMOF HKUST-1 prepared with ultrasonic treatment rinsing ethanol solution has the smallest surface roughness. This shows clearly that the introduction of ultrasonic instrument plays an important role in improving the quality of SURMOFs, in particular, ultrasonic treatment during the step of immersion of sample in rinsing ethanol.
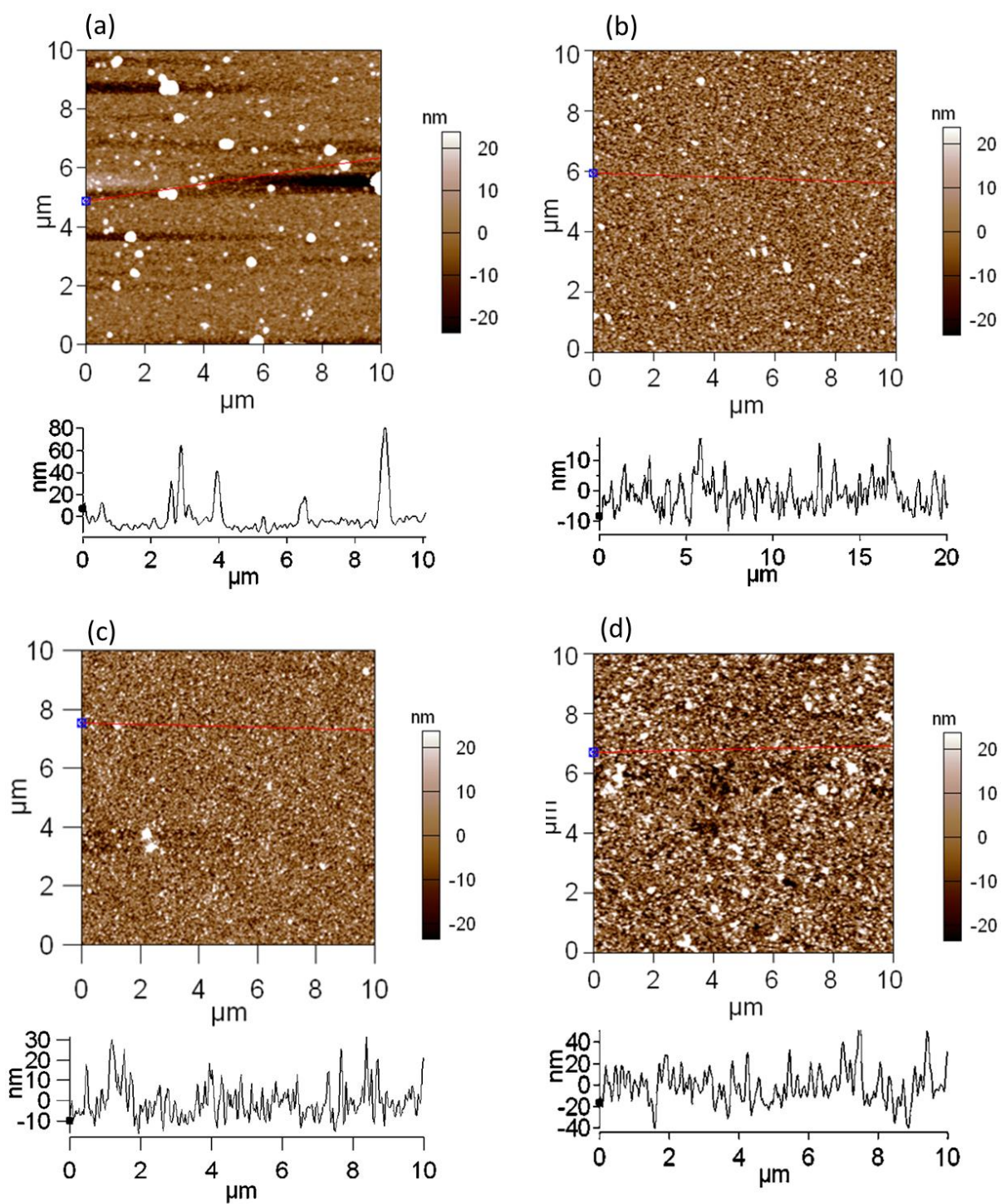
Figure 54. AFM images of HKUST-1 prepared without ultrasonic (a) and with ultrasonic treatment during immersion in rinsing ethanol (b), metal salts and ligands solutions (c) or all the solutions (metal salts, ligands and rinsing solutions) (d).

5.2 Patterned SURMOF

Micro contact printing (μCp) is an important technique for fabrication of patterns on

substrates.[112-113] An elastomeric polydimethylsiloxane (PDMS) stamp with different patterns, such as line, square, and circular pattern, etc can be used during the μCp process.
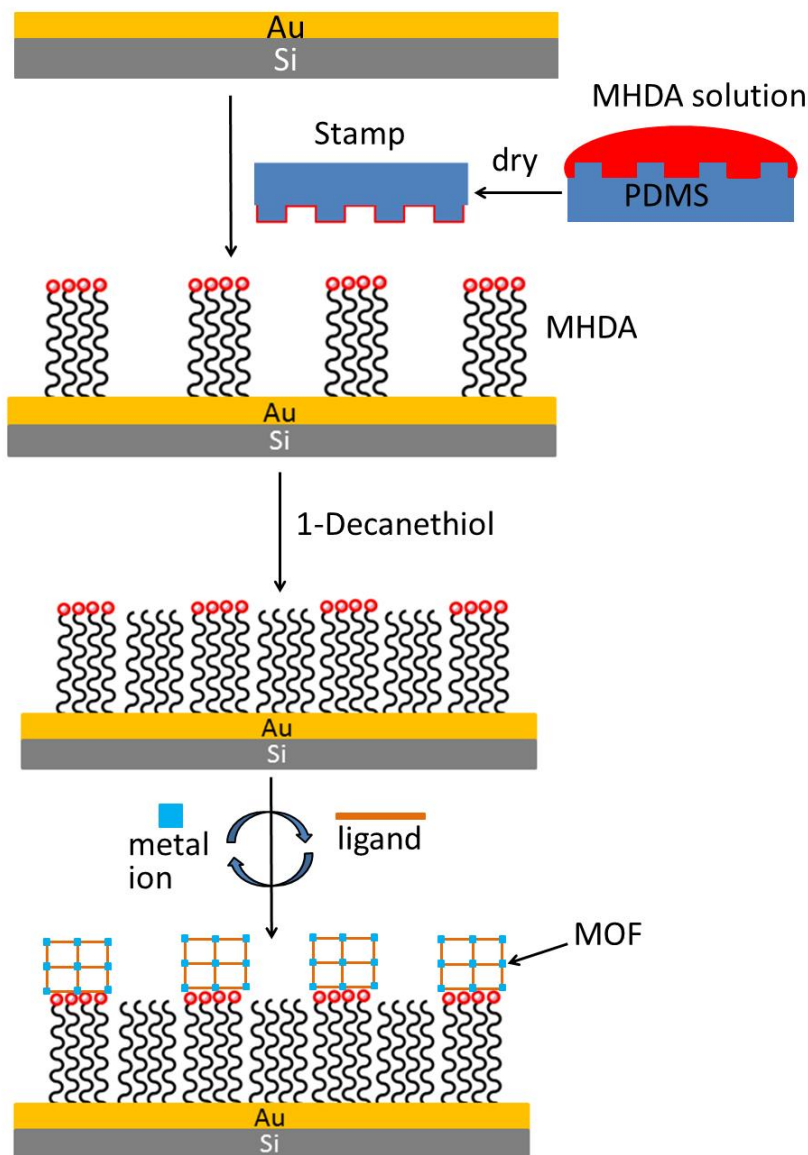
Figure 55. The patterned SURMOF grown on a patterned substrate prepared with Micro contact printing (μCp) stamp.

In this work, in order to get patterned SURMOFs, patterned MHDA substrate prepared by μCp technique are used to grow SURMOF. 1mM of MHDA solution is deposited on a clean polydimethylsiloxan (PDMS) stamp for 2 min. After drying with nitrogen, the stamp is gently pressed on the clean Au substrate for 1 min to get a patterned MHDA SAMs substrate. In order to enhance the quality of the patterned substrate, the patterned substrate is immersed into 1mM 1-Decanethiol solution for 1 min to block the non-patterned area with 1-decanethiol (*Figure 55*). This patterned substrate is used to prepare the patterned SURMOF by the LPE process, which has been described in detail by Ladnorg et al.[114]

For the purpose of comparison, two patterned SURMOF HKUST-1 samples (40 cycles) were prepared by μCp technique without and with ultrasonic treatment during the preparation. The out of plane XRD data of these two samples show two strong peaks at 6.7° and 13.4°, which correspond to (200) and (400) peaks in the calculated bulk XRD (*Figure 56*). This reveals the presence of highly oriented HKUST-1 thin film with a [100] growth direction in both cases.
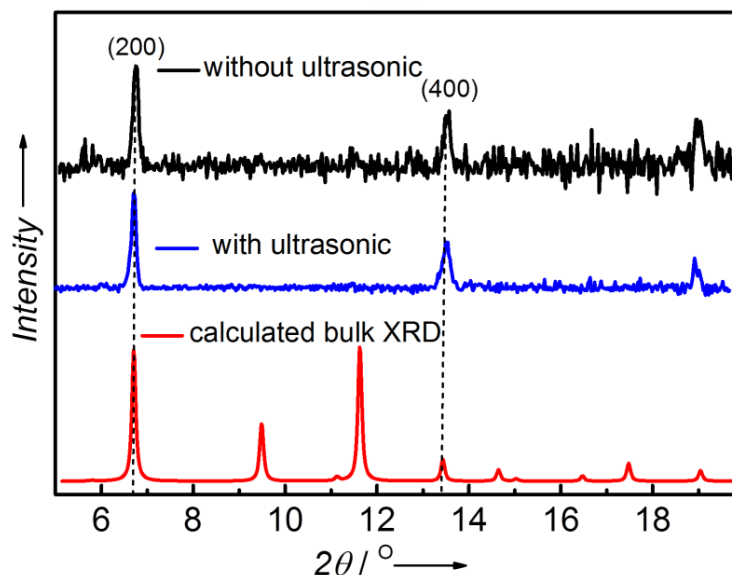
Figure 56. The out of plane XRD of patterned HKUST-1 prepared by dipping robot without and with ultrasonic treatment.

The morphologies of these two patterned samples (without and with ultrasonic treatment) were characterized with the optical microscopy. It clearly shows that the morphology of patterned SURMOF HKUST-1 prepared by using ultrasonic treatment (*Figure 57b*) is better than that of the SURMOF HKUST-1 prepared without ultrasonic treatment (*Figure 57a*). The sample prepared by ultrasonic bath shows the line patterns clearly and the SURMOF was grown only on the MHDA SAMs patterned area.
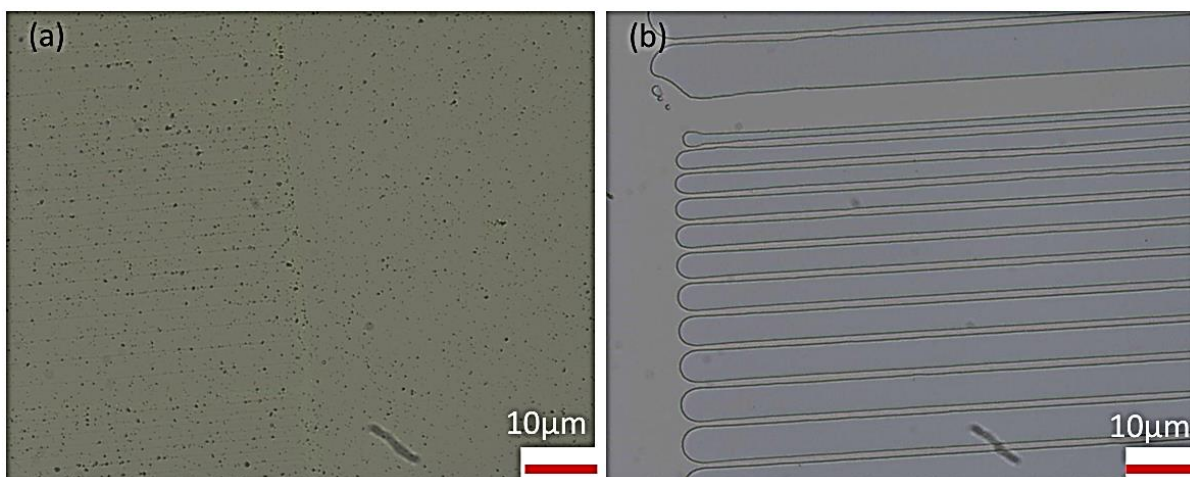
Figure 57. The optical microscopy images of patterned HKUST-1 prepared by dipping robot without (a) and with ultrasonic (b) treatment.
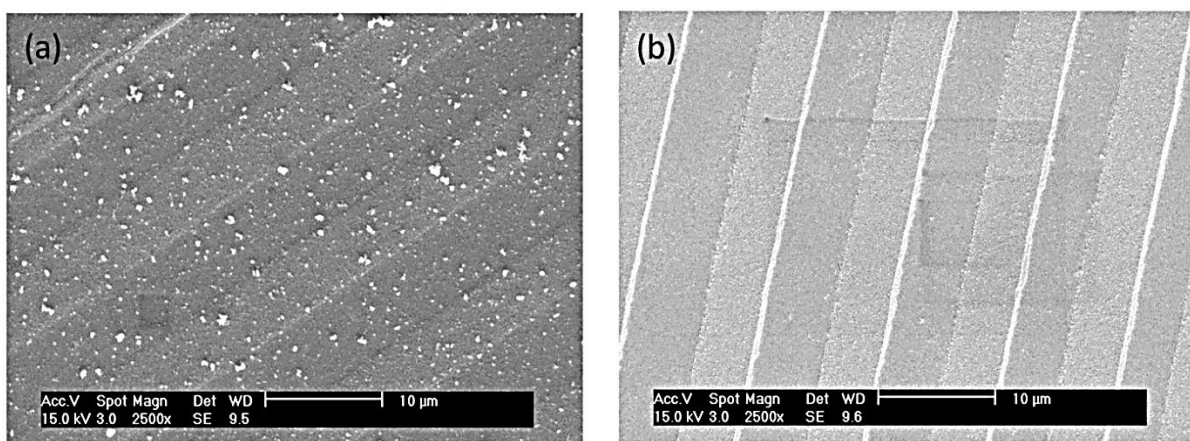
Figure 58. The SEM images of patterned HKUST-1 prepared by dipping robot without ultrasonic (a) and with ultrasonic (b) treatment.

The obvious difference between the patterned SURMOF HKUST-1 samples prepared without ultrasonic and with ultrasonic treatment during the preparations is also observed from the SEM images in *Figure 58*.
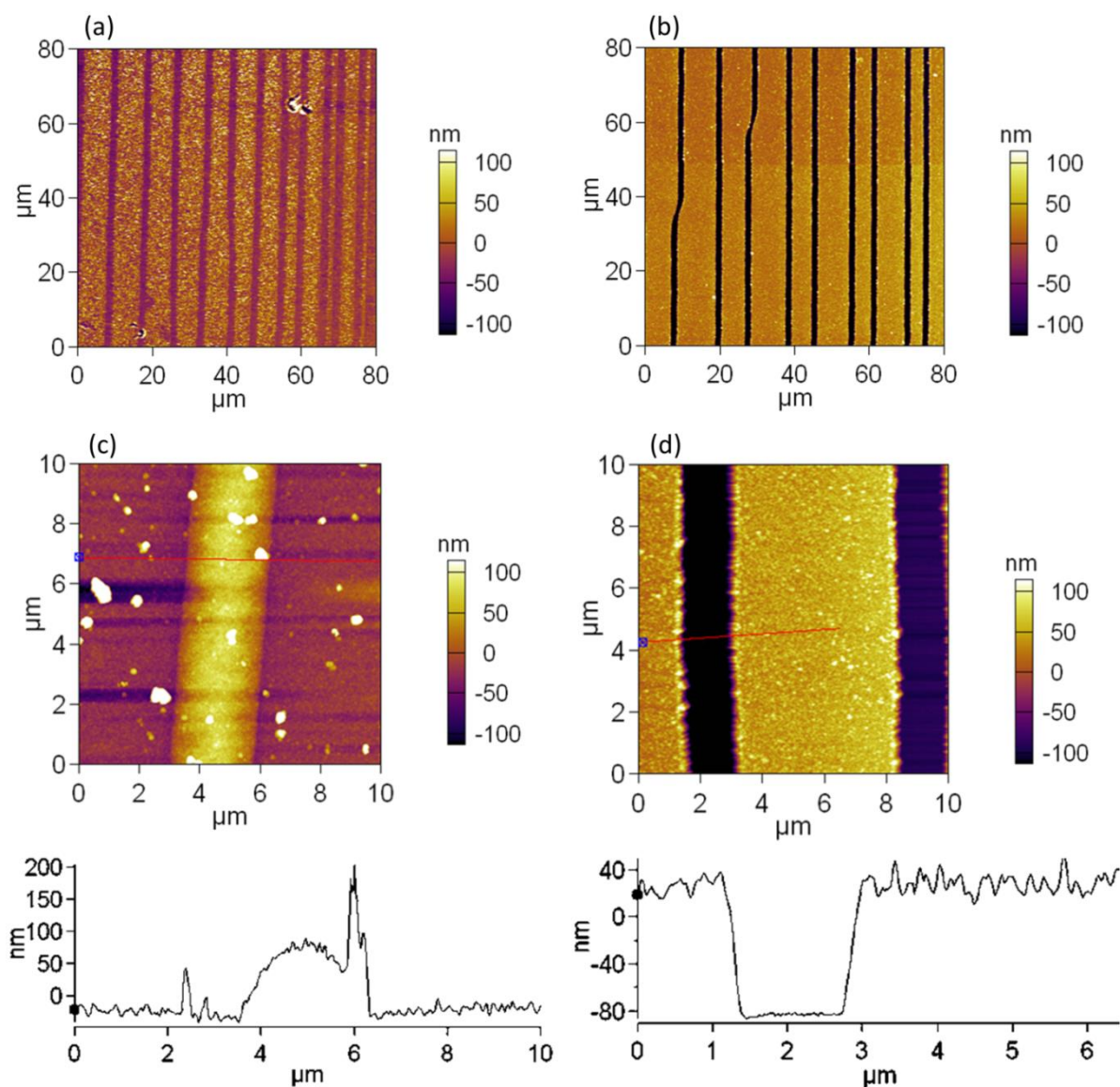
Figure 59. The AFM images and thickness measurement of patterned HKUST-1 prepared by dipping robot without (a, c) and with ultrasonic (b, d) treatment.

The AFM images of the patterned SURMOF HKUST-1 samples prepared without ultrasonic treatment are shown in the *Figure 59a and c*. Because of the remaining particles on the patterned and non-patterned areas, it is difficult to determine the film thickness on this patterned sample.

In contrast, the patterns of the sample prepared with ultrasonic treatment, are clearly visible. The HKUST-1 is grown only on the area with line patterns. The height histogram performed on a line is used to calculate the height of the SURMOF thin film. This shows that the height of patterned SURMOF HKUST-1 prepared with ultrasonic treatment is more accurate than that prepared without ultrasonic treatment (*Figure 59*).

5.3 Concentration dependence of the thickness and roughness of SURMOF HKUST-1

In order to improve the SURMOFs quality, the influence of the concentrations of the reagent (metal salts and organic ligands) solutions on the thickness and roughness of SURMOF was investigated. The SURMOF HKUST-1 was prepared with ultrasonic treatment during the rinsing ethanol step. The patterned Au substrate was prepared by μCp technique and was sequentially immersed into $Cu(OAc)_2$ and H_3btc ligands solutions by step by step fashion,[46] a patterned SURMOF HKUST-1 after 40 immersion cycles was obtained. Five SURMOF HKUST-1 samples were prepared by different concentrations: (a) 1 mM $Cu(OAc)_2$ and 0.2 mM H_3btc; (b) 0.1 mM $Cu(OAc)_2$ and 0.02 mM H_3btc; (c) 0.02 mM $Cu(OAc)_2$ and 0.004 mM H_3btc; (d) 0.01 mM $Cu(OAc)_2$ and 0.002 mM H_3btc; (e) 0.005 mM $Cu(OAc)_2$ and 0.001 mM H_3btc. The samples with smooth patterns are used to determine the thickness from the height histogram in AFM images (*Figure 60*). The thicknesses of the HKUST-1 prepared by using different concentrations are ~116 nm, ~88 nm, ~44 nm, ~24 nm and ~6 nm for the concentrations of a, b, c, d and e, respectively. The thickness of HKUST-1 increases with increasing concentration of metal and ligand solutions (*Figure 61a*).

This shows that with the here used parameters and a concentration of 0.01 mM $Cu(OAc)_2$ and 0.002 mM H_3btc, a SURMOF HKUST-1 growth is realized where (in average) one unit cell is synthesized every four synthesis steps-exactly the value which follows from a naive layer-by-layer method.

In order to study the roughnesses of SURMOF HKUST-1 prepared by using different reagent concentrations, a square area of 2 μm × 2 μm was chosen as shown in *Figure 60*. The roughness was calculated by root-mean-square (RMS) approach and the roughnesses of SURMOF HKUST-1 samples prepared with the different concentrations (a, b, c, d and e) are ~51 nm, ~35 nm, ~16nm, ~11 nm and ~3 nm, respectively (*Figure 61b*). The relative roughnesses (roughness/thickness) of SURMOFs HKUST-1 prepared by using different reagent concentrations are shown in *Figure 62*. This shows that the relative roughness of SURMOF is hardly influenced by concentrations of the reagent solutions.
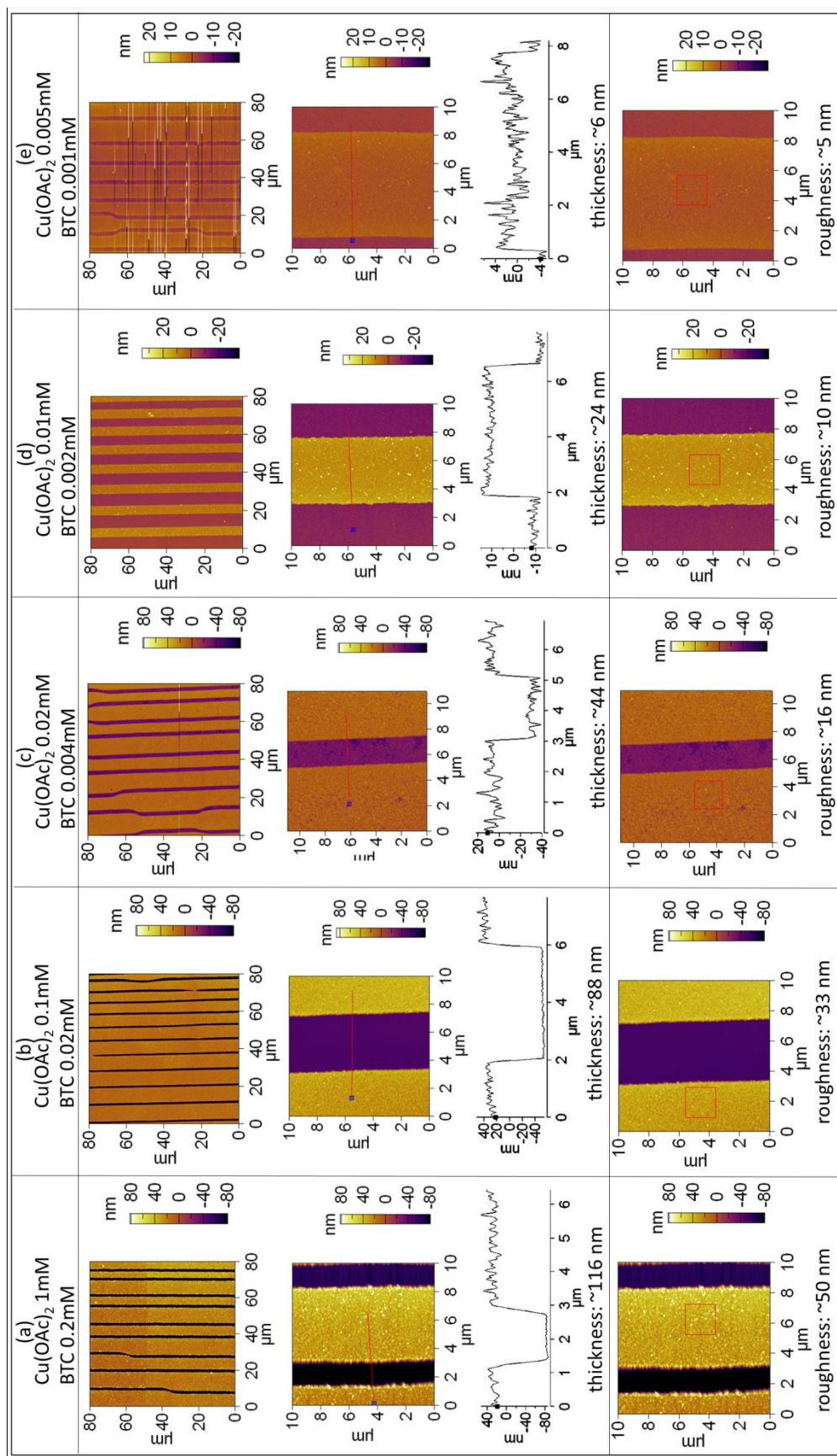
Figure 60. The AFM images, thickness and roughness measurement of SURMOF HKUST-1 prepared by different concentrations: (a) 1 mM Cu(OAc)$_2$ and 0.2 mM H$_3$btc; (b) 0.1 mM Cu(OAc)$_2$ and 0.02 mM H$_3$btc; (c) 0.02 mM Cu(OAc)$_2$ and 0.004 mM H$_3$btc; (d) 0.01 mM Cu(OAc)$_2$ and 0.002 mM H$_3$btc; (e) 0.005 mM Cu(OAc)$_2$ and 0.001 mM H$_3$btc. The same scales are measured by size of 80 μm × 80 μm and 10 μm × 10 μm, in which the thicknesses measurement was taken by 10 μm × 10 μm. The area of roughness calculation was taken by 2 μm × 2 μm.

77
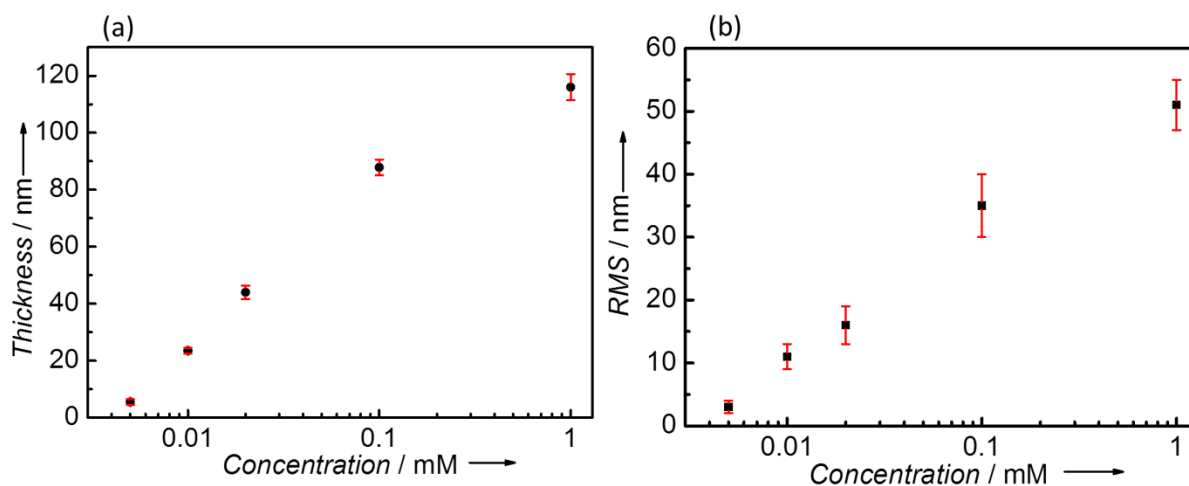
Figure 61. The thicknesses and root-mean-square (RMS) roughnesses of SURMOF HKUST-1 prepared by different concentrations: (a) 1 mM Cu(OAc)$_2$ and 0.2 mM H$_3$btc; (b) 0.1 mM Cu(OAc)$_2$ and 0.02 mM H$_3$btc; (c) 0.02 mM Cu(OAc)$_2$ and 0.004 mM H$_3$btc; (d) 0.01 mM Cu(OAc)$_2$ and 0.002 mM H$_3$btc; (e) 0.005 mM Cu(OAc)$_2$ and 0.001 mM H$_3$btc.
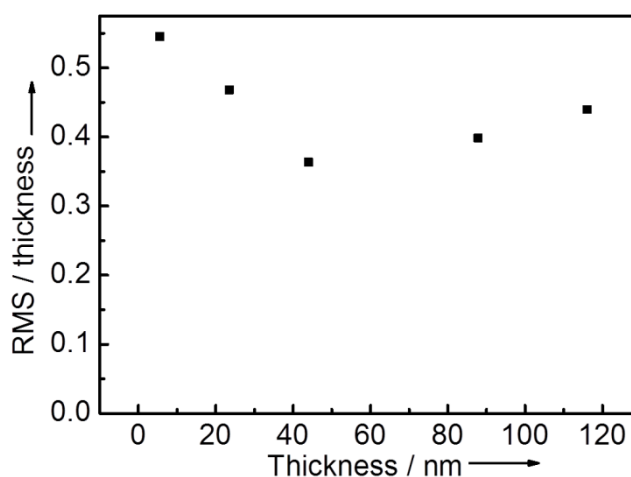
Figure 62. Relative roughness of SURMOF HKUST-1 prepared by different concentrations.

5.4 Concentration dependence of the thickness and roughness of SURMOF-2

The same optimization process for SURMOF HKUST-1 is also carried out for the SURMOF-2 Cu(bdc) synthesis. The sample was prepared with dipping time 600, 900 and 100 s for Cu(OAc)$_2$ (1 mM), H$_2$bdc (0.2 mM) and ethanol solutions, respectively. In each step, there is 3 s for showering. The XRD result of the Cu(bdc) sample shows there are two strong peaks at 8.3º and 16.6º, which correspond to (100) and (200) peaks in the calculated bulk XRD (*Figure 63b*), indicating a highly oriented SURMOF-2 film with a [100] growth direction

(*Figure 63a*). The patterned SURMOF-2 Cu(bdc) (40 cycles) grown on MHDA SAMs were prepared by dipping robot method using different concentrations of the reagent solutions (Cu(OAc)$_2$ and H$_2$bdc): (a) 0.05 mM Cu(OAc)$_2$ and 0.01 mM H$_2$bdc; (b) 0.02 mM Cu(OAc)$_2$ and 0.004 mM H$_2$bdc; (c) 0.01 mM Cu(OAc)$_2$ and 0.002 mM H$_2$bdc; (d) 0.005 mM Cu(OAc)$_2$ and 0.001 mM H$_2$bdc.
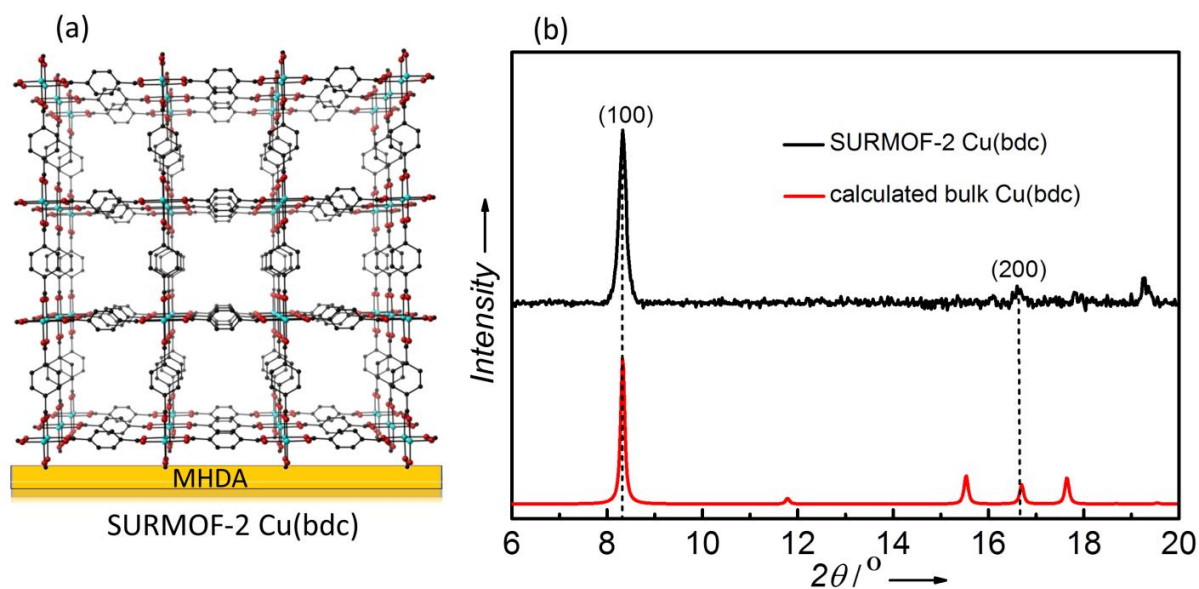
Figure 63. (a) The structure model of SURMOF-2 Cu(bdc); (b) The out of plane XRD of flat SURMOF Cu(bdc) prepared by dipping robot with ultrasonic treatment.

The AFM images of SURMOF-2 Cu(bdc) prepared using different concentrations are shown in *Figure 64*. The thicknesses of SURMOF-2 Cu(bdc) increase with increasing concentration of metal and ligand solutions: ~73 nm, ~42 nm, ~18 nm and ~7 nm for concentrations of a, b, c and d, respectively (*Figure 65a*). A square area of 4 µm^2 in SURMOF-2 Cu(bdc) samples prepared with the different concentrations a, b, c and d was chosen to calculate the roughness (*Figure 64*). The roughnesses are ~31 nm, ~16nm and ~9 nm and ~3 nm, respectively (*Figure 65b*).

This shows that by using a concentration of 0.02 mM Cu(OAc)$_2$ and 0.004 mM H$_2$bdc the thickness of the SURMOF-2 Cu(bdc) prepared in one growth step fits exactly the value of one unit cell in (1.1 nm). This means it follows the layer-by-layer growth model.
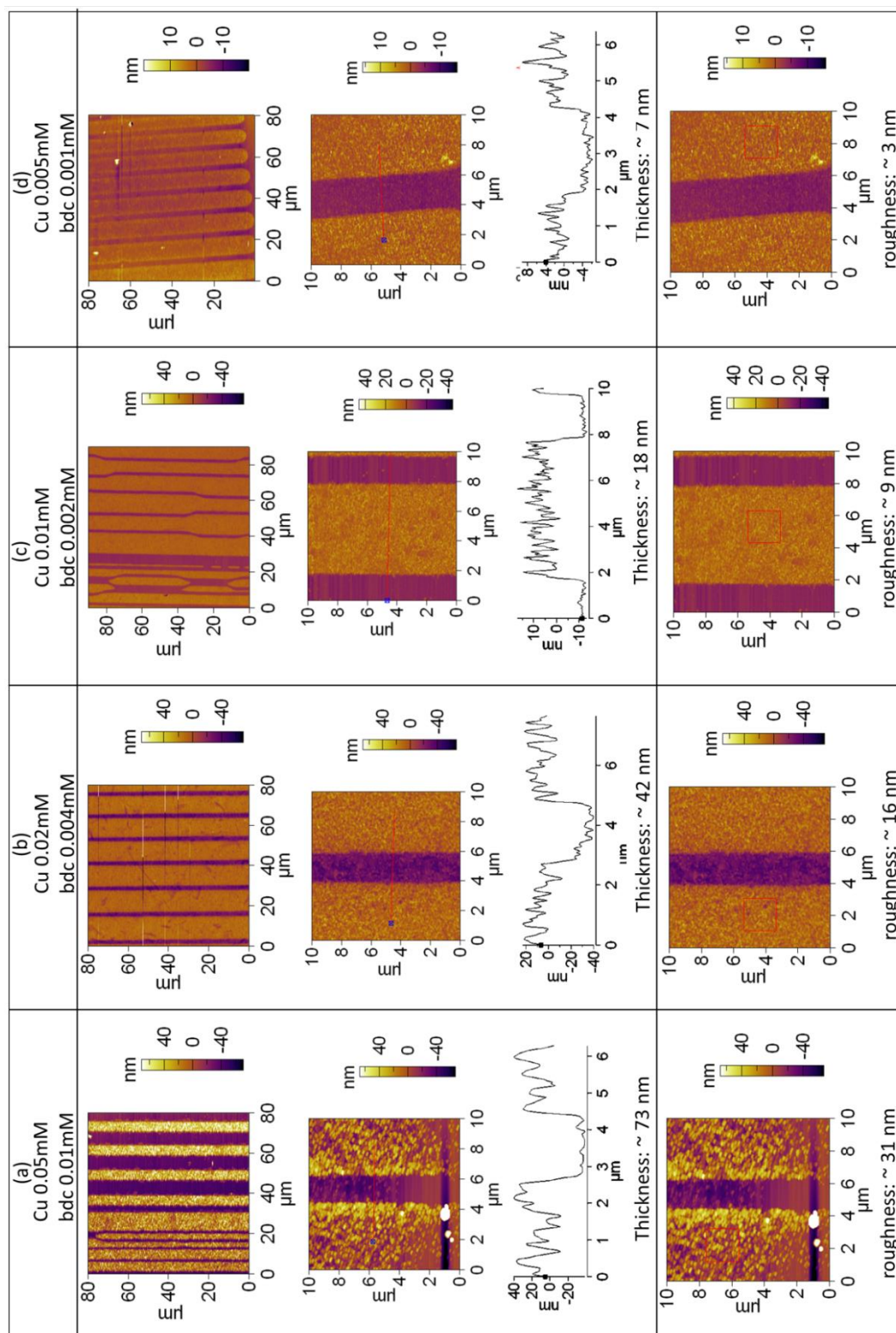
Figure 64. The AFM images and thickness measurement of SURMOF-2 Cu-BDC prepared by different concentrations: (a) 0.05 mM Cu(OAc)$_2$ and 0.01 mM H$_2$bdc; (b) 0.02 mM Cu(OAc)$_2$ and 0.004 mM H$_2$bdc; (c) 0.01 mM Cu(OAc)$_2$ and 0.002 mM H$_2$bdc; (d) 0.005 mM Cu(OAc)$_2$ and 0.001 mM H$_2$bdc.
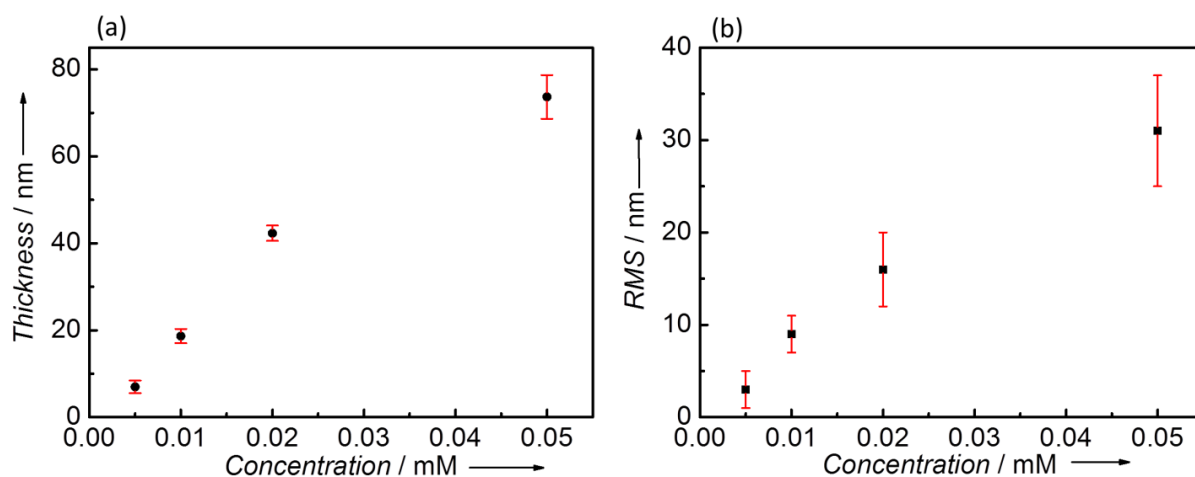
Figure 65. Thicknesses and root-mean-square (RMS) roughnesses of SURMOF-2 Cu(bdc) prepared by different concentrations: (a) 0.05 mM Cu(OAc)$_2$ and 0.01 mM H$_2$bdc; (b) 0.02 mM Cu(OAc)$_2$ and 0.004 mM H$_2$bdc; (c) 0.01 mM Cu(OAc)$_2$ and 0.002 mM H$_2$bdc; (d) 0.005 mM Cu(OAc)$_2$ and 0.001 mM H$_2$bdc.

5.5 Conclusion

Based on the results of HKUST-1 and SURMOF-2 Cu(bdc), the SURMOF quality can be dramatically improved by using a dipping robot. In this work, homogenous, compact and smooth SURMOFs were successfully prepared by using a dipping robot. This is not only because of the separated metal salts, organic ligands and rinsing solvent solutions into individual immersion containers, but also due to is the introduction of ultrasonic bath during the preparation process. The individual immersion fashion of reagent solutions can avoids the metal salts and organic ligands contaminating with each other during the preparation. Ultrasonic bath is a efficient instrument for cleaning the sample during the rinsing steps. In this work, the morphologies of the SURMOF were measured by optical microscopy, SEM and AFM. It shows that the samples prepared with ultrasonic treatment have very good quality. On the other hand, the thicknesses of SURMOF can be controlled by the numbers of deposition cycles exactly.[53] Furthermore, the thickness and roughness of the SURMOF are also controlled by adjusting the concentration of the reagent solutions during the SURMOF preparation with the dipping robot method. The thicknesses and roughnesses of the SURMOF increase with increasing reagent concentration. Therefore, a layer-by-layer SURMOF growth with one unit cell per cycle can be exactly controlled by using dipping robot method.

6 CONCLUSIONS

Metal organic frameworks (MOFs) consist of metal ions coordinated to organic ligands to build 1D, 2D or 3D crystalline frameworks. Numerous fields of science have shown that MOF materials can be used for various applications, such as gas storage, separation and catalysis. Chiral MOFs have shown potential applications in enantioselective adsorption and separation, as well as in asymmetric catalysis.

In this thesis, the objective focuses on preparation of new class surface mounted metal-organic frameworks (SURMOFs). SURMOFs grown on functionalized substrates by using liquid phase epitaxy (LPE) are highly oriented, homogeneous porous MOFs thin films.

The LPE approach of SURMOFs is based on sequentially immersion of functionalized substrate in the metal salts, organic ligands and rinsing solvent solutions, which can control the thickness and homogeneity of the MOF thin film. Therefore this method is suited for the fabrication of controllable layers with hetero-layers structure. In addition, the orientation of MOF crystallinity can be controlled by using different functional group on the substrate.

The primary focus of this work is to grow a series of homochiral SURMOFs with different pillaring ligands on substrates using LPE method. The isoreticular homochiral SURMOFs are not only chiral, they also possess different pore sizes with the same secondary building chiral layer unit. In this thesis, the enantioselectivty of a pair of chiral probe molecules, R- and S-Limonene, by three isoreticular chiral SURMOFs, $[Cu_2(Dcam)_2(dabco)]$, $[Cu_2(Dcam)_2(bipy)]$ and $[Cu_2(Dcam)_2(bipyb)]$ with identical chiral centers and different pore sizes was studied. It was found that the adsorption capacity increases with increasing pore size. For the enantiomer separation a more complex situation was found, where the highest enantiomer excess was found for SURMOF with the medium pore size while the enantiomer excess for very small and large pores is significantly smaller. This study shows that not only the chiral center also the pore size determine the enantioselectivity.

The quartz glass is chosen as substrate for the chirality investigation of SURMOFs. These chiral SURMOFs grown on quartz glass are sensitive to the signal of circular dichroism (CD), which is used to characterize the chirality of SURMOFs. There are some reports about the chirality of chiral bulk MOFs, displaying the mixed orientations in the chiral MOFs. However, the investigation of chirality in chiral MOF grown on different orientations has not been reported. In this work, the observed decrease in the oriented circular dichroism (OCD) band intensity going from a [001] to a [110] growth orientation of chiral SURMOF $[Cu_2(Dcam)_2(dabco)]$ demonstrates that SURMOFs are ideal materials for investigating the

dependence of CD on the orientation of the electric field vector to the corresponding transition dipole moment of the corresponding electronic excitation. In addition to demonstrate the huge potential of empty SURMOF lattices for OCD investigations, the enantioselective loading of the enantiopure SURMOFs [Cu_2(Dcam)$_2$(dabco)] and [Cu_2(Lcam)$_2$(dabco)] with (+)-ethyl-D-lactate and (-)-ethyl-L-lactate were also studied by using OCD. When exposing the homochiral SURMOFs to a racemic mixture of the ethyl lactate enantiomers, the OCD data directly demonstrated the selective enrichment of one of the enantiomers. A quantitative analysis of these data allowed for a determination of both, relative and absolute amounts of adsorbed guest molecules with different chirality. Therefore the combination of SURMOFs with CD spectroscopy carries a huge potential for investigations of the interactions of chiral host with enantiopure MOF materials with regard to applications as filter and membrane materials, which might contribute to the highly interesting filed of enantiomer separation.

The SURMOFs quality is optimized with the introduction of ultrasonic treatment in this thesis. The new setup dipping robot is an automated, computer controlled robot, which is used to improve the quality of SURMOFs by dipping the sample sequentially into the synthesis solutions. Due to the introduction of ultrasonic bath, the rising steps are efficiently enhanced for cleaning the sample. In this work, SURMOF HKUST-1 and SURMOF-2 Cu(bdc) were prepared by dipping robot method with different concentrations of reagent solutions. The morphologies of the SURMOFs were measured by optical microscopy, SEM and AFM. The thickness and roughness of the SURMOF is depended on the concentrations of metal salts and organic ligands solutions during the SURMOF preparation. The thicknesses and roughnesses of the SURMOF increase with increasing reagent concentrations, which show a naive layer-by-layer growth exactly according to the unit cell of MOF structure.

7 REFERENCES

[1]   Tranchemontagne, D. J.; Mendoza-Cortes, J. L.; O'Keeffe, M.; Yaghi, O. M., Secondary building units, nets and bonding in the chemistry of metal-organic frameworks. *Chemical Society Reviews* 2009, *38* (5), 1257-1283.

[2]   Makiura, R.; Motoyama, S.; Umemura, Y.; Yamanaka, H.; Sakata, O.; Kitagawa, H., Surface nano-architecture of a metal-organic framework. *Nature Materials* 2010, *9* (7), 565-571.

[3]   Horcajada, P.; Chalati, T.; Serre, C.; Gillet, B.; Sebrie, C.; Baati, T.; Eubank, J. F.; Heurtaux, D.; Clayette, P.; Kreuz, C.; Chang, J. S.; Hwang, Y. K.; Marsaud, V.; Bories, P. N.; Cynober, L.; Gil, S.; Ferey, G.; Couvreur, P.; Gref, R., Porous metal-organic-framework nanoscale carriers as a potential platform for drug delivery and imaging. *Nature Materials* 2010, *9* (2), 172-178.

[4]   Furukawa, H.; Ko, N.; Go, Y. B.; Aratani, N.; Choi, S. B.; Choi, E.; Yazaydin, A. O.; Snurr, R. Q.; O'Keeffe, M.; Kim, J.; Yaghi, O. M., Ultrahigh Porosity in Metal-Organic Frameworks. *Science* 2010, *329* (5990), 424-428.

[5]   Wang, B.; Cote, A. P.; Furukawa, H.; O'Keeffe, M.; Yaghi, O. M., Colossal cages in zeolitic imidazolate frameworks as selective carbon dioxide reservoirs. *Nature* 2008, *453* (7192), 207-212.

[6]   Cook, T. R.; Zheng, Y. R.; Stang, P. J., Metal-Organic Frameworks and Self-Assembled Supramolecular Coordination Complexes: Comparing and Contrasting the Design, Synthesis, and Functionality of Metal-Organic Materials. *Chemical Reviews* 2013, *113* (1), 734-777.

[7]   Corma, A.; Garcia, H.; Xamena, F. X. L., Engineering Metal Organic Frameworks for Heterogeneous Catalysis. *Chemical Reviews* 2010, *110* (8), 4606-4655.

[8]   Ferey, G.; Mellot-Draznieks, C.; Serre, C.; Millange, F.; Dutour, J.; Surble, S.; Margiolaki, I., A chromium terephthalate-based solid with unusually large pore volumes and surface area. *Science* 2005, *309* (5743), 2040-2042.

[9]   Hermes, S.; Schroder, F.; Amirjalayer, S.; Schmid, R.; Fischer, R. A., Loading of porous metal-organic open frameworks with organometallic CVD precursors: inclusion compounds of the type [L_nM]$_a$@MOF-5. *Journal of Materials Chemistry* 2006, *16* (25), 2464-2472.

[10]   Lin, Z. J.; Liu, T. F.; Huang, Y. B.; Lu, J.; Cao, R., A Guest-Dependent Approach to Retain Permanent Pores in Flexible Metal-Organic Frameworks by Cation Exchange.

Chemistry-A European Journal 2012, *18* (25), 7896-7902.

[11]   Spokoyny, A. M.; Kim, D.; Sumrein, A.; Mirkin, C. A., Infinite coordination polymer nano- and microparticle structures. *Chemical Society Reviews* 2009, *38* (5), 1218-1227.

[12]   Imaz, I.; Rubio-Martinez, M.; An, J.; Sole-Font, I.; Rosi, N. L.; Maspoch, D., Metal-biomolecule frameworks (MBioFs). *Chemical Communications* 2011, *47* (26), 7287-7302.

[13]   Cho, K. R.; Salter, E. A.; De Yoreo, J. J.; Wierzbicki, A.; Elhadj, S.; Huang, Y.; Qiu, S. R., Impact of Chiral Molecules on the Formation of Biominerals: A Calcium Oxalate Monohydrate Example. *Crystal Growth & Design* 2012, *12* (12), 5939-5947.

[14]   Georgiev, I. G.; MacGillivray, L. R., Metal-mediated reactivity in the organic solid state: from self-assembled complexes to metal-organic frameworks. *Chemical Society Reviews* 2007, *36* (8), 1239-1248.

[15]   Falcaro, P.; Buso, D.; Hill, A. J.; Doherty, C. M., Patterning Techniques for Metal Organic Frameworks. *Advanced Materials* 2012, *24* (24), 3153-3168.

[16]   Zou, F.; Yu, R. H.; Li, R. G.; Li, W., Microwave-Assisted Synthesis of HKUST-1 and Functionalized HKUST-1@$H_3PW_{12}O_{40}$: Selective Adsorption of Heavy Metal Ions in Water Analyzed with Synchrotron Radiation. *ChemPhysChem* 2013, *14* (12), 2825-2832.

[17]   Lam, F. L. Y.; Hu, X. J., In situ oxidation for stabilization of Fe/MCM-41 catalyst prepared by metal organic chemical vapor deposition. *Catalysis Communications* 2007, *8* (11), 1719-1723.

[18]   Kitagawa, S.; Kitaura, R.; Noro, S., Functional porous coordination polymers. *Angewandte Chemie-International Edition* 2004, *43* (18), 2334-2375.

[19]   Li, Y. Q.; Ben, T.; Zhang, B. Y.; Fu, Y.; Qiu, S. L., Ultrahigh Gas Storage both at Low and High Pressures in KOH-Activated Carbonized Porous Aromatic Frameworks. *Scientific Reports* 2013, *3*.

[20]   Adams, R.; Carson, C.; Ward, J.; Tannenbaum, R.; Koros, W., Metal organic framework mixed matrix membranes for gas separations. *Microporous and Mesoporous Materials* 2010, *131* (1-3), 13-20.

[21]   Sun, C. Y.; Qin, C.; Wang, C. G.; Su, Z. M.; Wang, S.; Wang, X. L.; Yang, G. S.; Shao, K. Z.; Lan, Y. Q.; Wang, E. B., Chiral Nanoporous Metal-Organic Frameworks with High Porosity as Materials for Drug Delivery. *Advanced Materials* 2011, *23* (47), 5629-5632.

[22]   Ma, L. Q.; Abney, C.; Lin, W. B., Enantioselective catalysis with homochiral metal-organic frameworks. *Chemical Society Reviews* 2009, *38* (5), 1248-1256.

[23]   Furukawa, H.; Cordova, K. E.; O'Keeffe, M.; Yaghi, O. M., The Chemistry and Applications of Metal-Organic Frameworks. *Science* 2013, *341* (6149), 974.

[24]   Eddaoudi, M.; Kim, J.; Rosi, N.; Vodak, D.; Wachter, J.; O'Keeffe, M.; Yaghi, O. M., Systematic design of pore size and functionality in isoreticular MOFs and their application in methane storage. *Science* 2002, *295* (5554), 469-472.

[25]   Chui, S. S. Y.; Lo, S. M. F.; Charmant, J. P. H.; Orpen, A. G.; Williams, I. D., A chemically functionalizable nanoporous material $[Cu_3(TMA)_2(H2O)_3]_n$. *Science* 1999, *283* (5405), 1148-1150.

[26]   Petit, C.; Bandosz, T. J., Synthesis, Characterization, and Ammonia Adsorption Properties of Mesoporous Metal-Organic Framework (MIL(Fe))-Graphite Oxide Composites: Exploring the Limits of Materials Fabrication. *Advanced Functional Materials* 2011, *21* (11), 2108-2117.

[27]   Larsen, R. W.; Wojtas, L.; Perman, J.; Musselman, R. L.; Zaworotko, M. J.; Vetromile, C. M., Mimicking Heme Enzymes in the Solid State: Metal-Organic Materials with Selectively Encapsulated Heme. *Journal of the American Chemical Society* 2011, *133* (27), 10356-10359.

[28]   Xiao, B.; Wheatley, P. S.; Zhao, X. B.; Fletcher, A. J.; Fox, S.; Rossi, A. G.; Megson, I. L.; Bordiga, S.; Regli, L.; Thomas, K. M.; Morris, R. E., High-capacity hydrogen and nitric oxide adsorption and storage in a metal-organic framework. *Journal of the American Chemical Society* 2007, *129* (5), 1203-1209.

[29]   Chae, H. K.; Siberio-Perez, D. Y.; Kim, J.; Go, Y.; Eddaoudi, M.; Matzger, A. J.; O'Keeffe, M.; Yaghi, O. M., A route to high surface area, porosity and inclusion of large molecules in crystals. *Nature* 2004, *427* (6974), 523-527.

[30]   Choi, J. R.; Tachikawa, T.; Fujitsuka, M.; Majima, T., Evaluating Host-Guest Interactions in a Metal-Organic Framework Using a Polarity-Sensitive Probe. *Journal of Physical Chemistry Letters* 2010, *1* (7), 1101-1106.

[31]   Koh, K.; Wong-Foy, A. G.; Matzger, A. J., Coordination Copolymerization Mediated by $Zn_4O(CO_2R)_6$ Metal Clusters: a Balancing Act between Statistics and Geometry. *Journal of the American Chemical Society* 2010, *132* (42), 15005-15010.

[32]   Dybtsev, D. N.; Chun, H.; Kim, K., Rigid and flexible: A highly porous metal-organic framework with unusual guest-dependent dynamic behavior. *Angewandte Chemie-International Edition* 2004, *43* (38), 5033-5036.

[33]   Boehle, T., Ausschnitt aus der Kristallstruktur von HKUST-1 im aktivierten Zustand. http://www.google.de/imgres?imgurl=http://upload.wikimedia.org/wikipedia/commons/4/4a/ HKUST-1_activated.png&imgrefurl=http://commons.wikimedia.org/wiki/File:HKUST-1_act ivated.png&h=1136&w=1140&sz=587&tbnid=6nPmZ765Dou9JM:&tbnh=96&tbnw=96&zo

om=1&usg=__xDW5Hy7SXqxDNwrJkwM-HpH4w0=&docid=ggQncAlORULoeM&sa=X &ei=RNgFU7e9FMWrhAen- oDgAw&ved=0CEYQ9QEwBA&dur=237, update 2014.

[34]   Cui, Y.; Evans, O. R.; Ngo, H. L.; White, P. S.; Lin, W. B., Rational design of homochiral solids based on two-dimensional metal carboxylates. *Angewandte Chemie-International Edition* 2002, *41* (7), 1159-15119.

[35]   Wu, C. D.; Lin, W. B., Highly porous, homochiral metal-organic frameworks: Solvent-exchange-induced single-crystal to single-crystal transformations. *Angewandte Chemie-International Edition* 2005, *44* (13), 1958-1961.

[36]   Han, Q. X.; He, C.; Zhao, M.; Qi, B.; Niu, J. Y.; Duan, C. Y., Engineering Chiral Polyoxometalate Hybrid Metal-Organic Frameworks for Asymmetric Dihydroxylation of Olefins. *Journal of the American Chemical Society* 2013, *135* (28), 10186-10189.

[37]   Jeong, K. S.; Go, Y. B.; Shin, S. M.; Lee, S. J.; Kim, J.; Yaghi, O. M.; Jeong, N., Asymmetric catalytic reactions by NbO-type chiral metal-organic frameworks. *Chemical Science* 2011, *2* (5), 877-882.

[38]   Nickerl, G.; Henschel, A.; Grunker, R.; Gedrich, K.; Kaskel, S., Chiral Metal-Organic Frameworks and Their Application in Asymmetric Catalysis and Stereoselective Separation. *Chemie Ingenieur Technik* 2011, *83* (1-2), 90-103.

[39]   Seo, J. S.; Whang, D.; Lee, H.; Jun, S. I.; Oh, J.; Jeon, Y. J.; Kim, K., A homochiral metal-organic porous material for enantioselective separation and catalysis. *Nature* 2000, *404* (6781), 982-986.

[40]   Dybtsev, D. N.; Yutkin, M. P.; Peresypkina, E. V.; Virovets, A. V.; Serre, C.; Ferey, G.; Fedin, V. P., Isoreticular homochiral porous metal-organic structures with tunable pore sizes. *Inorganic Chemistry* 2007, *46* (17), 6843-6845.

[41]   Zacher, D.; Shekhah, O.; Wöll, C.; Fischer, R. A., Thin films of metal-organic frameworks. *Chemical Society Reviews* 2009, *38* (5), 1418-1429.

[42]   Shekhah, O.; Liu, J.; Fischer, R. A.; Wöll, C., MOF thin films: existing and future applications. *Chemical Society Reviews* 2011, *40* (2), 1081-1106.

[43]   Hanke, M.; Arslan, H. K.; Bauer, S.; Zybaylo, O.; Christophis, C.; Gliemann, H.; Rosenhahn, A.; Wöll, C., The Biocompatibility of Metal-Organic Framework Coatings: An Investigation on the Stability of SURMOFs with Regard to Water and Selected Cell Culture Media. *Langmuir* 2012, *28* (17), 6877-6884.

[44]   Paz, F. A. A.; Klinowski, J.; Vilela, S. M. F.; Tome, J. P. C.; Cavaleiro, J. A. S.; Rocha, J., Ligand design for functional metal-organic frameworks. *Chemical Society Reviews* 2012, *41* (3), 1088-1110.

[45]   Love, J. C.; Estroff, L. A.; Kriebel, J. K.; Nuzzo, R. G.; Whitesides, G. M., Self-assembled monolayers of thiolates on metals as a form of nanotechnology. *Chemical Reviews* 2005, *105* (4), 1103-1169.

[46]   Shekhah, O.; Wang, H.; Kowarik, S.; Schreiber, F.; Paulus, M.; Tolan, M.; Sternemann, C.; Evers, F.; Zacher, D.; Fischer, R. A.; Wöll, C., Step-by-step route for the synthesis of metal-organic frameworks. *Journal of the American Chemical Society* 2007, *129* (49), 15118-15119.

[47]   Vericat, C.; Vela, M. E.; Benitez, G.; Carro, P.; Salvarezza, R. C., Self-assembled monolayers of thiols and dithiols on gold: new challenges for a well-known system. *Chemical Society Reviews* 2010, *39* (5), 1805-1834.

[48]   Parna, R.; Joost, U.; Nommiste, E.; Kaambre, T.; Kikas, A.; Kuusik, I.; Kink, I.; Hirsimaki, M.; Kisand, V., Effect of different annealing temperatures and $SiO_2/Si(100)$ substrate on the properties of nickel containing titania thin sol-gel films. *Physica Status Solidi a-Applications and Materials Science* 2012, *209* (5), 953-965.

[49]   More, P. S.; Raut, R. W.; Ghuge, C. S., Room temperature H_2S gas sensing characteristics of platinum (Pt) coated porous alumina (PoAl) thick films. *Materials Chemistry and Physics* 2014, *143* (3), 1278-1281.

[50]   Kelly, T. G.; Chen, J. G., Metal overlayer on metal carbide substrate: unique bimetallic properties for catalysis and electrocatalysis. *Chemical Society Reviews* 2012, *41* (24), 8021-8034.

[51]   Liu, J. X.; Shekhah, O.; Stammer, X.; Arslan, H. K.; Liu, B.; Schupbach, B.; Terfort, A.; Wöll, C., Deposition of Metal-Organic Frameworks by Liquid-Phase Epitaxy: The Influence of Substrate Functional Group Density on Film Orientation. *Materials* 2012, *5* (9), 1581-1592.

[52]   Velamakanni, A.; Torres, J. R.; Ganesh, K. J.; Ferreira, P. J.; Major, J. S., Controlled Assembly of Silane-Based Polymers: Chemically Robust Thin-Films. *Langmuir* 2010, *26* (19), 15295-15301.

[53]   Arslan, H. K.; Shekhah, O.; Wohlgemuth, J.; Franzreb, M.; Fischer, R. A.; Wöll, C., High-Throughput Fabrication of Uniform and Homogenous MOF Coatings. *Advanced Functional Materials* 2011, *21* (22), 4228-4231.

[54]   Silvestre, M. E.; Franzreb, M.; Weidler, P. G.; Shekhah, O.; Wöll, C., Magnetic Cores with Porous Coatings: Growth of Metal-Organic Frameworks on Particles Using Liquid Phase Epitaxy. *Advanced Functional Materials* 2013, *23* (9), 1210-1213.

[55]   Zhuang, Z. B.; Peng, Q.; Li, Y. D., Controlled synthesis of semiconductor

nanostructures in the liquid phase. *Chemical Society Reviews* 2011, *40* (11), 5492-5513.

[56]   Kressel, H.; Dunse, J. U.; Nelson, H.; Hawrylo, F. Z., Luminescence in Silicon-Doped Gaas Grown by Liquid-Phase Epitaxy. *Journal of Applied Physics* 1968, *39* (4), 2006-2011.

[57]   Arslan, H. K.; Shekhah, O.; Wieland, D. C. F.; Paulus, M.; Sternemann, C.; Schroer, M. A.; Tiemeyer, S.; Tolan, M.; Fischer, R. A.; Wöll, C., Intercalation in Layered Metal-Organic Frameworks: Reversible Inclusion of an Extended pi-System. *Journal of the American Chemical Society* 2011, *133* (21), 8158-8161.

[58]   Stavila, V.; Volponi, J.; Katzenmeyer, A. M.; Dixon, M. C.; Allendorf, M. D., Kinetics and mechanism of metal-organic framework thin film growth: systematic investigation of HKUST-1 deposition on QCM electrodes. *Chemical Science* 2012, *3* (5), 1531-1540.

[59]   Zacher, D.; Yusenko, K.; Betard, A.; Henke, S.; Molon, M.; Ladnorg, T.; Shekhah, O.; Schupbach, B.; de los Arcos, T.; Krasnopolski, M.; Meilikhov, M.; Winter, J.; Terfort, A.; Wöll, C.; Fischer, R. A., Liquid-Phase Epitaxy of Multicomponent Layer-Based Porous Coordination Polymer Thin Films of $[M(L)(P)_{0.5}]$ Type: Importance of Deposition Sequence on the Oriented Growth. *Chemistry-a European Journal* 2011, *17* (5), 1448-1455.

[60]   Liu, B.; Shekhah, O.; Arslan, H. K.; Liu, J. X.; Wöll, C.; Fischer, R. A., Enantiopure Metal-Organic Framework Thin Films: Oriented SURMOF Growth and Enantioselective Adsorption. *Angewandte Chemie-International Edition* 2012, *51* (3), 807-810.

[61]   Shekhah, O.; Hirai, K.; Wang, H.; Uehara, H.; Kondo, M.; Diring, S.; Zacher, D.; Fischer, R. A.; Sakata, O.; Kitagawa, S.; Furukawa, S.; Wöll, C., MOF-on-MOF heteroepitaxy: perfectly oriented $[Zn_2(ndc)_2(dabco)]_n$ grown on $[Cu_2(ndc)_2(dabco)]_n$ thin films. *Dalton Transactions* 2011, *40* (18), 4954-4958.

[62]   Zybaylo, O.; Shekhah, O.; Wang, H.; Tafipolsky, M.; Schmid, R.; Johannsmann, D.; Wöll, C., A novel method to measure diffusion coefficients in porous metal-organic frameworks. *Physical Chemistry Chemical Physics* 2010, *12* (28), 8092-8097.

[63]   Heinke, L.; Wöll, C., Adsorption and diffusion in thin films of nanoporous metal-organic frameworks: ferrocene in SURMOF $Cu_2(ndc)_2(dabco)$. *Physical Chemistry Chemical Physics* 2013, *15* (23), 9295-9299.

[64]   Streit, H. C.; Adlung, M.; Shekhah, O.; Stammer, X.; Arslan, H. K.; Zybaylo, O.; Ladnorg, T.; Gliemann, H.; Franzreb, M.; Wöll, C.; Wickleder, C., Surface-Anchored MOF-Based Photonic Antennae. *Chemphyschem* 2012, *13* (11), 2699-2702.

[65]   Leffingw.Jc; Royals, E. E., Conformational Effects in Opening of Cis/Trans 1,4-Dialkyl Substituted 1,2-Cyclohexene Epoxides with Acetic Acid. *Tetrahedron Letters* 1965, (43), 3829-3837.

[66]   Bringmann, G.; Mutanyatta-Comar, J.; Knauer, M.; Abegaz, B. M., Knipholone and related 4-phenylanthraquinones: structurally, pharmacologically, and biosynthetically remarkable natural products. *Natural Product Reports* 2008, *25* (4), 696-718.

[67]   Fortuna, A.; Alves, G.; Falcao, A., Chiral chromatographic resolution of antiepileptic drugs and their metabolites: a challenge from the optimization to the application. *Biomedical Chromatography* 2014, *28* (1), 27-58.

[68]   Landoni, M. F.; Lees, P., Pharmacokinetics and pharmacodynamics of ketoprofen enantiomers in calves. *Chirality* 1995, *7* (8), 586-597.

[69]   Ohtaki, H.; Radnai, T.; Yamaguchi, T., Structure of water under subcritical and supercritical conditions studied by solution X-ray diffraction. *Chemical Society Reviews* 1997, *26* (1), 41-51.

[70]   Dinnebier, R. E. and Friese, K., Modern XRD Methods in Mineralogy. *Eolss Publishers*, Oxford, 2003, 1-57.

[71]   Birkholz, M., *Thin Film Analysis by X-Ray Scattering*. Wiley-VCH Verlag GmbH & Co. KGaA, Weinheim, 2005, 1-41.

[72]   http://www.rigaku.com/applications/in_plane_diffraction, update 2014.

[73]   Beattie, I. R., Vibrational Infrared and Raman-Spectroscopy in Inorganic-Chemistry. *Chemical Society Reviews* 1975, *4* (1), 107-153.

[74]   Lynch, B. M.; Chisholm, S. L., A Simple, Effective, and General-Method of Enhancing Peak Intensities in Attenuated Total Reflectance Fourier-Transform Infrared-Spectra of Powdered Solids. *Langmuir* 1992, *8* (2), 351-352.

[75]   Atkins, P. A. and de Paula, J., Elements of physical chemistry (5th ed.). *W. H. Freeman and Company,* New York, 2009, 456-459.

[76]   Mendelsohn, R. and Flach, C. R., Infrared Reflection–Absorption Spectrometry of Monolayer Films at the Air-Water Interface. *John Wiley & Sons Ltd,* NewYork, 2002, 1028-1041.

[77]   Greenler, R. G., Reflection Method for Obtaining Infrared Spectrum of a Thin Layer on a Metal Surface. *Journal of Chemical Physics* 1969, *50* (5), 1963-1968.

[78]   Greenler, R. G., Infrared Study of Adsorbed Molecules on Metal Surfaces by Reflection Techniques. *Journal of Chemical Physics* 1966, *44* (1), 310-315.

[79]   Reviakine, I.; Johannsmann, D.; Richter, R. P., Hearing What You Cannot See and Visualizing What You Hear: Interpreting Quartz Crystal Microbalance Data from Solvated Interfaces. *Analytical Chemistry* 2011, *83* (23), 8838-8848.

[80]   http://en.wikipedia.org/wiki/File:Schema_MEB_(en).svg, uplate 2014.

[81]   Mcmullan, D., Scanning Electron-Microscopy 1928-1965. *Scanning*, *17* (3), 175-185.

[82]   Train, C.; Gruselle, M.; Verdaguer, M., The fruitful introduction of chirality and control of absolute configurations in molecular magnets. *Chemical Society Reviews* 2011, *40* (6), 3297-3312.

[83]   Sun, J.; Hu, J. S.; Guo, Z. X.; Qi, Y., Study on side-chain liquid-crystalline copolymer as a new beta-nucleating agent to induce phase behavior of isotactic polypropylene. *Colloid and Polymer Science* 2013, *291* (3), 735-742.

[84]   Nalam, P. C.; Daikhin, L.; Espinosa-Marzal, R. M.; Clasohm, J.; Urbakh, M.; Spencer, N. D., Two-Fluid Model for the Interpretation of Quartz Crystal Microbalance Response: Tuning Properties of Polymer Brushes with Solvent Mixtures. *Journal of Physical Chemistry C* 2013, *117* (9), 4533-4543.

[85]   Chura-Chambi, R. M.; Genova, L. A.; Affonso, R.; Morganti, L., Refolding of endostatin from inclusion bodies using high hydrostatic pressure. *Analytical Biochemistry* 2008, *379* (1), 32-39.

[86]   Deu, E.; Dhoot, J.; Kirsch, J. F., The Partially Folded Homodimeric Intermediate of Escherichia coli Aspartate Aminotransferase Contains a "Molten Interface" Structure. *Biochemistry* 2009, *48* (2), 433-441.

[87]   Santos, J.; Sica, M. P.; Buslje, C. M.; Garrote, A. M.; Ermacora, M. R.; Delfino, J. M., Structural Selection of a Native Fold by Peptide Recognition. Insights into the Thioredoxin Folding Mechanism. *Biochemistry* 2009, *48* (3), 595-607.

[88]   Ansari, M. A.; Zubair, S.; Atif, S. M.; Kashif, M.; Khan, N.; Rehan, M.; Anwar, T.; Iqbal, A.; Owais, M., Identification and Characterization of Molten Globule-Like State of Hen Egg-White Lysozyme in Presence of Salts Under Alkaline Conditions. *Protein and Peptide Letters* 2010, *17* (1), 11-17.

[89]   Shaw, A. K.; Pal, S. K., Resonance energy transfer and ligand binding studies on pH-induced folded states of human serum albumin. *Journal of Photochemistry and Photobiology B-Biology* 2008, *90* (3), 187-197.

[90]   Haghani, K.; Khajeh, K.; Salmanian, A. H.; Ranjbar, B.; Bakhtiyari, S., Acid-Induced Formation of Molten Globule States in the Wild Type Escherichia coli 5-Enolpyruvylshikimate 3-Phosphate Synthase and its Three Mutated Forms: G96A, A183T and G96A/A183T. *Protein Journal* 2011, *30* (2), 132-137.

[91]   Protasevich, I.; Yang, Z. R.; Wang, C.; Atwell, S.; Zhao, X.; Emtage, S.; Wetmore, D.; Hunt, J. F.; Brouillette, C. G., Thermal unfolding studies show the disease causing F508del mutation in CFTR thermodynamically destabilizes nucleotide-binding domain 1. *Protein*

Science 2010, *19* (10), 1917-1931.

[92]   Circular Dichroism (CD) Spectroscopy. http://www.photophysics.com/tutorials/circular-dichroism-cd-spectroscopy. update 2014.

[93]   Kobayashi, N. and Muranaka, A., Circular Dichroism and Magnetic Circular Dichroism Spectroscopy for Organic Chemists, *Royal Society of Chemistry*, Cambridge, 2012, 1-41.

[94]   Ezuhara, T.; Endo, K.; Aoyama, Y., Helical coordination polymers from achiral components in crystals. Homochiral crystallization, homochiral helix winding in the solid state, and chirality control by seeding. *Journal of the American Chemical Society* 1999, *121* (14), 3279-3283.

[95]   Liu, Y.; Xuan, W.; Cui, Y., Engineering Homochiral Metal-Organic Frameworks for Heterogeneous Asymmetric Catalysis and Enantioselective Separation. *Advanced Materials* 2010, *22* (37), 4112-4135.

[96]   Mo, K.; Yang, Y. H.; Cui, Y., A Homochiral Metal-Organic Framework as an Effective Asymmetric Catalyst for Cyanohydrin Synthesis. *Journal of the American Chemical Society* 2014, *136* (5), 1746-1749.

[97]   Wanderley, M. M.; Wang, C.; Wu, C. D.; Lin, W. B., A Chiral Porous Metal-Organic Framework for Highly Sensitive and Enantioselective Fluorescence Sensing of Amino Alcohols. *Journal of the American Chemical Society* 2012, *134* (22), 9050-9053.

[98]   Hatano, M.; Ishihara, K., Conformationally flexible chiral supramolecular catalysts for enantioselective Diels-Alder reactions with anomalous endo/exo selectivities. *Chemical Communications* 2012, *48* (36), 4273-4283.

[99]   Kaminker, R.; de Hatten, X.; Lahav, M.; Lupo, F.; Gulino, A.; Evmenenko, G.; Dutta, P.; Browne, C.; Nitschke, J. R.; van der Boom, M. E., Assembly of Surface-Confined Homochiral Helicates: Chiral Discrimination of DOPA and Unidirectional Charge Transfer. *Journal of the American Chemical Society* 2013, *135* (45), 17052-17059.

[100]   Olah, G. A.; Huang, H. W., Circular dichroism of oriented α helices. I. Proof of the exciton theory. *The Journal of Chemical Physics* 1988, *89* (4), 2531-2538.

[101]   Wu, Y.; Huang, H. W.; Olah, G. A., Method of oriented circular dichroism. *Biophysical Journal* 1990, *57* (4), 797-806.

[102]   Bürck, J.; Roth, S.; Wadhwani, P.; Afonin, S.; Kanithasen, N.; Strandberg, E.; Ulrich, A. S., Conformation and Membrane Orientation of Amphiphilic Helical Peptides by Oriented Circular Dichroism. *Biophysical Journal* 2008, *95* (8), 3872-3881.

[103]   Liu, B.; Shekhah, O.; Arslan, H. K.; Liu, J. X.; Wöll, C.; Fischer, R. A., Enantiopure

Metal-Organic Framework Thin Films: Oriented SURMOF Growth and Enantioselective Adsorption. *Angewandte Chemie-International Edition* 2012, *51* (3), 807-810.

[104]   Liu, B.; Tu, M.; Fischer, R. A., Metal-Organic Framework Thin Films: Crystallite Orientation Dependent Adsorption. *Angewandte Chemie-International Edition* 2013, *52* (12), 3402-3405.

[105]   Moffitt, W., Optical Rotatory Dispersion of Helical Polymers. *The Journal of Chemical Physics* 1956, *25* (3), 467-478.

[106]   Furche, F.; Ahlrichs, R.; Hättig, C.; Klopper, W.; Sierka, M.; Weigend, F., Turbomole. *Wiley Interdisciplinary Reviews: Computational Molecular Science* 2014, *4* (2), 91-100.

[107]   Weigend, F.; Ahlrichs, R., Balanced basis sets of split valence, triple zeta valence and quadruple zeta valence quality for H to Rn: Design and assessment of accuracy. *Physical Chemistry Chemical Physics* 2005, *7* (18), 3297-3305.

[108]   Rappoport, D.; Furche, F., Property-optimized Gaussian basis sets for molecular response calculations. *The Journal of Chemical Physics* 2010, *133* (13), 134105.

[109]   Becke, A. D., Density-functional thermochemistry. III. The role of exact exchange. *The Journal of Chemical Physics* 1993, *98* (7), 5648-5652.

[110]   Klamt, A., The COSMO and COSMO-RS solvation models. *Wiley Interdisciplinary Reviews: Computational Molecular Science* 2011, *1* (5), 699-709.

[111]   Shekhah, O.; Wang, H.; Strunskus, T.; Cyganik, P.; Zacher, D.; Fischer, R.; Wöll, C., Layer-by-layer growth of oriented metal organic polymers on a functionalized organic surface. *Langmuir* 2007, *23* (14), 7440-7442.

[112]   Nishimura, Y.; Manaka, T.; Iwamoto, M., Preparation and atomic force microscopy observation of lipid membranes on micro-patterned self-assembled monolayers. *Thin Solid Films* 2009, *517* (11), 3227-3229.

[113]   Kwak, C. K.; Kim, D. G.; Kim, T. H.; Lee, C. S.; Lee, M.; Lee, T. S., Simultaneous and Dual Emissive Imaging by Micro-Contact Printing on the Surface of Electrostatically Assembled Water-Soluble Poly(p-phenylene) Using FRET. *Advanced Functional Materials* 2010, *20* (22), 3847-3855.

[114]   Ladnorg, T.; Welle, A.; Heisser, S.; Wöll, C.; Gliemann, H., Site-selective growth of surface-anchored metal-organic frameworks on self-assembled monolayer patterns prepared by AFM nanografting. *Beilstein Journal of Nanotechnology* 2013, *4*, 638-648.

8 ABBREVIATIONS

1D	one-dimensional
2D	two-dimensional
3D	three-dimensional
AFM	atomic force microscopy
bdc	1,4-benzenedicarboxylate
BET	Brunauer-Emmett-Teller
bipy	4,4′-bipyridine
bpe	bis(4-pyridyl)-ethylene)
bipyb	1,4-bis(4-pyridyl)benzene
btb	1,3,5-benzenetribenzoate
btc	1,3,5-benzenetricarboxylate
cam	camphoric acid
CD	circular dichroism
COOH	carboxyl
$Cu(OAc)_2$	copper acetate
dabco	1,4-diazabicyclo[2.2.2]octane
Dcam	(1R,3S)-(+)-camphoric acid
DMF	dimethylformamide
DMSO	dimethylsulfoxide
ee	enantiomeric excess
FEG-ESEM	field emission gun environmental scanning electron microscope
FTIR	Fourier transform infrared spectroscopy
FWHM	full-width half-maximum
h	hour(s)
IRMOF	Isoreticular MOFs
IR	infrared
IRRAS	infrared reflection-adsorption spectroscopy
Lcam	(1S,3R)-(-)-camphoric acid
L-CPL	Left circularly polarized light
LPE	liquid phase epitaxy
MCT	mercury cadmium telluride
MHDA	16-Mercaptohexadecanoic acid

min	minute(s)
MOFs	metal-organic frameworks
MUD	11-mercapto-1-undecanol
OCD	Oriented circular dichroism
OH	hydroxyl
PCPs	porous coordination polymers
PDMS	polydimethylsiloxane
PDS	position sensitive detector
PEM	photo elastic modulator
PMT	Photo multiplier tube
PPMT	4,(4-pyridyl)phenyl)methanethiol
PSM	postsynthetic modification
QCM	quartz crystal microbalance
QCM-D	quartz crystal microbalance with dissipation monitoring
R-CPL	right circularly polarized light
R-HDO	(2R,5R)-2,5-hexanediol
SAMs	self-assembled monolayers
SBUs	secondary building units
SEM	scanning electron microscopy
S-HDO	(2S,5S)-2,5-hexanediol
SURMOFs	surface mounted metal-organic frameworks
T^2dc	thieno[3,2-b]thiophene-2,5-dicarboxylate
TDM	transition dipole moment
UV	ultraviolet
XRD	x-ray diffraction
(-)EtLt	(-)-ethyl-L-lactate
(+)EtLt	(+)-ethyl-D-lactate
μCp	micro contact printing

9 PUBLICATIONS

1. Z.-G. Gu, J. Bürck, A. Bihlmeier, J. Liu, O. Shekhah, P. G. Weidler, C. Azucena, Z. Wang, S. Heissler, H. Gliemann, W. Klopper, A. S. Ulrich, and C. Wöll, Oriented Circular Dichroism Analysis of Chiral Surface-Anchored Metal-Organic Frameworks Grown by Liquid-Phase Epitaxy and upon Loading with Chiral Guest Compounds; *Chem. Eur. J.* (2014), 20, 9879-9882.

2. L. Heinke, Z.-G. Gu, C. Wöll, The surface barrier phenomenon at the loading of metal-organic frameworks; *Nat. Commun. (2014), DOI: 10.1038/ncomms5562*.

3. Z. Wang, J. Liu, B. Lukose, Z.-G. Gu, P. Weidler, H. Gliemann, T. Heine and C. Wöll, Nanoporous Designer Solids with Huge Lattice Constant Gradients: Multi-heteroepitaxy of Metal-Organic Frameworks; *Nano Lett.* (2014), 14, 1526-1529.

4. Z.-G. Gu, L. Heinke, C. Wöll, Tuning the Enantioselectivity in Thin Films of Isoreticular Homochiral Metal-Organic Frameworks; *In preparation*.

10 ACKNOWLEDGEMENTS